INFORMATION TO USERS

This reproduction was made from a copy of a document sent to us for microfilming. While the most advanced technology has been used to photograph and reproduce this document, the quality of the reproduction is heavily dependent upon the quality of the material submitted.

The following explanation of techniques is provided to help clarify markings or notations which may appear on this reproduction.

1. The sign or "target" for pages apparently lacking from the document photographed is "Missing Page(s)". If it was possible to obtain the missing page(s) or section, they are spliced into the film along with adjacent pages. This may have necessitated cutting through an image and duplicating adjacent pages to assure complete continuity.

2. When an image on the film is obliterated with a round black mark, it is an indication of either blurred copy because of movement during exposure, duplicate copy, or copyrighted materials that should not have been filmed. For blurred pages, a good image of the page can be found in the adjacent frame. If copyrighted materials were deleted, a target note will appear listing the pages in the adjacent frame.

3. When a map, drawing or chart, etc., is part of the material being photographed, a definite method of "sectioning" the material has been followed. It is customary to begin filming at the upper left hand corner of a large sheet and to continue from left to right in equal sections with small overlaps. If necessary, sectioning is continued again—beginning below the first row and continuing on until complete.

4. For illustrations that cannot be satisfactorily reproduced by xerographic means, photographic prints can be purchased at additional cost and inserted into your xerographic copy. These prints are available upon request from the Dissertations Customer Services Department.

5. Some pages in any document may have indistinct print. In all cases the best available copy has been filmed.

University Microfilms International
300 N. Zeeb Road
Ann Arbor, MI 48106

TZEGHAI, GHEBRE E.

MASS TRANSPORT WITH MIXED BOUNDARY CONDITIONS WITH SPECIAL APPLICATION TO PROBLEMS IN ATHEROGENESIS

City University of New York PH.D. 1984

MASS TRANSPORT WITH MIXED BOUNDARY CONDITIONS WITH SPECIAL APPLICATION TO PROBLEMS IN ATHEROGENESIS

By

GHEBRE E. TZEGHAI

A dissertation submitted to the Graduate Faculty in Engineering in partial fulfillment of the requirements for the degree of Doctor of Philosophy, The City University of New York.

1983

This manuscript has been read and accepted for the Graduate Faculty in Engineering in satisfaction of the dissertation requirement for the degree of Doctor of Philosophy.

11/21/83
date

Robert Pfeffer, Chairman of
Examining Committee

11/21/83
date

Paul Karmel
Executive Officer

Shu Chien, M.D.*

Peter Ganatos, Ph.D.

Charles Maldarelli, Ph.D.

Robert Pfeffer, Ph.D.
Chairman

Sheldon Weinbaum, Ph.D.

Supervirory Committee

*Columbia University Faculty of Medicine

The City University of New York

ABSTRACT

MASS TRANSPORT WITH MIXED BOUNDARY CONDITIONS WITH SPECIAL APPLICATION TO PROBLEMS IN ATHEROGENESIS

By

Ghebre E. Tzeghai

Adviser : Professor Robert Pfeffer
Co-Advisers: Professor Sheldon Weinbaum
Professor Peter Ganatos

This thesis deals with the construction of new theoretial models to help elucidate and quantify the fundamental mechanisms by which cholesterol carrying and related macromolecules first cross the arterial endothelium and subsequently diffuse into the underlying tissue. Atherosclerosis, an arterial disease which is recognized as the leading cause of death in most developed countries is associated with the accumulation of these macromolecules in the arterial wall.

Thus far, the existing large body of experimental and theoretical findings strongly suggest that the mechanisms which govern transport of macromolecules across arterial wall are strongly dependent on the structural integrity of the arterial endothelium. The theoretical work presented herein offers some explanations to these findings.

The predictions from the first model show that the endothelium is the major resistance to transarterial transport of macromolecules greater than 40Å and that only a small fraction of the endothelial junctions need be disrupted to produce a significant change in the concentration distribution of macromolecules in the wall. An extension

of this model shows that convection will produce about a 20% increase in flux of macromolecules into the wall for small endothelial damage (<1%), but that the effect of convection will increase dramatically as the damage size or the number of leaky junctions increases.

For the first time, 1) the coupling of the endothelial junction resistance with that of the media has been examined quantitatively so that the rate of water filtration and the pressure distribution in the arterial wall can be estimated. From this model it is found that when the tight junction width is 26Å, more than half of the transmural pressure drop can be sustained by the endothelium for a wall whose media thickness is less than 200μm, and 2) the arterial distribution volume has been quantified. The latter results clearly show that the artery wall consists essentially of two distinct regions of relatively constant diffusion coefficient, the media and the adventitia with an abrupt change in diffusion coefficient occurring at their interface. Furthermore, it is indicated that the distribution volume is larger in the adventitia than in the media.

All of the findings indicated above are in a very favorable agreement with experimental physiological data.

ACKNOWLEDGEMENT

I wish to thank Professor Robert Pfeffer, Professor Sheldon Weinbaum and Professor Peter Ganatos for introducing me to a research field that I found to be highly challenging and educational. I wish to thank them also for their continuous guidance and many contributions in directing this research. Also, I wish to thank the staff of The City University of New York Computer Center for their technical assistance and the use of their facilities.

This research was supported by the National Science Foundation, Grant No. CPE-8200301 and by the National Institutes of Health Award HL 19454. In addition, I received a one year Graduate Fellowship from the Northeast Resource Center for Science and Engineering at The City College of New York. These are gratefully acknowledged.

TABLE OF CONTENTS

LIST OF FIGURES

Figure | Page

CHAPTER III

CHAPTER I

INTRODUCTION

Solutions of heat and mass transfer equations have long been of interest in many areas of science and engineering. Very often, problems with planar or cylindrical geometries arise where the boundary conditions on the same coordinate surface are mixed. In particular, a Dirichlet or Newmann type boundary condition may be required on one part of the surface, while the solution must satisfy a boundary condition of the third kind, such as a convective boundary condition in heat or mass transfer, on another part of the same surface. An additional complication that may arise is that the medium in which conduction or diffusion is taking place may be stratified requiring that the problem be treated assuming a variable conductivity or diffusivity.

Various special solution methods to this type of boundary value problems are presented here in with specific applications in mass transfer and pressure distribution problems in biological systems, in particular to theoretical studies on the pressure drop and transport of macromolecules across an arterial wall. In the following paragraphs, some of the previous theoretical studies which are closely related to the work presented here, and the experimental findings that motivated such studies are summarized.

The structure of a typical mammalian artery consists of three morphologically distinct layers: the intima (which consists of the endothelial call monolayer), the media and the adventitia. The passage of the cholesterol-carrying low-density lipoproteins (LDL) and related macromolecules across the arterial endothelium and the rate of wall transfer in the underlying arterial structure have been the subject of many in vivo and in vitro experiments, electron microscopic studies and numerous theoretical studies. These studies have been motivated in large measure by the considerable importance

of the transport of macromolecules between lumen (blood) and arterial wall in the understanding of the causes of atherogenesis in the larger arteries of humans and animals. The importance of atherosclerosis as a principal arterial disease has been appreciated for many years (see Thurn, 1982 for historical background). Nevertheless, its causes and pathogenesis remain unsolved. A major problem is that the disease progresses insidiously for years before symptoms develop (Ross et al., 1976), making it difficult to follow the early stages of the disease.

In the arterial wall, the innermost layer or the intima consists of a very narrow region bounded on the luminal or blood side by a single continuous layer of endothelial cells that serve as the interface between the lumen and the arterial tissue, and by a fenestrated sheet of elastic fibrils, the internal elastic lamina. The endothelial cells rest on a connective tissue matrix that consists of a basement membrane intermixed with collagen fibrils. Between the endothelium and the basement membrane, the intima consists of various components of extracellular connective tissue and occasional smooth muscles, the presence of which is found to increase with age. It is within this region that lipoproteins from blood passing through an artery tend to accumulate and also it is in this region where the proliferation of smooth muscle cells is observed. These events are believed to be the beginnings of the formation of atheromatous lesions and eventually plaques. Furthermore, migration of smooth muscle cells from the media into the intima and the subsequent proliferation of these cells in the intimal space is an important event in atherogenesis (Ross et al., 1976).

The large body of the experimental data already gathered strongly suggests that the controlling resistance and the fundamental mechanisms which govern transport of macromolecules across the wall are mainly related to the highly specialized ultrastructure of the arterial endothelium. The experimental evidence also shows that the rate of macromolecule transport across the arterial wall is sensitive to mechanical factors, e.g. shear stresses, pressure oscillations and mechanical stretches.

From electron microscopic studies, the largest macromolecules that can effectively pass the narrowest constrictions of the intercellular channels between adjacent endothelial cells are approximately 20-40Å. Larger molecules, such as albumin (42Å) and the LDL that carry cholesterol (150-200Å) are transported through vesicles which are an important ultrastructural feature of the endothelieal cells that can transport molecules larger than 40Å across the endothelium, (see Chien and Weinbaum, 1981) and through open channels which might exist during cell turnover (death).

A problem of great current interest because of its implication for arterial disease is why in certain regions of the larger vessels the uptake of lipoproteins is 50 to 100 percent larger than in neighboring areas. Intravenous injection of protein-bound Evans blue dye into experimental animals leads to a characteristic focal pattern of the distribution of blue areas in the arterial wall. The uptake of ^{3}H-cholesterol is greater in the blue areas (Somer et al., 1971, 1972) than in the contiguous white areas. The endothelial cells in the blue areas exhibit altered morphology, a higher incidence of focal injuries (Gerrity et al., 1977) and a higher cell turnover rate. In situ experiments with

elevated pressure and mechanical oscillation, and the supporting vesicle transport theory reported in Chien and Weinbaum (1981) strongly suggest that the observed regional differences in uptake of macromolecules are difficult to explain on the basis of vesicular transport. The alternate explanation is that the variation in the transport are mediated by subtle changes in the permeability of the endothelial cell as might occur during cell turnover. Recent ultrastructural studies (Schwartz et al., 1981) suggest that the increased cholesterol uptake in areas with high rates of cell turnover results from enhanced permeability around regenerating cells, Chien and Weinbaum (1981), and Lezczynski and Kummerow (1981) have shown that elevated luminal pressure produces an increase in uptake that does not vary linearly with increased luminal area. These and the ultrastructural studies suggest that the intercellular clefts between adjoining endothelial cells may become leaky to larger macromolecules (> 40Å) at elevated pressure or during the cell turnover process or due to both pressure and cell turnover.

According to the response-to-injury hypothesis (Virchow, 1856), atherogenesis results from the response of the arterial wall to blood factors following the loss of endothelium (e.g. Björkerud, 1969, Sheppard and French, 1971), and the ensuing release of platelet derived growth factor (PDGF) has been proposed to be an important factor in atherogenesis (Ross et al., 1976). PDGF induces smooth muscle cell proliferation and degradation of LDL in cultured smooth muscle cells (Ross and Vogel, 1978). Ultrastructural studies, however, have failed to demonstrate areas of exposed subendothelium under normal conditions or in response to atherosclerotic risk factors (Schwartz et al., 1981). Furthermore, accumulation of lipids occurs only beneath regions of regenerated endo-

thelium, but not on areas of denudation (Stemermen, 1974 and Minick et al., 1977). Hence, it appears that the presence of endothelium contributes to lipid accumulation in the intima. Endothelial cells have shown to produce factors which stimulate the proliferation of smooth muscle cells (Gajdusek et al., 1980) and also inhibit their growth and DNA synthesis. Endothelial cells in culture produce factor(s) which stimulate LDL binding, but, unlike PDGF, inhibit LDL degradation (Witte et al., 1982). The relation of the endothelial derived growth factor(s) to atherogenesis remains to be elucidated.

The findings from the studies described above raise several fundamental questions about the mass transfer in the artery wall. In particular, how much damage in the endothelial cell monolayer is required to account for the observed nearly two-fold increase in the uptake of LDL and related macromolecules into the arterial wall? What is the transport mechanism(s) in the wall when the endothelium suffers a damage(s)? The central focus of the work presented in the following chapters is to theoretically explain the observed increase in uptake and provide possible mass transfer mechanism(s) in the arterial wall when the integrity of the endothelium is not maintained, so as, in part, to help elucidate the early stages of the atherogenesis.

The basic model for macromolecule transport in arterial vessels is presented in Weinbaum and Caro (1976). In this model, the arterial media is considered to be a medium consisting of two phases, an interstitial fluid phase and a uniformly dispersed cellular phase representing the large number of smooth muscle cells which are present in the wall tissue. Application of this model predicts that the intact endothelium, although typically much less than one percent

of the arterial wall in thickness, represents more than 80 percent of the total resistance to macromolecule transport in major arteries. This important conclusion was also made from both in vivo and in vitro experimental studies (e.g. Fry, 1973 and Bratzler et al., 1977).

Nir and Pfeffer (1979) in an effort to explain the experimentally observed increase in uptake, extended the basic model, to take into account the presence of a single local endothelial injury in an otherwise undamaged endothelial cell layer. It was hypothesized that during cell turnover, the dying cell itself become permeable across its entire surface. By neglecting any interaction between damaged cells, these authors obtained analytic solutions for the flux, uptake and concentration profile in the arterial media as a function of damage size and a fraction of damaged surface. The results strongly support the possibility that the increased permeability of the arterial wall to macromolecules in localized regions of the arterial tree is due to loss of endothelial integrity and that only a very small portion of the endothelium need be damaged for its resistance to be significantly reduced. The theory, however, could not be directly compared with physiological experimental data since cell turnover studies have shown that the spacing between dying cells is too close for the interaction between damaged sites to be neglected.

Pfeffer et al. (1981) overcame this limitation by introducing a periodic model for multiple interacting damages in which the damages are arranged in a two-dimensional array where the spacing between damages can be chosen arbitrarily. Using the periodic model, Pfeffer et al. explained the observed increase in uptake of macromolecules in Evans stained blue areas as compared to unstained white areas, and obtained

results that are also quantitatively in favorable agreement with physiological experimental data.

Specific Studies

As stated earlier, recent electron microscopic studies (Schwartz et al., 1981) have shown that the process of cell turnover associated with naturally occurring hemodynamic factors does not casue denudation, suggesting that a dying cell may not be permeable to macromolecules over its entire surface but that only its junctional complex may become disrupted allowing the passage of macromolecules. Since under normal in vivo condition 0.1 to 1 percent of the endothelial surface is involved in cell turnover (Schwartz et al., 1981), and the intercellular cleft is only 0.1 percent of the cell surface area, the feasibility of the leaky junction hypothesis as a mechanism of enhanced transport has to be critically examined on quantitive grounds. The study presented in Chapter II deals with the plausibility of this potentially very important hypothesis.

The significance of water transport in the artery wall is of prime importance in testing the validity of the filtration theory of atherogenesis in which arterial thickening is attributed to the filtration and entrapment of plasma borne constituents (Wilens, 1951). Also of interest in atherogenesis are the forces acting on the endothelium and their relationship to endothelial permeability. One of these forces is the luminal pressure, which results in a pressure gradient across the endothelium and the media (Harrison and Massero, 1976).

Experimental studies on the movement of water across the arterial wall due to a pressure driving force and the hydraulic conductivity of the various layers of the wall suggest that as much as half of the total hydraulic resistance

occurs in the endothelial cell monolayer (Vargas et al., 1978). This finding is rather surprising considering that the endothelial thickness is a very small fraction of the arterial wall thickness. A mathematical model for the water movement across the wall is presented in Chapter III. The aim is, for the first time, to provide fundamental insight into the fine structure of the water movement and pressure distribution in the arterial wall and, in particular, to show quantitatively how the dimensions of the intercellular cleft is related to both the water movement and pressure distribution in the subendothelial space. The movement of water across the artery wall is also important in studying the effect of convection on macromolecule transport in the arterial media. With the findings from Chapter II and III, a more general theory and model are presented in Chapter IV quantifying the effect of both diffusive and convective transport on the steady-state concentration of macromolecules in the artery wall, in the presence of multiple interacting endothelial injuries or leaky junctions.

In Chapter V, the last of the major chapters, a theoretical model is presented for estimating the interstitial concentration and distribution volume in the arterial wall. The plan here is to develop a model which, 1) could explain the resistance to the transport of macromolecules by the different layers in the wall and 2) could predict the distribution volume in the different layers, thus allowing the computation of the actual concentration of macromolecules across the arterial wall which otherwise is difficult to determine.

Atherosclerosis is an arterial disease that is recognized as the leading cause of death in most of the developed countries. It is also a multifactor problem which requires

the involvement of many disciplines including physiology, bio-physics, engineering, cell biology, electron microscopy, medicine and fluid mechanics. Therefore, the work presented herein has been only one part of many ongoing studies.

This manuscript is presented in the form of four independent papers each of which will be submitted for publication in a scientific journal. Each of the main chapters (II, III, IV and V), therefore, has its own summary, introduction and reference list.

REFERENCES

Bratzler, R.L., Colton, C.K. and Smith, V.A. (1977). In G.W. Manning and M.D. Haust, Atherosclerosis: Metabolic, Morphologic and Clinical Aspects, Plenum Press, New York, pp. 943.

Björkerud, S. (1969). J. Athers. Res. 9, 209.

Chien, S. and Weinbaum, S. (1981). ASME J. Biomech. Eng., 103, 176.

Fry, D.L. (1973). Ciba Foundation Symposium, 12, 93. Amsterdam: Elsevier Assoc. Sci. Publ.

Gajdusek, C., Dilorleto, P., Ross, R. and Schwartz, S.M. (1980). J. Cell Biol. 85, 467.

Gerrity, R.G., Richardson, M., Somer, J.B., Bell, F.B., and Schwartz, C.J. (1977). J. Amer. Path. 99, 131.

Harrison, G.R., and Massaro, T.A. (1976). Am. J. Physiol. 231, 1806.

Lezczynski, D.E. and Kummerow, F.A. (1981). J. Biomech. 14, 307.

Minick, C.R., Stemerman, M.G. and Insull, W. (1977). Proc. Natl. Acad. Sci. 74, 1724.

Nir, A. and Pfeffer, R. (1979). J. Theor. Biol. 81, 685.

Pfeffer, R., Ganatos, P., Nir, A. and Weinbaum, S. (1981). ASME J. Biomech. Eng., 103, 197.

Ross, R. and Glomset, J.A. (1976). N. Engl. J. Med. 295, 369.

Ross, R. and Vogel, A. (1978). Cell. 14, 203-210, (Review).

Schwartz, S.M., Gajdusek, C.M., and Selden, S.C. III, (1981). Atherosclerosis, 1, No. 1.

Sheppard, B.L. and French, J.E. (1971). Proc. Roy. Soc. Lond. (Biol.) 176, 427.

REFERENCES (cont.)

Somer, J.B. and Schwartz, C.J. (1971). Atherosclerosis, 13, 293.

Somer, J.B. and Schwartz, C.J. (1972). Atherosclerosis, 16, 377.

Stemermen, M.B. (1974). Prog. in Thrombosis and Hemostasis (ed. T.H. Spaet), 2, 1. Grune and Stratton, New York.

Thurn, A.L. (1982). Columbia University, doctoral thesis.

Vargas, C.B., Vargas, F.F., Pribyl, J.G. and Blackshear, P.L. (1978). Amer. J. Physiol. 236, H53.

Virchow, R. (1856). In. Ges Abha Wissenschaftlichen Med. Frankfurt-au-Main: Meidinger, pp. 458.

Wilens, S.L. (1951). Science, 14, 389.

Witte, L.D., Corneicelli, J.A., Miller, R.W. and Goodman, D.S. (1982). J. Biol. Chem, 257, 5392.

CHAPTER II

EFFECT OF CELL TURNOVER AND LEAKY JUNCTIONS ON THE TRANSPORT OF MACROMOLECULES ACROSS THE ARTERIAL WALL

SUMMARY

A new theoretical model for endothelial cell turnover is presented herein which has provided a very plausible mechanism to explain the large local differences in macromolecule permeability in an arterial wall that have been observed in vivo. In previous models (Nir and Pfeffer, 1979 and Pfeffer et al., 1981), it was assumed that a damaged or dying endothelial cell offered no resistance to transport, i.e., such a cell becomes permeable to macromolecules over its entire surface. The present model is based on recent experimental evidence (Schwartz et al., 1981) which suggests that dying endothelial cells do not leave demonstrable areas of exposed tissue but rather that the junctional complex around such cells may become leaky to macromolecules. Since the width of a leaky junction is very small when compared to the arterial wall thickness (about 10^{-5} to 1), a special solution technique has been developed to determine the fine structure of the solution in the vicinity of the junctional complex. The results from the present model clearly show that the transport rate of macromolecules into the wall is largely controlled by the perimeter of the dying cell rather than its area. Furthermore, the leaky junction hypothesis is not only qualitatively a reasonable explanation of the increased uptake found in certain regions of the arterial tree, but also is in very favorable quantitative agreement with experimental physiological results reported by Bell et al. (1974a).

1 INTRODUCTION

The studies on the transport of macromolecules between the lumen (blood) and the arterial wall are vast and of considerable importance in understanding the pathogenesis of atherosclerosis in larger arteries of humans and animals. Figure 1, taken from Bratzler et al. (1975), is a conceptual illustration of the three distinct layers present in a typical mammalian artery: the intima, the media, and the adventitia. The intima is a very thin region bounded on the blood side by a single continuous layer of endothelial cells which act as the interface between the blood and the arterial tissue, and bounded in the arterial wall by the elastic laminae. It is widely agreed that the endothelium, despite its small thickness (1/2000)of the media in a dog carotid artery), represents the main barrier to the trans-arterial transport of macromulecules. Molecules from the lumen such as, among many others, the cholesterol carrying low-density lipoproteins (LDL) tend to accumulate in the intima. It is also in this region that the proliferation of smooth muscle cells is observed, leading to the development of atheromatus lesions.

From electron microscopic studies, the largest molecules which can effectively pass through the narrowest constrictions of the intercellular clefts (frequently called tight junctions) separating healthy endothelial cells are approximately 20-40Å. Larger molecules such as albumin (42Å) and the cholesterol carrying LDL (150-200Å), are transported via plasmalemma vesicles (as first suggested by Palade, 1953) which are present in endothelial cells, and also through intercellular clefts whose tight junctions have been opened (probably a disruption of intramembranous protein strands which are observed in freeze fracture electron micrographs of tight junction regions) by either mechanical factors such as hypertension or normal cell turnover (death and replacement of endothelial cell). Both of these

mechanisms can facilitate the transport of larger molecules across the endothelial monolayer (Oko, 1979). Such junctions are referred to here as leaky junctions.

About 90 percent of the vesicles present in the arterial endothelium are open and attached at either the luminal or the intimal surface of the cell. It was first hypothesized by Palade (1953) that the vesicles fill with micromolecules through diffusion in their attached state, then break off from their attaching stalks, migrate in a closed spherical shape across the endothelial cell by Brownian diffusion and reattach at the opposite surface where they discharge their contents. This process is called vesicular transport and proceeds in both directions, but if the concentration of molecules in the lumen is greater than that in the tissue, there will be a net transfer of molecules from the blood to the arterial tissue. The process just described has been experimentally observed in mammalian endothelium using time dependent labeled tracer techniques (Casley-Smith et al., 1971; Simionescu et al., 1973). An alternate hypothesis which has been recently advanced by Louden et al. (1979) and Clough et al. (1981), based on their experiments with frog capillary endothelium, is that the vesicles do not undergo a transendothelial diffusion but fuse with one another forming transient patent channels across the cell. At present, it is not known which hypothesis is correct or if both occur and the difference is due to experimental species differentiation. Detailed summaries of the existing theoretical models in vesicular transport and their extensions are presented in Weinbaum and Chien (1980), and Arminski et al. (1980). The necessary conditions for vesicle fusion and the formation of patent channels has been theoretically examined in Arminski et al. (1982).

A problem of great current interest because of its implication in arterial disease is why in certain regions of the larger arterial vessels, the uptake of labeled

macromolecules (transendothelial transport) is 50 to 100 percent larger than in neighboring areas. Numerous in vivo experiments with pig, canine and rabbit aorta by Adams et al. (1968, 1970), Bell et al. (1974a,b) and Schwartz et al. (1974) just to name a few, have confirmed that the transport of molecules across endothelium is severely restricted except in some regions of enhanced permeability where roughly a twofold increase in uptake of macromolecules is observed. These regions, which stain more readily with protein binding Evans blue dye than other areas which appear white, have been shown to exhibit a significant increase in cell turnover as has been demonstrated using thymidine labelling and silver nitrate staining techniques. However, Schwartz et al. (1981) and DeBruijn et al. (1974) have reported that the silver stain itself is noxious and will produce changes in the endothelial cell complicating the determination of the cell turnover rate. Figure 2, taken from Gerrity (1977) is a silver stained Hautchen preparation of endothelial cells for pig aorta showing two dying or dead endothelial cells in the process of turnover. In general the cell turnover rate predicted by silver staining is five to tenfold greater than that reported using thymidine labelling.

The in situ experiments with elevated pressure and mechanical oscillation, and the supporting vesicle transport theory reported in Chien and Weinbaum (1981) strongly suggest that the observed regional differences in uptake of macromolecules are difficult to explain on the basis of vesicular transport. These authors argue that vesicle attachment/detachment as opposed to vesicle diffusion, is the rate limiting process and the former process is not significantly affected by mechanical disturbances. However, the above authors, and Lezczynski and Kummerow (1981) show that elevated pressure produces an increase in uptake that does not vary linearly with increased luminal area. This behavior

suggests that the intercellular clefts between adjoining endothelial cells may become leaky at elevated pressure. The above findings raise several fundamental questions in arterial mass transport. In particular, how many leaky junctions are required to account for the observed, nearly twofold increase in the uptake of LDL and related macromolecules in the arterial wall? How does the uptake and permeability of the artery wall change when the endothelial cells are in the process of cell turnover? The central focus of the work presented here is to theoretically explain the observed increase in uptake and provide possible mass transfer mechanism(s) in the arterial wall when the integrity of the endothelium is not maintained.

2. THEORETICAL BACKGROUND

The basic model used in this study for macromolecule transport in an arterial vessel is presented in Weinbaum and Caro (1976). In this model, the arterial media is considered to be a medium consisting of two phases, an interstitial fluid phase and a uniformly dispersed cellular phase representing the large number of smooth muscle cells which are present in the wall tissue. The entire interstitial space is described by an effective diffusion coefficient which takes into account the presence of the collagen fibers and other concomitant material present in the interstitial space. The smooth muscle cells are assumed to be uniformly distributed and act as a continuous distribution of sinks since the dimension of the cells is small compared to the thickness of the arterial media. Application of this model predicts that the intact endothelium, although typically less than 0.1 percent of the arterial wall in thickness, represents more than 80 percent of the total resistance to macromolecule transport in major arteries.

Nir and Pfeffer (1979) in an effort to explain the experimentally observed increase in uptake, extended the basic model developed by Weinbaum and Caro (1976), to take into account the presence of a single local endothelial injury in an otherwise undamaged endothelial cell layer. It was hypothesized that during cell turnover, the dying cell itself becomes permeable across its entire surface. The dying cell, Figure 3, was modeled as a circular hole of radius ε in an otherwise intact endothelium of infinite extent. All lengths were nondimensionalized by the thickness of the media L. The endothelium is at $z = 1$, and was treated as a vanishingly thin high resistance layer in accord with the model. The basement membrane in the focal regions of damage was also assumed to be disrupted and in the region of intact endothelium to offer a resistance which is

combined with the endothelial resistance. By neglecting any interaction between damaged cells, these authors were able to obtain an analytic solution for the flux, uptake and concentration profile in the arterial media as a function of damage size and fraction of damaged surface for an inert tracer molecule that does not react with wall components. The results strongly support the possibility that the increased permeability of the arterial wall to macromolecules in localized regions of the arterial tree is due to loss of endothelial integrity and that only a very small portion of the endothelium need be damaged for its resistance to be significantly reduced. The theory, however, could not be directly compared with physiological experimental data since cell turnover studies have shown that the spacing between dying cells is too close for the interaction between damaged sites to be neglected.

Pfeffer et al. (1981) overcame this limitation by introducing a periodic model for multiple interacting damages in which the dying endothelial cells are arranged in a two-dimensional array as shown in Figure 4. Here, 2ξ is the distance between two neighboring damages or dying cells which are represented as circular holes, and this spacing can be chosen arbitrarily. Using the periodic cell turnover model, Pfeffer et al. examined the quantitative feasibility of a small fraction of dying cells accounting for the observed increase in uptake of macromolecules in Evans stained blue areas as compared to unstained white areas, and obtained results that were also quantitatively in favorable agreement with physiological experimental data. While precise numerical comparison with experiment is not meaningful, because of the simplified nature of the model and the neglect of chemical kinetic processes associated with the dissociation and recombination of the Evans blue dye with the wall substance, the model clearly showed that for endothelial wall dimensions and arterial wall thicknesses of interest the

steady state increase in flux and uptake would be a hundred fold larger than one would expect on the basis of the area of the dying cells.

3. ENDOTHELIAL CELL TURNOVER AND LEAKY JUNCTIONS

In the previous models which describe the transport of macromolecules by considering the uptake at the luminal surface and the subsequent diffusion in the arterial tissue, it was assumed that damaged or dying endothelial cells offered no resistance to transport of macromolecules over their entire area. Thus the concentration underneath such cells was assumed to be the same as in the lumen. Recent electron microscopic studies (Schwartz et al., 1981) have shown that the process of cell turnover associated with naturally occurring hemodynamic factors does not cause denudation, suggesting that a dying cell may not be permeable to macromolecules over its entire surface but that only its junctional complex may become disrupted allowing the passage of macromolecules. Since under normal in vivo conditions 0.1 to 1 percent of the endothelial surface is involved in cell turnover (Schwartz et al., 1981), and the intercellular cleft is only 0.1 percent of the cell surface area, the feasibility of the leaky junction hypothesis as a mechanism of enhanced transport has to be critically examined on quantitative grounds. In essence one would like to know whether it is indeed possible on the basis of fundamental diffusion mechanisms to have a twofold increase in permeability arise from a very small fraction of leaky endothelial junctions which account for only 10^{-5} to 10^{-6} of the endothelial surface. The present study will focus on the plausibility of this new hypothesis.

A. Mathematical Formulation

The main difference between the new model presented here and the previous models, Nir and Pfeffer (1979) and Pfeffer et al. (1981), which study the effect of local endothelial damage is the assumption that an endothelial cell that is in the process of turnover becomes leaky only along its perimeter, and that the macromolecules larger than 40Å can be transported through the disrupted junctional

complexes between dying and normal cells. This model like the previous ones involves the solution of a mixed boundary value problem. However, since the width of a leaky junction is very small compared to the wall thickness of the spacing between leaky junctions, special solution techniques must be used to find the fine structure of the solution in the vicinity of the junctional complex.

A schematic diagram of the geometry of the problem is shown in Figure 5, where R_1 is the radius of a damaged or dying endothelial cell, $R_2-R_1 = \varepsilon'$ is the width of the leaky junction, and all lengths are nondimensionalized by the thickness of the arterial wall. As in the model of Pfeffer et al. (1981), the damaged cells (or leaky junctions) are arranged in a two-dimensional array (Figure 4), in which 2ξ is the distance to the next leaky junction so that ξ is the effective radius of a unit cell of the model. In the present model the existence of a diffuse basement membrane needs no separate treatment. This membrane would function in exactly the same way as the endothelium itself and would offer a resistance which would be small compared to the endothelium if only 1 part in 10^5 of its surface area were permeable. The arterial media is represented by a dispersed cellular phase and interstitial fluid phase as in the model of Weinbaum and Caro (1976), and diffusion in the media is described by an effective diffusion coefficient. The chemical kinetics of the diffusing tracer is again neglected since this adds mathematical complexity without elucidating the fundamental hypothesis. Wall kinetics can be easily added later as a refinement of the basic model.

At steady state, the concentration of macromolecules in the two phases is the same. Thus the governing mass transfer equation is

$$\nabla^2 c = 0 \qquad (1)$$

where c is the dimensionless concentration of macromolecules at any position defined as $c = (C-C_A)/(C_L-C_A)$, in which C_A is the macromolecule concentration at the adventitial and C_L is the concentration in the lumen.

The boundary condition at the adventitial surface (z=0) is

$$c(r,0) = 0 \qquad 0 < r < \xi \tag{2}$$

where it is assumed that macromolecules are effectively removed by the lymphatic system.

At r=0, due to symmetry

$$\frac{\partial c}{\partial r}(0,z) = 0 \qquad 0 < z < 1 \tag{3}$$

and at the edge of the unit cell, $r=\xi$, the periodicity of the model requires that there be no net mass transfer. Therefore,

$$\frac{\partial c}{\partial r}(\xi,r) = 0 \qquad 0 < z < 1 \tag{4}$$

Once the junctional complex becomes leaky we assume that its dimensions are sufficiently larger than the tracer molecule so that the transport resistance of the intercellular cleft around the perimeter of the dying cell can be neglected. Thus, the concentration of the exit of the intercellular cleft is the same as in the lumen:

$$c(r,1) = 1 \qquad R_1 < r < R_2 \tag{5}$$

For the overwhelming fraction of the luminal surface where the endothelium is intact, the net flux of macromolecules across the endothelial cell layer by vesicular transport must equal the net flux by molecular diffusion in the intima directly beneath the endothelium. Hence, the appropriate boundary condition in this region is

$$\frac{\partial c}{\partial z}(r,1) = \sigma[1-c(r,1)] \qquad R_2 < r < \xi \tag{6}$$

In the present model, condition (6) is also satisfied in the region $0<r<R_1$. Since the vesicular contribution of the dying cell is negligible, boundary condition (6) or a zero flux boundary condition would lead to essentially the same result. Here, σ is the Biot number which is shown in Weinbaum and Caro (1976) to physically represent the ratio of the resistance to macromolecule transport of the arterial media to that of the intact endothelium. Convective transport of molecules due to water movement through the junctions between cells has been neglected in the present model and will be considered in a future effort.

The mathematical solution of the boundary value problem just outlined is not straightforward because of the complexity of the mixed boundary conditions at the endothelial surface and the large difference in the required scale representation between R_1-R_2 (leaky junction width), and the unit cell radius ξ. Therefore, a special analytical procedure was developed and is described as follows: The solution of (1) for the steady-state concentration distribution $c(r,z)$ is obtained using a superposition of two contributions

$$c = C_1 + C_2, \tag{7}$$

in which C_1 corresponds to the solution for the case where the endothelium is undamaged. At $z = 1$, we require that C_1 satisfy boundary condition (6) everywhere,

$$\frac{\partial C_1}{\partial z}(r,1) + \sigma C_1(r,1) = \sigma \qquad 0 < r < \xi \tag{8}$$

The C_2 in (7) accounts for the presence of the leaky junctions. From (5,6,7 and 8) the boundary conditions for C_2 at $z = 1$ are,

$$C_2(r,1) = \frac{1}{1+\sigma} \qquad R_1 < r < R_2 \tag{9}$$

$$\frac{\partial C_2}{\partial r}(r,1) + \sigma C_2(r,1) = 0 \quad 0 < r < R_1,\ R_2 < r < \xi \tag{10}$$

For the case where the endothelium is intact, the concentration equation, i.e., Eq. (1) reduces to

$$\frac{d^2C_1}{dz^2} = 0 \tag{11}$$

and the solution to C_1 is easily found by integrating (11) and applying conditions (2) and (8),

$$C_1 = \frac{\sigma}{1+\sigma} z \tag{12}$$

The general solution for C_2 which satisfies boundary conditions (2,3 and 4), is of the form

$$C_2 = a_0 z + \sum_{j=1}^{\infty} a_j \sinh(\lambda_j z) J_0(\lambda_j r) \tag{13}$$

where J_0 is Bessel function of the first kind of order zero, and the coefficients a_j, j=0,1,2,---, are unknown constants. The crucial mathematical problem is to determine these unknown coefficients by satisfying the mixed boundary conditions (9,10) at z=1.

Due to the small width of the leaky junctional complex compared to both the cell dimensions and the spacing between neighboring damaged cells 30,000 to 240,000 of the a_j coefficients are required to adequately represent the solution $C_2(r,z)$, depending on the cell turnover rate. The eigenfunction $J_0(\lambda_j r)$ is orthogonal in the region $0<r<\xi$, and the eigenvalues λ_j, which are the roots of the eigenfunction $J_1(\lambda_j \xi)=0$, j=1,2,3,---, are approximately equal to $j\pi/\xi$. The wave length of $J_0(\lambda_j r)$ is $2\pi/\lambda_j = 2\xi/j$, and the solution first senses the presence of the junction when the wavelength of the lowest order eigenmode describing the junction satisfies $2\xi/j = \varepsilon' = R_2 - R_1$, or $j=2\xi/\varepsilon'$. Furthermore, if one lets

$\emptyset$ represent the cell turnover ratio, for example $\emptyset$ = 1 percent represents one damaged cell or one leaky junction out of every one hundred endothelial cells, then the radius ξ of the model unit cell is related to $\emptyset$ as $\emptyset = R_2^2/\xi$. Therefore, $\xi = R_2/\sqrt{\emptyset}$, and $j = 2R_2/\varepsilon'\sqrt{\emptyset}$. Using an endothelial cell length (for pig aorta) or 30μm (Caplan and Schwartz, 1973), a leaky junction width of 200Å (0.02μm), and arterial wall thickness L, the critical number of the a_j terms needed (lowest order eigenmode) for $\emptyset$ = 1 percent are therefore, $j = (2 \times 15/L/(\sqrt{0.01} \times 0.02/L) = 15000$. However, four or more higher order eigenmodes are required for satisfactory conversion of the series in the solution. Thus, about 60,000 a_j coefficients are necessary. Similarly, for $\emptyset$ = 0.1 percent and considering only the first four eigenmodes for the junctional region, 190,000 of the a_j are required in the series solution (Equation 13).

The number of the a_j coefficients required in the series solution is related inversely to the turnover rate, and small turnover rates ($\emptyset \leq 1\%$) are of most physiological interest. Therefore, to determine the a_j coefficients it would be necessary to invert huge (j by j) matrices which would require long computation times and a very large computer space (at least 10^9 K), easily exceeding the capacity of the computer (IBM 4341). Thus we would like to develop a double orthogonalization technique which is able to pick out the structure of both variations in length scale of the periodic cell spacing and the much smaller junctional scale. We proceed with the new solution technique which is described as follows. At z = 1, we require that

$$\frac{\partial C_2}{\partial z}(r,1) + \sigma C_2(r,1) = f(r), \qquad R_1 < r < R_2 \quad (14)$$

where f(r) is an unknown function. f(r) can easily be shown to be the unknown local flux in $R_1<r<R_2$ if one writes

$$C_2 = c - C_1 \quad (15)$$

and then substitutes (15) in (14)

$$\frac{\partial c}{\partial z}(r,1) + c(r,1) - \frac{\sigma}{1+\sigma} - \frac{\sigma}{1+\sigma} = f(r) \qquad R_1 < r < R_2 \tag{16}$$

However, $c(r,1) = 1$ for $R_1<r<R_2$; therefore,

$$\frac{\partial c}{\partial z}(r,1) = f(r) \tag{17}$$

indicating that $f(r)$ is the local flux at $z = 1$, in $R_1<r<R_2$.

To determine the a_j coefficients in terms of $f(r)$, we first evaluate (10) using (13) and then apply (14) to obtain

$$\frac{\partial C_2}{\partial z}(r,1) + \sigma C_2(r,1) = (1+\sigma)a_0 + \sum_{j=1}^{\infty} a_j[\lambda_j \cosh\lambda_j + \sigma \sinh\lambda_j] J_0(\lambda_j r)$$

$$= \begin{cases} 0 & 0<r<R_1,\ R_2<r<\xi \qquad (18a) \\ f(r) & R_1<r<R_2 \qquad (18b) \end{cases}$$

Then, using the orthogonality of $J_0(\lambda_j r)$ in the region $0<r<\xi$ and using (18) we obtain the following expressions for the a_j coefficients in terms of the unknown flux function $f(r)$

$$a_0 = \frac{1}{1+\sigma}\,\frac{2}{\xi^2} \cdot \int_{R_1}^{R_2} r' f(r')\,dr' \tag{19}$$

$$a_j = \frac{2}{\lambda_j \cosh\lambda_j + \sigma \sinh\lambda_j} \cdot \frac{1}{\xi^2 J_0^{\,2}(\lambda_j \xi)} \cdot \int_{R_1}^{R_2} r' f(r') J_0(\lambda_j r)\,dr' \tag{20}$$

$$j = 1,2,3,---$$

Substituting Equations (19) and (20) in (13) gives

$$C_2(r,z) = \frac{z}{1+\sigma}\frac{2}{\xi^2}\int_{R_1}^{R_2} r'f(r')dr' + \frac{2}{\xi^2}\sum_{j=1}^{\infty}\frac{\sinh(\lambda_j z)}{\lambda_j\cosh\lambda_j+\sigma\sinh\lambda_j}\frac{J_0(\lambda_j r)}{J_0^2(\lambda_j\xi)}\int_{R_1}^{R_2} r'f(r')J_0(\lambda_j r')dr' \tag{21}$$

Thus (21) satisfies boundary condition (10) exactly regardless of the functional representation of f(r). For this series representation (21) to also satisfy boundary condition (9), we multiply through by a Kernel solution function Kn(r), which is general enough to represent any solution function in the region R_1 to R_2 and can also be integrated when multiplied by the J_0 eigenfunction. Integrating this result from R_1 to R_2 and rearranging, one obtains

$$\frac{1}{1+\sigma}\left[1 - \frac{2}{\xi^2}\int_{R_1}^{R_2} r'f(r')dr'\right]\int_{R_1}^{R_2} Kn(r') = \frac{2}{\xi^2}\sum_{j=1}^{\infty}\frac{1}{(\sigma+\lambda_j/\tanh\lambda_j)J_0^2(\lambda_j\xi)} \cdot \int_{R_1}^{R_2} r'f(r')J_0(\lambda_j r')dr' \cdot \int_{R_1}^{R_2} Kn(r')J_0(\lambda_j r)dr' \tag{22}$$

In Equation (22), there are two integrals of interest; one consists of $f(r)\cdot J_0$ and the other consists of $Kn(r)\cdot J_0$. We seek a functional representation of f(r) and Kn(r) that is integrable when multiplied by J_0 and satisfies an appropriate Sturm-Liouville problem at the end points R_1 and R_2. To accomplish this we choose a general series representation for the flux f(r) of the form

$$f(r) = D_0 + \sum_{j=1}^{\infty}[D_m J_0(\alpha_m r) + E_m Y_0(\alpha_m r)] \tag{23}$$

where Y_0 is Bessel function of the second kind of order zero. We next need to define an appropriate Sturm-Liouville problem for the flux which is orthogonal (Hildebrand, 1962) on the interval $R_1<r<R_2$. However, in the present model, neither f(r) nor df(r)/dr vanish at the end points (R_1,R_2). Therefore, in order to ensure that the f(r) provides a general representation of the flux f(r) for $R_1<r<R_2$, the series representation (23) is made orthogonal in a slightly bigger integration interval $R_1 - \Delta r$ and $R_2 + \Delta r$, by satisfying the artificial conditions

$$\text{at } r = R^- = R_1 - \Delta r, \quad \frac{df(r)}{dr} = 0 \tag{24}$$

$$\text{and at } r = R^+ = R_2 + \Delta r, \quad \frac{df(r)}{dr} = 0 \tag{25}$$

Here Δr is a small non-zero ($\Delta r << \varepsilon'$) length used to guarantee that the eigenfunctions in (23) provide a proper representation of the function f(r) at the end points $r = R_1$, and $r = R_2$ despite the artificial boundary conditions imposed to make the eigenfunctions orthogonal.

Using (24) in (23) gives

$$f(r) = D_0 + \sum_{m=1}^{\infty} D_m \left[J_0(\alpha_m r) - \frac{J_1(\alpha_m R^-)}{Y_1(\alpha_m R^-)} Y_0(\alpha_m r)\right] \tag{26}$$

and (25) in (26) gives

$$- J_1(\alpha_m R^+) + \frac{J_1(\alpha_m R^-)}{Y_1(\alpha_m R^-)} Y_1(\alpha_m R^+) = 0 \tag{27}$$

in which the D_m are unknown constants still to be determined and the α_m are eigenvalues obtained from the roots of the eigenfunction equation (27).

Having derived a suitable representation for f(r), Equations (26) and (27), we next will choose a Kernel

function Kn(r) with the following properties: (1) it is general enough to represent any function in the interval $R_1<r<R_2$, (2) is integrable when multiplied by the J_0 function, and (3) enables the generation of n linearly independent equations to determine the unknown D_m, m = 0,1,2---, coefficients in (26). A convenient form of the Kernel solution function with the above properties is

$$Kn(r) = \begin{cases} r & n = 0 \qquad (28a) \\ r\left[J_o(\alpha_n r) - \dfrac{J_1(\alpha_n \bar{R})}{Y_1(\alpha_n \bar{R})} Y_0(\alpha_n r)\right] & \qquad (28b) \end{cases}$$

Substituting (26) and (28) in (22), performing the necessary integration and rearranging gives

$$D_0 \left\{ \frac{\bar{R}_2^2}{1+\sigma} + \sum_{j=1}^{\infty} f_7 \left[\frac{R_2 J_1(\lambda_j R_2) - R_1 J_1(\lambda_j R_1)}{\lambda_j}\right]^2 \right\} +$$

$$\sum_{m=1}^{\infty} D_m \left\{ \frac{\bar{R} f_1}{1+\sigma} + \sum_{j=1}^{\infty} f_7 (f_3 - f_4) \cdot \frac{R_2 J_1(\lambda_j R_2) - R_1 J_1(\lambda_j R_1)}{\lambda_j} \right\}$$

$$= \frac{\bar{R}\xi^2}{2(1+\sigma)} \quad , \text{ for } n = 0 \qquad (29)$$

and

$$D_0 \left\{ \frac{\bar{R} f_2}{1+\sigma} + \sum_{j=1}^{\infty} f_7 (f_4 - f_6) \cdot \frac{R_2 J_1(\lambda_j R_2) - R_1 J_1(\lambda_j R_2)}{\lambda_j} \right\} +$$

$$\sum_{m=1}^{\infty} D_m \left\{ \frac{f_1 f_2}{1+\sigma} + \sum_{j=1}^{\infty} f_7 (f_3 - f_4) \cdot (f_5 - f_6) \right\} = \frac{f_2 \xi^2}{2(1+\sigma)} \qquad (30)$$

for n>0

The definitions of $\bar{R}$, f_1 to f_7 and details of the required steps are given in the Appendix.

From Equations (29) and (30), for every value of n, a linearly independent equation is obtained. If the infinite series indexed by j is truncated at some large number j, and the m series is truncated at some number where m = n, a system of (m + 1) linear algebraic equations are obtained for the unknown coefficients D_m, m = 0,1,2,---,m. The coefficient matrix of the system of equations may be solved for the D_m coefficients via standard matrix reduction techniques.

Applying (26) in (19) and (20) and integrating gives

$$a_0 = \frac{2\bar{R}}{1+\sigma} D_0 + \left(\frac{2}{1+\sigma}\right) \frac{1}{\xi^2} \sum_{m=1}^{\infty} D_m f_1 \tag{31}$$

$$a_j = \frac{2}{\lambda_j \cosh\lambda_j + \sigma \sinh\lambda_j} \frac{1}{\xi^2 J_0^2(\lambda_j \xi)} \cdot \left\{ D_0 \frac{R_2 J_1(\lambda_j R_2) - R_1 J_1(\lambda_j R_1)}{\lambda_j} + \sum_{m}^{\infty} D_m (f_3 - f_4) \right\} \tag{32}$$

In (32), when the index j is large, the hyperbolic functions become very large and the a_j coefficients approach zero. This leads to overflow problems with the computer. This problem is remedied by redefining the a_j as

$$A_j = a_j \sinh\lambda_j \tag{33}$$

This completes the solution of the concentration distribution which is given as the sum of $C_1(z)$ and $C_2(r,z)$.

The average axial flux across any plane in the arterial media is defined by

$$\psi = \frac{2\pi}{\pi\xi^2} \int_0^{\xi} \frac{\partial c}{\partial z} \, r dr \tag{34}$$

In the absence of endothelial damage of leaky junctions, i.e., the case where the endothelium is intact

$$\psi_i = \frac{\sigma}{1+\sigma} \tag{35}$$

whereas with damage(s) or leaky junctions

$$\psi = \frac{\sigma}{1+\sigma} + a_0 \tag{36}$$

Similarly, the total uptake of macromolecules per unit volume is

$$u = \frac{2\pi}{\pi\xi^2}\int_0^1\int_0^\xi crdrdz \tag{37}$$

For an intact endothelium

$$U = \frac{1}{2}\,\frac{\sigma}{1+\sigma} \tag{38}$$

whereas with damage(s) or leaky junctions

$$U = \frac{1}{2}\,(\frac{\sigma}{1+\sigma} + a_0) \tag{39}$$

Here again, as was shown for the single damage (Nir and Pfeffer, 1979) and the periodic model (Pfeffer et al., 1981), the flux and the uptake depend only on the leading coefficient a_0, and differ only by a factor of a 1/2.

B. Summary of Formulation

To summarize the special features of the method of solution described above, first, the total concentration was given as a superposition of two solutions, one for intact endothelium and the other to account for the leaky junctions. The solution (13) which accounts for the presence of the leaky junctions (or endothelial injuries) requires the evaluation of thousands or hundreds of thousands of the a_j coefficients which involves the inversion of matrices beyond the capability of our computational equipment (IBM 4341). Second, a flux function f(r) is introduced which is a local series valid in the junctional space. To ensure that f(r) correctly represents the solution in the junction, we required that its orthogonality properties be satisfied in the region $R_1<r<R_2$. Thus, f(r) coupled with the Kernel

solution $K_n(r)$ provides a small matrix for the unknown D_m in (26) at every leaky junction. In this manner we have devised a method of locally amplifying the overall solution in an otherwise unnoticed space. Furthermore, this representation reduces the extremely large matrix that would have been generated for the unknown a_j coefficients to a simple summation. Consequently, the computer space and time requirements are markedly reduced, making the solution feasible. The above solution is exact, and is valid for any endothelial damage size and any number of leaky junctions.

4. NUMERICAL RESULTS AND DISCUSSIONS

In determining the flux, uptake and concentration profiles of the macromolecules in the arterial wall, the analytical model described above required only a small number of terms in the m series ($m = n \leqslant 21$), for accurate convergance for the entire range of the cell turnover rates of interest. However, as indicated earlier, a very large number of terms are required in the j series ($j > 30{,}000$), especially for small turnover rates like 0.1 percent ($j > 100{,}000$). But, since the j terms enter the solution in the form of a summation, this presents no difficulty.

The principle results of the model are shown in Figure 6, which is a plot of the ratio of the steady state flux (ψ/ψ_i), for a damaged to an intact endothelial cell layer, as a function of cell turnover rate and a leaky junction width of 200Å (lower curve). In preparing the figure, a Biot number of 0.2, endothelial cell length of 30μm (Caplan and Schwartz, 1973) and arterial media thickness of 1 mm have been assumed. Figure 6 also predicts the ratio of the uptake in the artery wall, since in the steady state the uptake and flux ratios are equal to one another. For very small $\emptyset$, the results approach the behavior of an intact endothelium, and for larger $\emptyset$, the results approach that of a completely denuded endothelium. It is interesting to note that as the number of damaged cells or turnover rate increases from 1/1000 to 5/1000, the flux or the uptake ratio increases roughly by 67 percent, clearly indicating the rate controlling effect of the endothelial cell monolayer. Thus large changes in the equilibrium balance of the cholesterol carrying LDL molecules in the arterial wall can occur for very small cell turnover rates due to a small fraction of leaky junctions.

Also shown in Figure 6 (dashed curve) are the results from the previous model reported in Pfeffer et al. (1981) in which the dying endothelial cell was treated as an open

hole. In the present model, with a junctional width of 200Å, the exposed area of the intercellular cleft is less than 0.1 percent of the surface area of a single dying cell. Thus, the area of the leaky junction is less than 10^{-5} of the endothelial surface when $\emptyset < 1$ percent. The closeness of the results obtained from the model assuming leaky junctions and the model assuming holes, shows that the transport rate of an artery wall of 1 mm thickness and specified cell turnover rate, is largely controlled by the perimeter of the dying cell rather than its area. Since the endothelium is the main barrier to the transarterial transport of macromolecules, the above findings are not very sensitive to changes in arterial wall thickness.

A deeper insight into the mechanism by which a small fraction of damaged cells can effectively destroy the diffusional resistance of the endothelium can be obtained by examining the radial concentration profiles in Figures 7a and 7b, which are for $\emptyset = 3$ percent and $\emptyset = 1$ percent respectively. Due to the small dimensions of the leaky junctions, steep concentration gradients are found only in the vicinity of the leaky junctions, but the radial spread of macromolecules is very large and is nearly independent of r away from the damage. The solution for an intercellular cleft width of 100Å is nearly indistinguishable from the 200Å solution shown, indicating that the transport rate is relatively insensitive to the width of the intercellular cleft provided its dimensions are sufficiently large to permit the rapid passage of the diffusing molecule.

Bell et al. (1974a), reported the experimental finding of a 66 percent increase in albumin influx rate in the Evans blue stained area of a pig aorta as compared to the unstained or white area. And, Gerrity et al. (1977) reported that, using silver nitrate staining, the frequency of cell turnover was found to be 2.91 percent in the blue area as compared to 0.7 percent in the white area. Interpreting the above

finding as the ratio of fluxes $(\psi/\psi_i)_{\phi blue}/(\psi/\psi_i)_{\phi white}$ and then referring to Figure 6, it is found that $(\psi/\psi_i)_{\phi=0.03}/(\psi/\psi_i)_{\phi=0.007} = 1.76$ or a 76 percent increase. Hence, it appears that the leaky junction cell turnover hypothesis is not only a qualitatively reasonable explanation of the increased uptake found in certain focal regions of the arterial tree, but also is in favorable quantitative agreement with experimental physiological results. For the reasons mentioned earlier rigorous numerical comparisons between theory and experiment have to be viewed cautiously, both because of the simplifications introduced in the model and the uncertainty of the silver nitrate staining procedure as a reliable index of cell turnover. The results of the model show, however, that even if the lower cell turnover statistics obtained from the thymidine labelling technique are used, the proposed leaky junction mechanism is still quantitatively feasible. At present there is no clearly defined experiment which shows that the intercellular junctions of dying or newly formed endothelial cells are leaky to macromolecules while the junctions of their normal neighboring cells are not. Double labelling techniques are currently being developed by our colleagues S. Chien and A. Baldwin to see if this basic supposition can be documented.

5. REFERENCES

Adams, C.W.M., Virag, S., Morgan, R.S. and Orken, C.C., (1968) J. Athero. Res. 8, 679.

Adams, C.W.M., Morgan, R.S. and Bayliss, O.B (1970), Athero. 11, 119.

Arminski, L., Weinbaum, S. and Pfeffer, R. (1980), J. Theor. Biol. 85, 13.

Bell, F.P., Adamson, T.L. and Schwartz, C.J. (1974a), Exp. Mol. Path. 20, 57.

Bell, F.P., Gallus, A.S. and Schwartz, C.J. (1974b), Exp. Mol. Path. 20, 281.

Bratzler, R.L., Colton, C.K. and Smith, V.A. (1977), in G.W. Manning and M.D. Haust Atherosclerosis: Metabolic, Morphologic and Clinical Aspects, Plenum Press, New York, pp. 943.

Caplan, B.A. and Schwartz, C.J. (1973), Atherosclerosis 17, 401.

Casley-Smith, J.R. and Chin, J.C (1971), Microscopy 93, 167.

Chien, S. and Weinbaum, S. (1981), ASME J. Biomech. Eng., 103, 176.

Clough, G. and Michel, C.C. (1981), J. Physiol. 315, 127.

DeBruijn, W.L., Van Naurik, W. and Basveld, I.J. (1974), J. Cell. Sci. 16, 221.

Gerrity, R.G., Richardson, M., Somer, J.B., Bell, F.B. and Schwartz, C.J. (1977), J. Amer. Path. 99, 131.

Hildebrand, F.B. (1962), "Advanced Calculus for Applications", Prentice-Hall, Inc., New Jersey, 2nd Ed., pp. 208.

Loudon, M.F., Michel, C.C. and White, I.F., J. Physiol. 296, 97.

Lezczynski, D.E. and Kummenow, F.A. (1981), J. Biomech. 14, 307.

Nir, A. and Pfeffer, R. (1979), J. Theor. Biol. 81, 685.

Oko, S. (1979), Biorheology 16, 2-3.

Palade, G.E. (1953), J. Appl. Phys. 24, 1424.

Pfeffer, R., Ganatos, P., Nir, A. and Weinbaum, S. (1981), ASME J. Biomech. Eng. 103, 197.

Schwartz, C.J., Bell, F.P., Somer, J.B. and Gerrity, R. (1974), Proc. of NSF Specialists Meetings of Fluid Dynamic Aspects of Arterial Disease, Ohio State Univ., 46.

Schwartz, S.M., Gajdusek, C.M. and Seldon, S.C., III (1981) Atherosclerosis 1, No. 1.

Simionescu, N., Simionescu, M. and Palade, G.E. (1973), J. Cell Biol. 54, 434.

Weinbaum, S. and Caro, C.G. (1976), J. Fluid 74, 611.

Weinbaum, S. and Chien, S. (1980), Mathematics of Microcirculation Phenomena, Eds., J.F. Gross and A. Papel, Raven Press, New York, 109-131.

6. APPENDIX

The procedure used to evaluate the integrals in (22) and consequently determine the D_m=0,1,2,---, and the A_j, j =0,1,2,---, coefficients is as follows: substitute the series representations of the junctional flux, Equation (26), and of the Kernal solution, Equation (28), in (22)

$$\frac{1}{1+\sigma}\left\{1 - \frac{2}{\xi^2}\int_{R_1}^{R_2} r'\left[D_0+\sum_{m=1}^{\infty} D_m\left[J_0(\alpha_m r') - T_m Y_0(\alpha_m r')\right]\right]dr'\right\}$$

$$\cdot \int_{R_1}^{R_2} r[1+J_0(\alpha_n r') - T_n Y_0(\alpha_n r']dr =$$

$$\frac{2}{\xi^2}\sum_{j=1}^{\infty}\int_{R_1}^{R_2} r'\left[D_0+\sum_{m=1}^{\infty} D_m\left[J_0(\alpha_m r') - T_m Y_0(\alpha_m r')\right]\right]J_0(\lambda_j r)dr'$$

$$\cdot \int_{R_1}^{R_2} r'[1+J_0(\alpha_n r') - T_n Y_0(\alpha_n r')]J_0(\lambda_j r)dr' \qquad (A.1)$$

where $T_m = \dfrac{J_1(\alpha_m R^-)}{Y_1(\alpha_m R^-)}$ and $T_n = \dfrac{J_1(\alpha_n R^-)}{Y_0(\alpha_n R^-)}$

We now define the following functions:

$$f_1 = f_1(m) = \int_{R_1}^{R_2} [J_0(\alpha_m r') - T_m Y_0(\alpha_m r')]r'dr'$$

$$= \left\{r' \frac{J_1(\alpha_m r')}{\alpha_m} - T_m r' \frac{Y_1(\alpha_m r')}{\alpha_m}\right\}\Bigg|_{R_1}^{R_2} \qquad (A.2)$$

$f_2 = f_2(n) = f_1(m)$, i.e., replace m by n in (A.2) (A.3)

$$f_3 = f_3(m,j) = \int_{R_1}^{R_2} r' J_0(\alpha_m r') J_0(\lambda_j r') dr'$$

$$= \left\{ -r' \frac{\lambda_j J_0(\alpha_m r') J_1(\lambda_j r') + r' \alpha_m J_1(\alpha_m r') J_0(\lambda_j r')}{\alpha_m^2 - \lambda_j^2} \right\} \Bigg|_{R_1}^{R_2} \quad (A.4)$$

$$f_4 = f_4(m,j) = T_m \int_{R_1}^{R_2} r' Y_0(\alpha_m r') J_0(\lambda_j r') dr'$$

$$= \left\{ -r \frac{\lambda_j Y_0(\alpha_m r') J_1(\lambda_1 r) + r' \alpha_m Y_1(\alpha_m r') J_0(\lambda_j r')}{\alpha_m^2 - \lambda_j^2} \right\} \Bigg|_{R_1}^{R_2} \quad (A.5)$$

$f_5 = f_5(n,j) = f_3(m,j)$, i.e., replace m by n in (A.4) (A.6)

$f_6 = f_6(n,j) = f_4(m,j)$, i.e., replace m by n in (A.5) (A.7)

and

$$f_7 = \frac{1}{\sigma + \lambda_j / \tanh \lambda_j} \frac{1}{J_0^2(\lambda_j \xi)} \quad (A.8)$$

Note that all the integrals appearing in equation (A.1) can be evaluated analytically. Thus, for the case where n = 0, Equation (A.1) gives

$$\frac{1}{1+\sigma}\left(\frac{R_2^2 - R_1^2}{2}\right) - \frac{2}{(1+\sigma)\xi^2}\left[\frac{R_1^2 - R_1^2}{2}\right]^2 D_0 - \frac{2}{(1+\sigma)\xi^2} \sum_{m=1}^{\infty} D_m f_1 \left(\frac{R_2^2 - R_1^2}{2}\right)$$

$$= \frac{2}{\xi^2} \sum_{j=1}^{\infty} f_7 D_0 \cdot \left[r' \frac{J_1(\lambda_j r')}{\lambda_j} \Bigg|_{R_1}^{R_2} \right]^2 + \frac{2}{\xi^2} \sum_{j=1}^{\infty} f_7 \sum_{m=1} (f_3 - f_4)$$

$$\cdot \left(r' \frac{J_1(\lambda_j r')}{\lambda_j} \Bigg|_{R_1}^{R_2} \right) \quad (A.9)$$

rearranging (A.9) yields

$$D_0\left\{\frac{\bar{R}^2}{1+\sigma}+\sum_{j=1}^{\infty} f_7\left[\frac{R_2J_1(\lambda_jR_2)-R_1J_1R_1(\lambda_jR_2)}{\lambda_j}\right]^2\right\}+$$

$$\sum_{m=1}^{\infty} D_m\left\{\frac{\bar{R}f_1}{1+\sigma}+\sum_{j=1}^{\infty} f_7(f_3-f_4)\cdot\frac{R_2J_1(\lambda_jR_2)-R_1J_1(\lambda_jR_1)}{\lambda_j}\right\}$$

$$=\frac{\bar{R}\,\xi^2}{2(1+\sigma)} \qquad \text{(A.10)}$$

$$\text{where } \bar{R}=\frac{R_2^2-R_1^2}{2}$$

Similarly for n > 0, performing the necessary integrations and rearranging gives

$$D_0\left\{\frac{\bar{R}f_2}{1+\sigma}+\sum_{j=1}^{\infty} f_7(f_5-f_6)\cdot[R_2J_1(\lambda_jR_2)-R_1J_1(\lambda_jR_1)]\right\}+$$

$$\sum_{m=1}^{\infty} D_m\left\{\frac{f_1f_2}{1+\sigma}+\sum_{j=1}^{\infty} f_7(f_3-f_4)(f_5-f_6)\right\}=\frac{f_2\xi^2}{2(1+\sigma)} \qquad \text{(A.11)}$$

For every value of n, a linearly independent equation for the D_m coefficients is obtained from (A.10) and (A.11). The matrix of D_m coefficients associated with the n independent equations may be solved for the D_m coefficients via standard matrix reduction methods. Because of the relationship in the series forms that were assumed for f(r) and $K_n(r)$, the D_m coefficient matrix is symmetric. This symmetry will further reduce the required computation time.

Once the D_m coefficients are known, the A_j coefficients can be easily determined by substituting the D_m in (31) and (32).

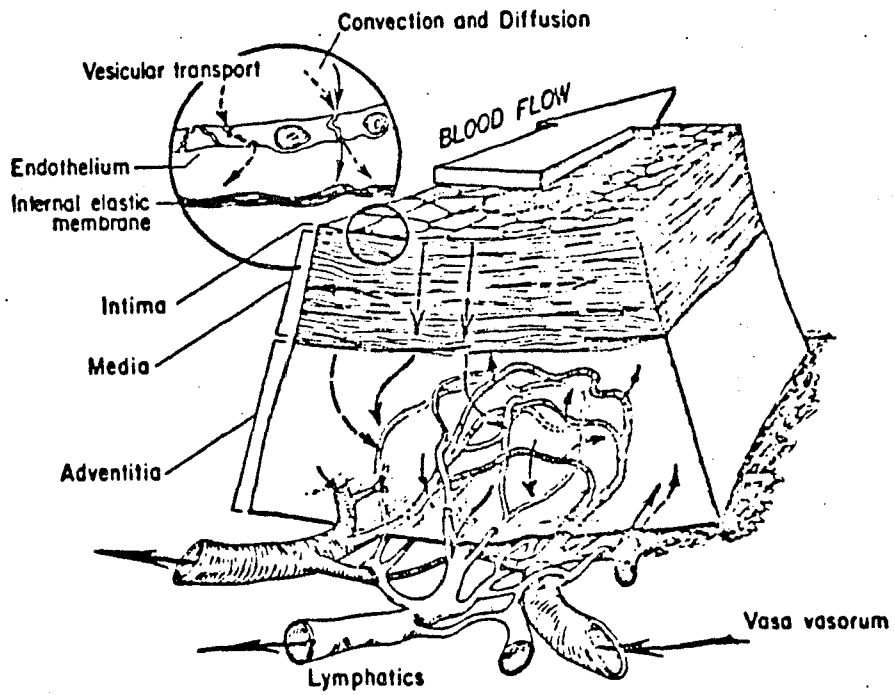

Figure 1. Conceptual illustration of the three distinct layers in a typical mammalian artery (courtesy of Bratzler et al., 1975).

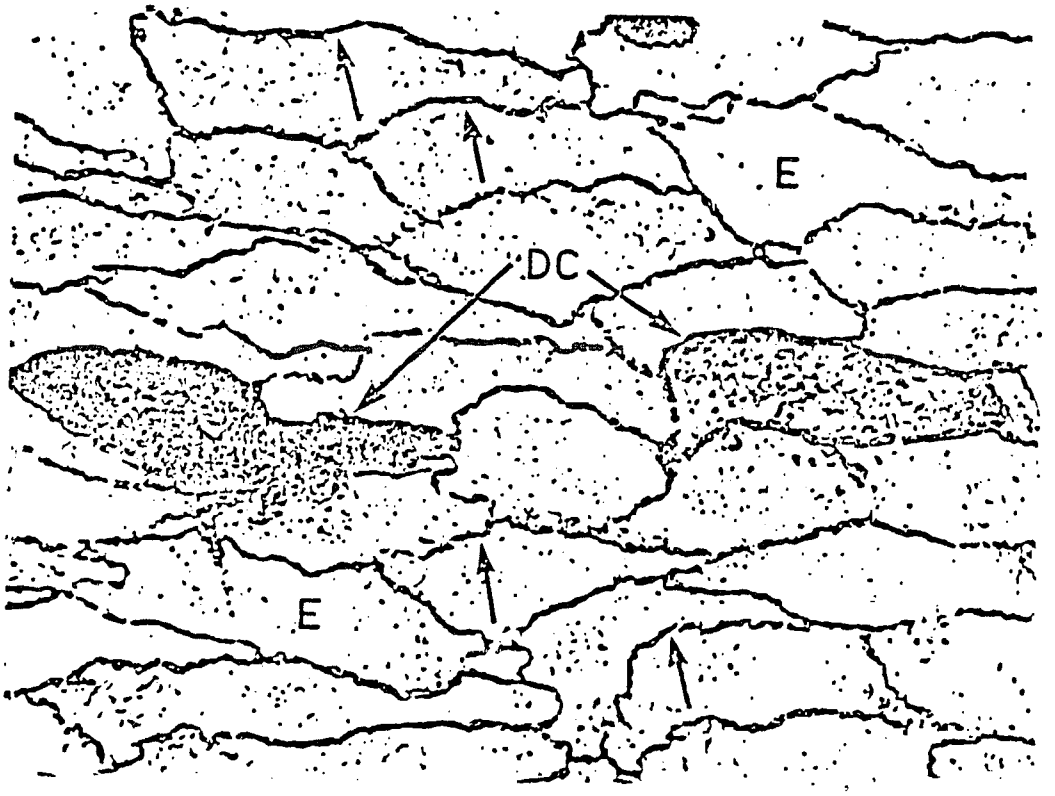

Figure 2. Light micrograph of silver-stained endothelial cells; injured and dead cells show intense uptake of silver stain (courtesy of Gerrity et al.,1977)

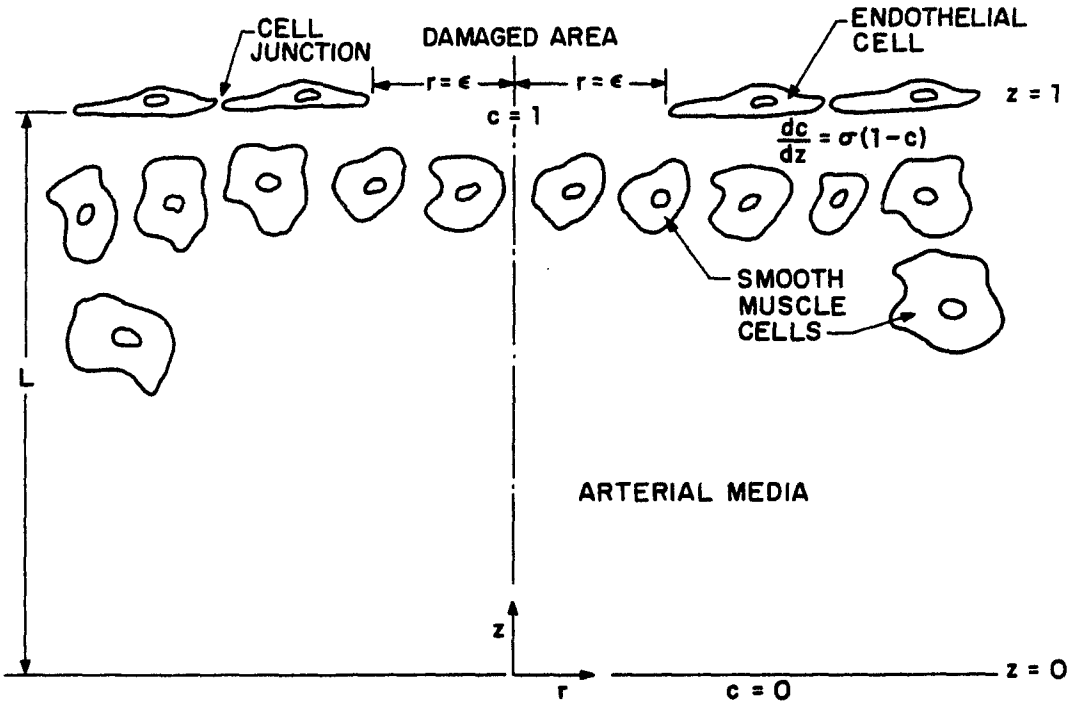

Figure 3. Schematic diagram of arterial wall with local endothelial damage (cells not drawn to scale).

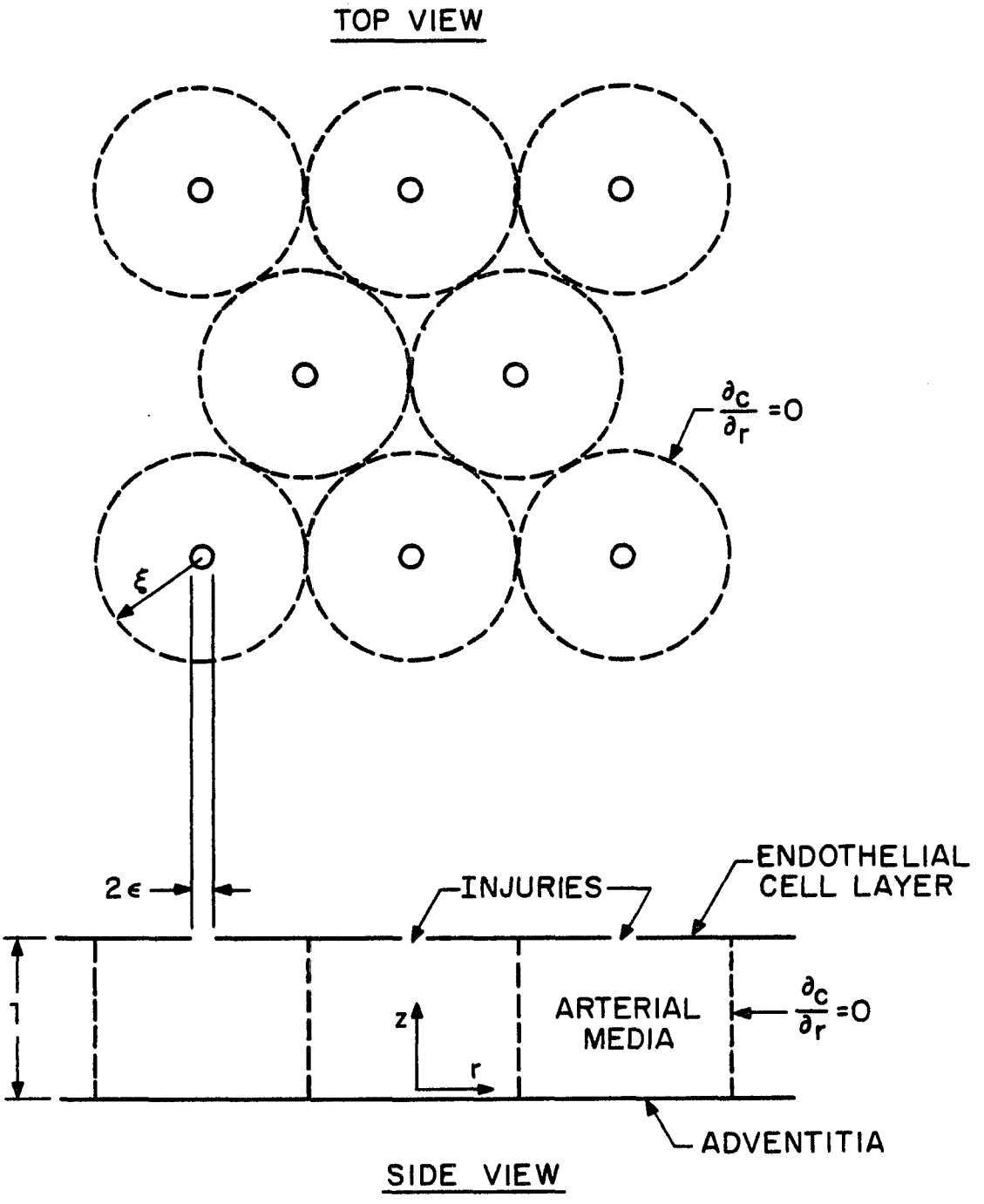

Figure 4. Schematic diagram of mathematically idealized model of artery wall with periodically distributed dying endothelial cells.

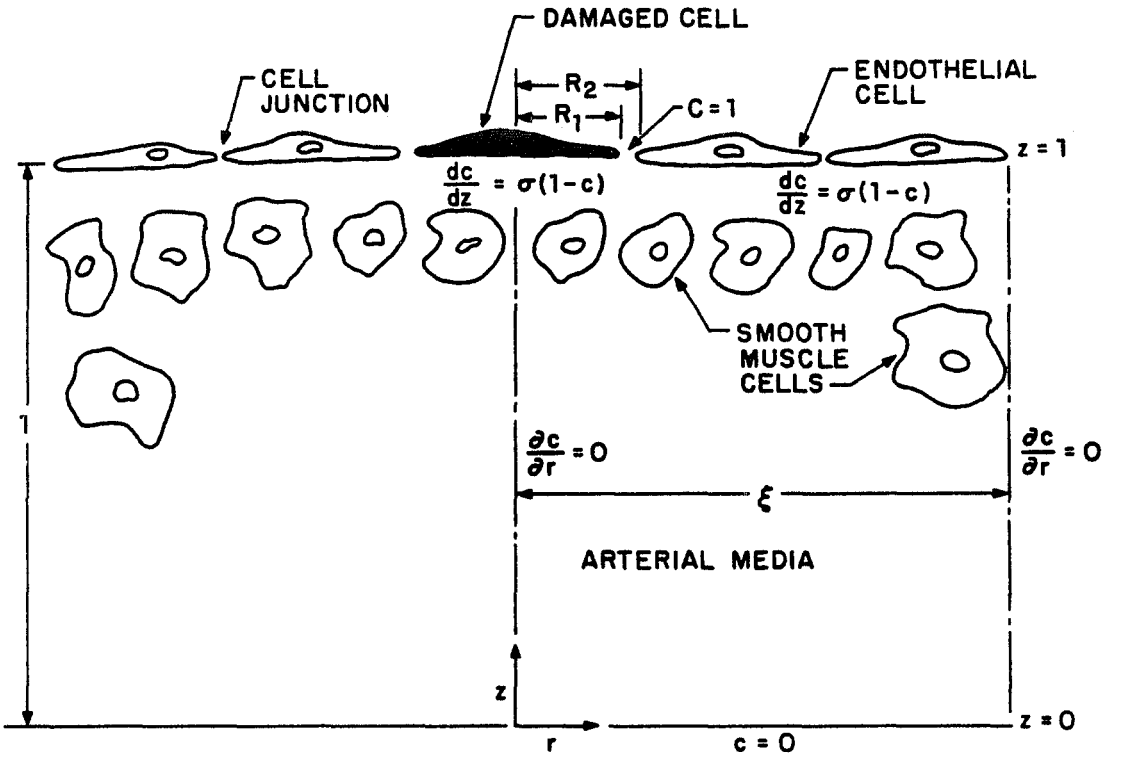

Figure 5. Schematic diagram of a unit cell in a periodic model artery for case where dying cell (shown in black) becomes leaky to macromolecules only through its junctional complex.

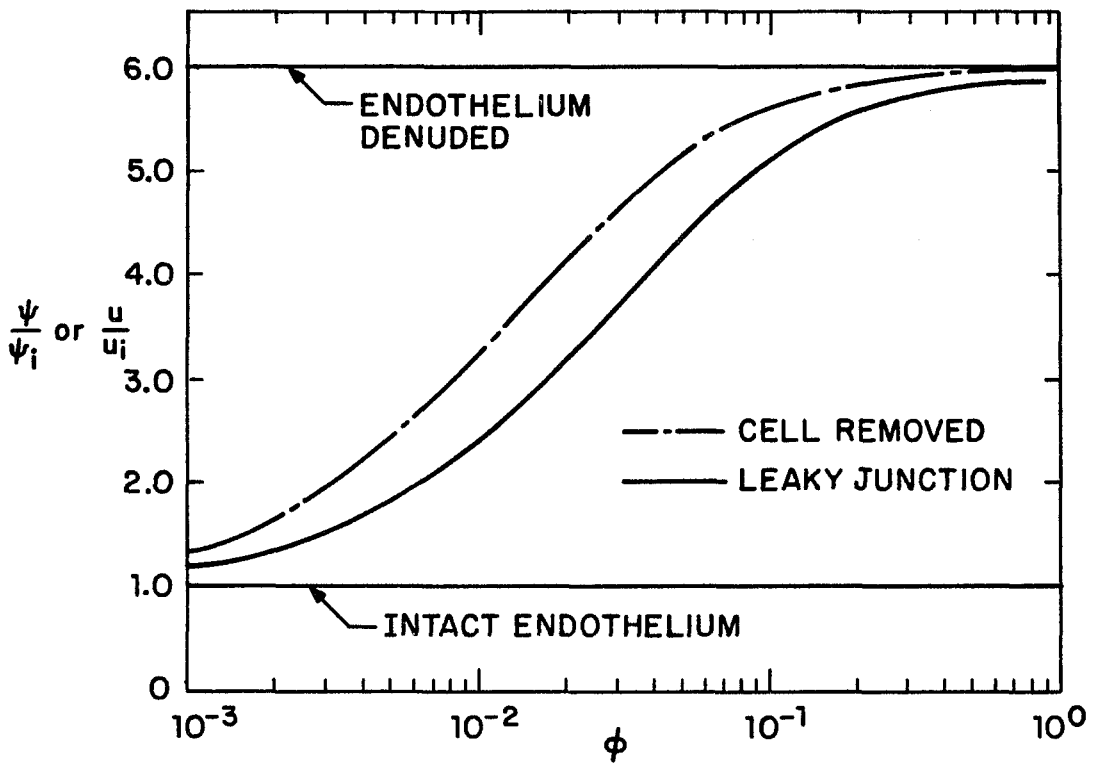

Figure 6. Relative enhancement of flux or uptake as a function of cell turnover for the leaky junction model; width of intercellular junction 200Å, wall thickness 1mm. Dashed curve represents equivalent results if entire endothelial cell is removed.

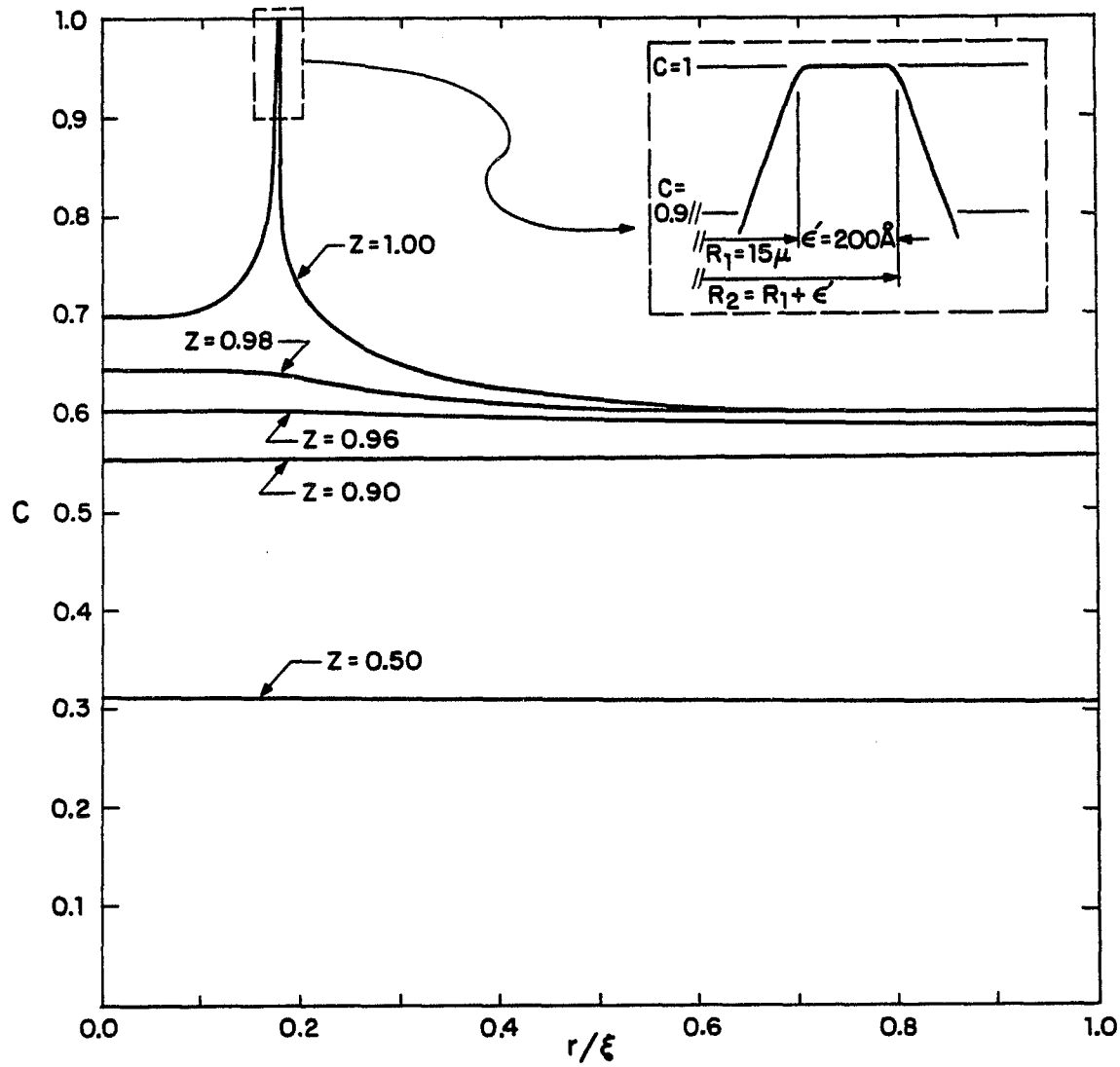

Figure 7a. Radial concentration profiles for case where dying cell is permeable to macromolecules only through its junctional complex; $\sigma = 0.2$, $\phi = 0.03$.

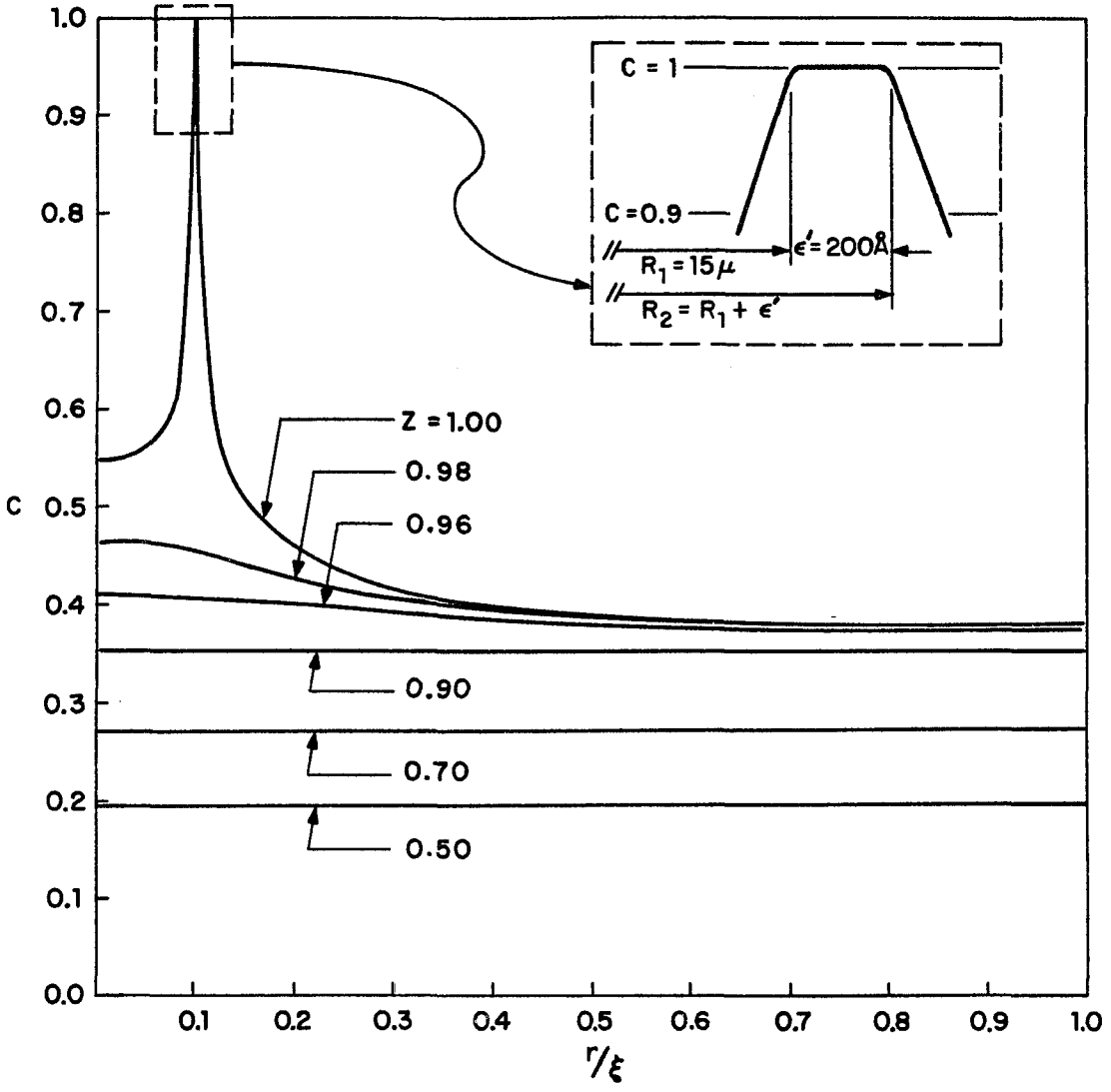

Figure 7b. Radial concentration profile for case where dying cell is permeable to macromolecules only through its junctional complex; $\sigma = 0.2$, $\phi = 0.01$.

CHAPTER III

THEORETICAL MODEL FOR THE STEADY STATE WATER MOVEMENT AND PRESSURE DISTRIBUTION IN SMALL AND LARGE VESSELS

SUMMARY

It is now generally accepted that the intercellular cleft between adjacent endothelial cells is the primary pathway for the transluminal movement of water and small ions in the vasculature. A steady state theoretical model has been developed to show quantitatively how the geometry of the intercellular cleft between adjacent endothelial cells is related to both the water movement and pressure distribution in the subendothelial space and to examine how the existence of a subendothelial interaction layer affects the hydraulic resistance of the media of vessels of varying wall thickness. The velocity and pressure fields in the media are described using porous matrix theory based on Darcy's law and a lubrication type analysis is used to describe the flow in a variable geometry intercellular cleft. These two equations are solved simultaneously to determine the unknown pressure distribution beneath the endothelium and the flow in the arterial media.

Application of this model shows that, when the tight junction in the cleft is 26Å or less, more than half of the total hydraulic resistance of the wall occurs across the endothelial cell monolayer, for a vessel whose wall thickness is less than 0.02 cm. This finding is in good agreement with the experimental findings of Vargas et al. (1979) for rabbit aorta. Contrary to previous belief, the model shows that the filtration resistance of an arterial wall with intact endothelium does not scale linearly with wall thickness due to the highly non-linear resistance of the endothelial interaction layer.

1. INTRODUCTION

The transmural movement of water across the vasculature provides nutrients, removes wastes and furnishes the fluid for the lymphatic circulation. The movement of water in the arterial wall significantly affects the pressure and mechanical stress distribution in the wall. The flux of lipids, proteins, ions and other small solutes is also influenced by the water movement. While convection in the media is currently thought to play a small role in macromolecule transport in the larger vessels, the water movement could have a significant affect on transport across the endothelium if the filtration pressure could alter the geometry of the intercellular clefts between adjacent endothelial cells.

There is no prior study to the authors knowledge that has theoretically examined the detailed hydraulic interaction between the endothelial channels and the underlying wall tissue, the pressure distribution in the subendothelial space or the dependence of the steady state filtration flow on the geometry of the intercellular channels. In the present study the geometry of the intercellular channels is prescribed. A comparison study is in progress to study the effect of the fluid pressure on the intercellular channel geometry. While the primary interest of the investigators is in transport across large vessels, the theoretical model can be applied down to vessels of approximately 25 μm diameter or roughly 3-5 μm wall thickness. The results for vessels whose wall thickness is between 5 and 150 μm show the existence of an important interaction layer where the hydraulic resistance of the media does not scale linearly with thickness.

Experimental studies by Vargas et al. (1979) on the movement of water across the rabbit aorta due to a steady pressure driving force and the hydraulic conductivity of

the various layers of the wall indicate that as much as one-half of the total transmural pressure drop occurs across the endothelial cell monolayer. This finding is rather surprising considering that the thickness of the endothelial cell layer is less than 1/500 the thickness of the arterial wall media for the larger arteries of most mammals and humans. Vargas et al. (1979) have estimated the magnitude of creep in their experiments and have reported steady state hydraulic conductivity data based on the assumption that the creep can be attributed to the change in the internal radius of the vessel and not the wall volume. Using Kenyon's (1979) consolidation model they show that for 0.02 cm wall thickness, the time required for wall volume consolidation is of the order of one minute. Since their experiments were conducted for 30 minutes, and since they have allowed an initial period of equilibration, the initial consolidation should not affect their steady state measurements. These steady state filtration studies should not be confused with earlier studies by Harrison and Massaro (1976) in which the vessel wall is cut open, layed upon a porous support and the hydraulic permeability measured during the consolidation process.

Two primary pathways have been hypothesized for transendothelial water movement; small hydrophilic pores and the intercellular clefts. The 3-4 Å hydrophilic pores, which are an integral part of the phospholipid bilayer membrane of the endothelial cell, are crucial in the movement of water and small ions into and between (communicating junctions) the endothelial cells themselves. However, this small pore system is of lesser importance in transendothelial water transport than the intercellular junctions because of its much

larger hydraulic resistance. Thus, the hydraulic conductivity of the endothelium principally corresponds to its junctions as suggested by Landis et al. (1964) and Vargas et al. (1979) for capillary and aortic endothelia respectively. Another important experimental observation is that the hydraulic conductivity (Vargas et al., 1964) and cell junction morphology (Huttner et al., 1973) of the aortic and capillary endothelium are very similar in the same species, indicating that models based on larger vessels could provide important insights into some small vessel functions that are otherwise difficult to study due to vessel size limitations.

The above experimental studies provide some insight into the hydraulic resistance of the different layers of the arterial wall. They also provide basic data for constructing a quantitative mathematical model for describing the fine structure of the steady state water movement and pressure distribution in the arterial wall. In the steady state model developed herein, we wish to show quantitatively how the specialized geometry of the intercellular cleft between adjacent endothelial cells is related to both the water movement and pressure distribution in the subendothelial space. We also wish to further examine how the interaction between the water jets issuing from the intercellular channels is related to the hydraulic resistance of the arterial media. The model can be used in addition to obtain an independent estimate of the size of the largest molecules that can pass through normal intercellular junctions in arterial endothelium.

2. MATHEMATICAL MODEL

The vessel wall is treated as a slab of uniform thickness. Figure 1 is a schematic diagram for the mathematical model (not to scale) for pressure filtration across the vessel wall, in which, the top view shows the endothelial cells and the section view shows the endothelial cell monolayer and the vessel media. The driving force for the water movement can either be a colloidal osmotic pressure applied across the junctional complexes of the intercellular cleft or a transmural hydrostatic pressure difference. Since the arrangement of endothelial cells is of the form shown in Figure 1, it appears reasonable to develop a two-dimensional model as shown in section "AA" and to adjust for the small contribution to water movement through the cell ends by using an equivalent spacing between clefts that conserves total cell perimeter. The mathematical boundary value problem for a unit cell in this two-dimensional periodic arrangement is shown in Figure 2. The intercellular clefts are separated by a distanc 2ξ, where $o \leq x \leq \xi$ represents half a unit cell in our model. All lengths have been non-dimensionalized by the thickness of the arterial media L. The endothelium and the media meet at $z=1$, and the media-adventitial interface is at $z=0$. The intercellular space is treated as a parallel channel with a localized constriction of length w which narrows down from 200Å in the parallel channel section to $2\ell_{min}$ in the region frequently called the junctional complex. The length of the intercellular cleft is ℓ. P_1, P_2 and P_3 are the dimensionless pressures in the lumen, in the subendothelial space at the channel exit and in the adventitia respectively. These pressures are defined as $P_i = (\mathbb{P}_i - \mathbb{P}_3)/(\mathbb{P}_1 - \mathbb{P}_3)$, $i = 1,2,3$, where $\mathbb{P}_3$ is the pressure at the media-adventitia interface and $\mathbb{P}_1$ is the lumen pressure. The

important unknown is the steady state pressure distribution in the media and in particular in the subendothelial space at the channel exit. In developing the model, we have divided the problem into three parts: A) A porous media diffusion equation is solved for the pressure field in the media, and then using Darcy's Law, an expression is derived for the volumetric flow across the arterial media in terms of an unknown average pressure $\bar{P}_2$ at the exit of the intercellular channels. B) A second equation is obtained by applying lubrication theory to determine the fluid motion and pressure distribution in an intercellular channel of variable geometry. The pressure drop across the entire channel is then expressed in terms of a parallel wall channel of the same length. C) These equations are then solved simultaneously to determine $\bar{P}_2$. Once $\bar{P}_2$ is known, one can find the flow across the arterial wall and the pressure distribution along the cleft, beneath the endothelium and in the media.

A. Media

We assume in the steady state that the filtration flow obeys Darcy's Law ($\bar{v} = \frac{k}{\mu}\nabla p$) and that the wall is incompressible and thus satisfies the continuity equation ($\nabla \cdot \bar{v} = o$). These conditions require that the pressure distribution in the media be given by:

$$\frac{\partial^2 P}{\partial x^2} + \frac{\partial^2 P}{\partial z^2} = 0 \qquad (1)$$

The relevant boundary conditions in dimensionless form are:

$$P(x,o) = P_3 = 0 \qquad o \le x \le \xi \qquad (2)$$

$$\frac{\partial P}{\partial x}(o,z) = \frac{\partial P}{\partial x}(\xi,z) = 0 \qquad o \le z \le 1 \qquad (3), \ (4)$$

$$\frac{\partial P}{\partial z}(x,1) = \begin{cases} V_2^* & o \le x \le \epsilon \\ o & o < x \le \xi \end{cases} \qquad \begin{matrix} (5a) \\ (5b) \end{matrix}$$

where ϵ is one half of the width of the intercellular channel exit and V_2^* is the dimensionless total fluid velocity which is defined as $V_2^* = V_2 L\mu/K(P_1-P_3)$, in which K is the media conductivity and μ is the viscosity of the flowing fluid. Equation (2) is the boundary condition for the dimensionless steady state pressure distribution at the adventitial surface. The condition that the pressure at the adventitial surface be nearly constant will be approximately satisfied provided the total transmural resistance across the media is large compared to the resistance of the loose connective tissue at the adventitial surface. This is a reasonable approximation for vessels whose wall thickness is greater than 5 μm. The symmetry condition along the centerline of the unit cell is given by equation (3). At the edge of the unit cell, $x=\xi$, we require that the water flux vanish (equation (4)) due to the periodic arrangement of the unit cells. Equation (5) is based on the assumption that there is negligible water movement across the membranes of the endothelial cells and that filtration is due solely to the transendothelial pressure difference, P_1-P_2, across the intercellular clefts.

The formulation of this boundary value problem for the pressure field is similar to that of Kelman (1965) and Keller et al. (1967) for mass transfer across a boundary layer with a perforated interface consisting of a two-dimensional array of cylindrical pores with a prescribed uniform flux. The present problem differs in that the flux is unknown, the geometry is two-dimensional and the channels (pores) have variable geometry. The solution to (1) subject to conditions (2) to (4) is:

$$P(x,z) = B_o z + \sum_{m=1}^{\infty} B_m \sinh(\lambda_m z)\cos(\lambda_m x) \qquad (6)$$

in which, the B_m, m=o,1,2,---coefficients are unknown constants and the λ_m are eigenvalues determined from the roots of $\sin(\lambda_m \xi)$.

To determine the b_m constants, we first apply conditions (5a) and (5b) to (6)

$$\frac{\partial P}{\partial z} = B_o + \sum_{m=1}^{\infty} B_m \lambda_m \cosh(\lambda_m x)$$

$$= \begin{cases} V_2^* & o<x<\epsilon \qquad (7a) \\ o & \epsilon<x<\xi \qquad (7b) \end{cases}$$

Then, using the orthogonality properties of $\cos(\lambda_m x)$ in the interval $o \le x \le \xi$, we obtain the following implicit representations of the constants.

$$B_o = \frac{1}{\xi}\int_o^{\epsilon} V_2^* \, dx = V_2^* \phi \qquad (8a)$$

where $\phi = \epsilon/\xi$ and

$$B_m = \frac{2}{\xi}\frac{V_2^*}{\lambda_m \cosh\lambda_m}\int_o^{\epsilon}\cos(\lambda_m x)dx = \frac{2V_2^*\varphi\sin(\lambda_m \epsilon)}{\epsilon\lambda_m{}^2\cosh\lambda_m} \qquad (8b)$$

Substituting equations (8a) and (8b) in (6) gives the expression for the pressure field, P(x,z), in terms of the unknown channel flux V_2^*. Integrating this expression for the pressure across half the channel exit and and dividing by ϵ gives the average pressure $\bar{P}_2$ at the channel exit,

$$\bar{P}_2(x,1) = \frac{1}{\epsilon}\int_o^{\epsilon} P(x,1)$$

$$= V_2^*\phi\left\{1+\frac{2}{\epsilon^2}\sum_{m=1}^{\infty}\frac{\tanh\lambda_m}{\lambda_m}\left[\frac{\sin(\lambda_m \epsilon)}{\lambda_m}\right]^2\right\} \qquad (9a)$$

Equation (9a) may be denoted simply by:

$$\bar{P}_2 = V_2^* \phi \, Sm \qquad (9b)$$

in which Sm is the quantity in parenthesis in (9a).

B. Intercellular Cleft

The pressure drop in the intercellular channel is the sum of two contributions, one from the section of local constriction and the second from the region outside the constriction. In the later region we have a parallel wall channel with a two-dimensional Poiseuille flow whose average velocity is given by:

$$V = \frac{Q}{A_c} = -\frac{(2\varepsilon_n)^2}{12\mu}\frac{dP}{dz'} \tag{10}$$

where Q is the volumetric flow rate, $2\varepsilon_n$ is channel width and $A_c = y \times 2\varepsilon_n$ is the channel cross sectional area in which y is the distance along the cell perimeter. In the region of constriction, we apply lubrication theory type analysis and express the local velocity as:

$$V = \frac{Q}{y(2\varepsilon(z'))} = \frac{(2\varepsilon(z'))^2}{12\mu}\frac{dp}{dz'} \tag{11}$$

where $\varepsilon(z')$ is the variable channel width. A reasonable parametric representation of the channel geometry based on high magnification electron microscopic observations is the cosine distribution

$$\varepsilon(z') = \left(\frac{\varepsilon_n + \varepsilon_{min}}{2}\right) + \left(\frac{\varepsilon_n - \varepsilon_{min}}{2}\right)\cos\left(\frac{2\pi}{w}\right)z' \tag{12a}$$

Equation (12a) has the simple form:

$$(z') = \quad + b \cos cz' \tag{12b}$$

From (10) and (11) the total pressure drop in the channel is:

$$\Delta P = \frac{12\mu Q}{y}\left[\int_o^w \frac{dz'}{[2\varepsilon(z')]^3} + \int_w^{\ell} \frac{dz'}{[2\varepsilon_n]^3}\right] \tag{13}$$

Evaluating the integrals in equation (13) one obtains:

$$\Delta P = \frac{12\,\mu Q}{y}\left[\frac{w\left(a^2+(b^2)/2\right)}{8\left(a^2-b^2\right)^{5/2}} + \frac{\ell-w}{(2\epsilon_n)^3}\right] \qquad (14a)$$

To compare the relative importance of the pressure drop from the parallel and constricted sections of the cleft, we non-dimensionalize equation (14) with respect to the constriction length w and the minimum width of the junction in the constricted region ϵ_{min},

$$\gamma = 8\Delta P y\,\epsilon_n^3 \,/\, 12\,\mu Q w$$

$$= 8\left(\frac{\epsilon_n}{\epsilon_{min}}\right)^3 \frac{\left[\frac{3}{2}\left(\frac{\epsilon_n}{\epsilon min}\right)^2 + \frac{\epsilon_n}{\epsilon min} + \frac{3}{2}\right]}{\left(4\,\frac{\epsilon_n}{\epsilon_{min}}\right)^{5/2}} + \frac{\ell}{w} - 1 \qquad (14b)$$

Denoting the contribution form the constricted section, i.e., the first term in the right side of Equation (14b) by A and plotting A/γ as a function of $\epsilon_n/\epsilon_{min}$ for various $\ell/_w$ ratios, we obtain the curves shown in figure 3. In the limit of small vessels of capillary size $\ell/_w$ is typically about 5. For the larger vessels considered herein a reasonable range for $\ell/_w$ is $10 \le \ell/_w \le 30$. From Figure 3, it is evident that for $\epsilon_n/\epsilon_{min} > 10$ (or $2\epsilon_{min} < 20\mathring{A}$) most of the pressure drop occurs across the junction region. However, we shall show later that the most likely range for minimum junction width is between 25 and $30\mathring{A}$. For this range both contributions for the pressure drop in the intercellular cleft are important.

The hydraulic resistance of the variable geometry model can be represented by an equivalent parallel plane channel of the same length and of width $2\epsilon_o$ as illustrated in Figure 4. The pressure drop in this equivalent model is:

$$\Delta P = \frac{12\mu Q}{y}\,\frac{\ell}{(2\epsilon_o)^3} \qquad (15)$$

Equating (14) and (15) gives the relationship between ϵ_o and ϵ_{min}, that is:

$$\epsilon_o = \left(\ell \Big/ \left[\frac{w(a^2+(b^2)/2)}{(a^2-b^2)^{5/2}} + \frac{\ell - w}{\epsilon_n^3}\right]\right)^{1/3} \tag{16}$$

Using equation (16) one can solve the coupled boundary value problem for the endothelium and media using the parallel plane representation for the intercellular cleft and then relate the pressure drops in the two geometries shown in ing Figure 4. From equation (15):

$$Q = \frac{2}{3}\frac{(P_1-\bar{P}_2)}{\mu\ell}\epsilon_o^3 y \tag{17}$$

The average fluid velocity (flux) becomes:

$$V_1 = \frac{P_1-\bar{P}_2}{R_1} \tag{18}$$

in which $R_1 = \frac{3\mu\ell}{\epsilon^2}$ is the channel resistance. In dimensionless form:

$$V_1^* = (1-\bar{P}_2) \;/\; R_1^* = \frac{V_1\epsilon}{\mu(P_1-P_3)} \tag{19}$$

where R_1^* is defined as $R_1^* = \frac{R_1\epsilon}{\mu}$.

c. Matching

The overall solution to the problem is obtained by requiring that at the channel exit, the average pressure be continuous and that the volumetric flow entering the media be compatible with the total pressure drop across the intercellular channels. If the average velocities V_1 and V_2 are equal, it then follows that V_1^* and V_2^* are related by:

$$V_2^* = \Psi V_1^* \tag{20}$$

where $\Psi = (\mu^2 L)/(\epsilon K)$.

Therefore, using (20) and solving (9b) and (19) simultaneously yields:

$$\bar{P}_2 = \underline{\psi}\phi Sm/(\underline{R}_1^* + \underline{\psi}\phi Sm) \tag{21}$$

$$V_1^* = 1/(\underline{R}_1^* + \underline{\psi}\phi Sm) \tag{22a}$$

and

$$V_2^* = \underline{\psi}/(\underline{R}_1^* + \underline{\psi}\phi Sm) \tag{22b}$$

With V_2^* known the B_m coefficients are found from (8a,b). Then, the final solution for the pressure field is:

$$P(x,z) = \frac{\underline{\psi}}{(\underline{R}_1^* + \underline{\psi}\phi Sm)} \cdot \phi \left\{ z + \frac{2}{3} \sum_{m=o}^{\infty} \frac{\sinh(\lambda_m z)}{\cosh\lambda_m} \frac{\sin(\lambda_m \epsilon)}{\lambda_m^2} \cos(\lambda_m x) \right. \tag{23}$$

Also, having found $\bar{P}_2$ and the total fluid velocity V_2^*, the dimensionless media hydraulic resistance $\underline{R}_2^*$ is easily determined from its definition:

$$\underline{R}_2^* = \frac{\bar{P}_2 - P_3}{V_2^*} = \phi Sm \tag{24}$$

The two components of the arterial media velocity field are the x and z gradients of the steady state pressure distribution given in (23). That is:

$$V_x = -\frac{\partial P}{\partial x}(x,z) = \left(\frac{\underline{\psi}}{\underline{R}_1^* + \underline{\psi}\phi Sm}\right)\phi \frac{2}{3} \sum_{m=o}^{\infty} \frac{\sinh(\lambda_m z)}{\cosh\lambda_m} \frac{\sin(\lambda_m \epsilon)}{\lambda_m} \sin(\lambda_m x) \tag{25}$$

and

$$V_z = -\frac{\partial P}{\partial z}(x,z)$$

$$= \left(\frac{-\underline{\psi}}{\underline{R}_1^* + \underline{\psi}\phi Sm}\right)\phi \left\{ 1 + \frac{2}{3} \sum_{m=1}^{\infty} \frac{\cosh(\lambda_m z)}{\cosh\lambda_m} \frac{\sin(\lambda_m \epsilon)}{\lambda_m} \cos(\lambda_m x) \right\} \tag{26}$$

3. RESULTS AND DISCUSSION

We shall first want to compare the predictions of the theoretical model with the experimental results of Vargas et al. (1978), for rabbit aorta. In particular, we want to examine the effect of the intercellular cleft geometry on the average channel exit pressure $\bar{P}_2$. The theoretical predictions can also be combined with the experimental measurements to provide an independent estimate of the minimum width of the junctional complexes. We shall then explore the effect of wall thickness on the resistance of the media and the development of the velocity field in the interaction layer as a function of wall thickness. Finally, we shall look at the detailed development of the pressure profiles in the subendothelial tissue for vessels of different thickness.

A. Effect of Intercellular Cleft Geometry

All the results in this section will pertain to rabbit aorta since this is the only vascular tissue where we currently have accurate steady state measurements of the hydraulic conductivity of a vessel with both its endothelium intact and denuded. Figures 5,6 and 7 are, therefore, all based on a wall thickness of 200 μm and a measured hydraulic conductivity ($k \cdot L = 1.55 \times 10^{-9}$ cm^2/sec. cm-H_2O) of a denuded wall as given by Vargas et al. (1978). The average interjunctional spacing corrected for cell end effects in our two-dimensional equivalent model is $2\xi = 12\,\mu$m. The parameters which are not known in the experimental measurements for the aorta with intact endothelium are those relating to the geometry of the intercellular cleft. The model, however, provides the flexibility for varying the intercellular cleft geometry and seeing the effect this has on the relative resistance of the endothelium to that of the entire wall, the quantity which is calculated in the experiments.

Figure 5 shows the solution for the average pressure, $\bar{P}_2$, at the entrance to the subendothelial space as a function of ϵ_o (parallel plane model), for a cleft length, ℓ, ranging from 1 μm to 3 μm and a transmural pressure of 100 cm of water. The relationship between ϵ_o and ϵ_{min} is given by Equation (16) and is plotted in Figure 6 for an assumed cosinosoidal constriction length, w, of 1000 Å. The values for ℓ, 1 μm to 3 μm, are based on measurements made by Ann Baldwin (private discussion) and w = 1000 Å has been estimated from transmission electron microscopic studies of endothelial junctions Simionescu, Simionescu and Palade, 1975; Simionescu and Simionescu 1977). From these estimates $10 \leq \frac{\ell}{w} \leq 30$ should be representative of the range of values found in rabbit aorta. Figures 5 and 6 may be combined easily to give $\bar{P}_2$ as a function of ϵ_{min} as shown on Figure 7. For $\ell/w = 10$, one observes that when $\epsilon_{min} = 13$Å, ($\epsilon_o = 50$Å), or when the narrowest point in the junctional complex, $2\epsilon_{min}$, is 26Å or less, more than half of the transmural pressure drop can be sustained by the endothelium for a vessel whose media thickness is less than 200 μm. The equivalent result for $\ell/w = 30$ μm is a junction whose minimum constriction $2\epsilon_{min}$ is 29.6Å.

The experimental measurements of Vargas et al. would predict that roughly one-half of the total hydraulic resistance in rabbit aorta resides in the endothelium and, therefore, that $\bar{P}_2$ should be approximately 50 cm of H_2O. The results in Figure 7 indicate that for $2\epsilon_{min}$ less than 40Å varying ℓ/w from 10 to 30 changes the prediction for $\bar{P}_2$ by less than 15 percent and, hence, that $\bar{P}_2$ is primarily a function of a minimum gap width when $\epsilon_{min} < 20$Å.

The above observations suggest that the theoretical model can be combined with macroscopic water permeability measurements to provide a novel means for estimating the largest molecules that can pass through the intercellular cleft. The only existing technique for making such estimates is the use of labelled electron dense marker molecules that can be observed in transmission electron micrographs of the junction region. Much of the existing work is on capillary junctions on the arterial side. The results are believed to apply, however, to larger arterial vessels. Karnovsky (1965) and Flory and Sheppard (1970) using horseradish peroxidose as the tracer molecule have suggested 40Å as close to the upper limit, whereas Simionescu et al. (1975) using small hemopeptides as the tracer have proposed a limit closer to 20Å. The prediction of the present theory, a molecule with effective diameter between 26 and 30Å for rabbit aorta endothelium, therefore, lies in the middle of the range of commonly accepted values.

Another problem of interest that is easily answered by Figure 7 is how much does the intercellular cleft have to open up for the endothelium to behave as if it where entirely leaky. In the recent experiments reported by Blackshear et al. (1982) the lumen of the rabbit aorta is pressurized by air instead of being fluid filled. These vessels had nearly the same hydraulic conductivity as vessels denuded using a baloon catheter yet at the light microscopic level the endothelium appeared almost intact. One observes in Figure 7 that for $\ell/w = 10$ and $\epsilon_{min} > 50$Å nearly 90 percent of the pressure drop is taken up by the media assuming that the spacing of the cleft outside the junction region is held at 200Å. If the cleft itself is opened up to 400Å the endothelial resistance would drop

to less than three percent of the vessel wall even for $\ell = 3\mu m$. It is evident that only minute injuries in the endothelium are required to make it totally leaky in large vessels.

B. Media Resistance

It is commonly assumed that the hydraulic resistance of a homogeneous tissue scales linearly with thickness. This is, of course, only true if the velocity profile is one dimensional (uniform). This behavior would be a reasonable but rough approximation for a vessel denuded of its endothelium. For this case variations would be due principally to inhomogeneities in wall structure. For a vessel with intact endothelium this behavior is altered drastically since there are localized regions in the subendothlial space near the exits of the intercellular clefts where the velocity is two or more orders of magnitude larger than more distant regions of the media. One thus anticipates the existence of an interaction layer where the porous media jets first spread, then interact with one another and finally at some distance which is large compared to the jet spacing, asymptotically achieve a one-dimensional velocity profile. Since the pressure drop for a homogeneous medium is proportional to the velocity, the apparent resistance must exhibit three different types of behavior as the wall thickness is varied relative to the interaction layer thickness.

In Figure 8 the hydraulic resistance of the media $\underline{R}_2$ is presentd as a fuction of media thickness L, for $2\epsilon_{min} = 26\mathring{A}$ and $\ell/w = 10$, and for $2\epsilon_{min} = 29.6\mathring{A}$ and $\ell/w = 30$. One observes that when the media thickness increases fivefold, i.e., from that of an arteriole or venule (5 μm), to that of a small artery or vein (20μm), the media resistance $\underline{R}_2$ increases by only 50 percent. However, if the media thickness is greater than 150 μm, $\underline{R}_2$ varies linearly with L. This varying behavior of the media

resistance is clearly shown again in Figure 9, where the resistance of the media is presented as a resistance per unit length ($\underline{R}_2/L$). $\underline{R}_2/L$ is nearly constant for $L > 150$ μm. However, for $5 < L < 100$ μm there is a large variation in the resistance. That is $\underline{R}_2/L$ for $L = 5$ μm is about 5 times greater than that for $L = 100$ μm. This obsevation of the nonlinear behavior is new and contrary to previous studies that assumed that the media resistance per unit length is constant (for example, Kenyon, 1977, Vargas et al., 1979, Harrison et al., 1976).

The behavior exhibited in Figures 8 and 9 is readily explained in terms of the comments at the beginning of this subsection. For wall thickness smaller than the spacing between clefts the resistance is the same as the volumetric spreading of an isolated jet in a porous media. The problem is equivalent to the diffusion from a line source into a half space. Provided the wall thickness is large compared to the exit width of the jet (200Å), this resistance is independent of wall thickness and as seen in Figure 8 would approach a constant value if the curves were continued beyond $L = 5$ μm. For $L > 200$ μm $\underline{R}_2/L$ is a constant and one retrieves the linear scaling with thickness that one associates with a uniform profile. The range $10 < L < 200$ μm is a transition region between these two regimes. The behavior in the transition region is more easily understood from the detailed pressure and velocity profiles showing the interaction between the jets in the media. The curious result that we shall find is that the jet interaction is essentially completed and a one-dimensional velocity profile obtained after only 20 μm yet one has to go to 200 μm before $\underline{R}_2$ varies linearly with L. This is not a contradiction, but simply an expression of the fact that the initial spreading resistance is large because of the

relative velocities involved and can be neglected compared to the far field media resistance only when the latter region is roughly 10 times the thickness of the jet interaction layer. Note too that the definition of $\underline{R}_2$ is ambiguous since it varies with the geometry of the intercellular cleft. The difficulty is that $\bar{P}_2$ and hence the velocity at the exit of the cleft is a function of its geometry.

C. Velocity Profiles

Figures 10a,b,c, show the development of the axial velocity profiles in the vessel media for three representative wall thicknesses, L = 10,20 and 200 μm and an intercellular cleft geometry defined by $\ell/w = 30$ and $2\varepsilon_{min} = 29.6\mathring{A}$. Note that the scale on both axes is logarithmic. Peak velocities are nearly three orders of magnitude larger at the cleft exit than in the far field and that $x/\xi = 0.1$, which appears on the right-hand side of the figure, is still a small region in the neighborhood of the cleft exit when compared to the interaction distance between jets.

The axial velocity profiles for L=10 μm show that even at the adventitial surface z = 0, the jet interaction is incomplete and that the velocity beneath the center of the cell is still noticeably different that beneath the cleft. However, much of the interaction has been completed in the first five μm. The results for 20 μm wall thickness show, however, an essentially one-dimensional profile at the outer wall of the vessel. Again most of the interaction is completed in the first five μm. Finally, the solutions for the 200 μm wall show that the axial velocity profile has achieved one-dimensionality to within less than one percent at z=0.935 or at a distance 17 μm beneath the endothelial surface. Based on the foregoing, we shall consider 20 μm as a conservative estimate of the thickness the subendothelial interaction layer for water movement.

The striking result illustrated by Figure 10c is that for all major vessels one has a boundary layer like structure in which there is a thin region of non-uniformity beneath the endothelium and the vast majority of the wall has a one-dimensional profile. This behavior suggests that if one wishes to take account of filtration in the media in mass transport of large vessels a uniform velocity profile could be used as a reasonable approximation for the entire wall.

D. Pressure Profiles

A question that has been the subject of considerable speculation is the detailed pressure distribution under the endothelial cell layer. It is well-known that the endothelium is rather fragile and that an artery wall can be easily denuded of its endothelium at shearing stresses of as little as 40 dynes/cm^2, Fry (1976). It may therefore appear surprising that the endothelium can support normal stress differences that are several orders of magnitude larger without rupturing. The answer is, of course, that while a large hydrostatic pressure difference can exist across the endothelium when the lumen pressure is higher than the subendothelial pressure, the unbalanced pressure must be taken up as a contact stress in the subendothelial tissue matrix. When the direction of the transendothelial pressure difference is reversed either osmotically or by suddenly reducing the lumen pressure endothelial blistering does occur and the tethers that attach the endothelial cells to the basement membrane are easily torn Blackshear et al. (1982). The pressure difference to lift the endothelial cells from their substratum can only be maintained if the intercellular clefts maintain their integrity. The solutions in Figures 5,6, and 7 are valid for either an outward or inward flow of water and,

therefore, might be used to provide an estimate of the back-pressure that can be built up in subendothelial blisters. To obtain a realistic estimate of this pressure one would need to know more about the geometry of the intercellular cleft between blistered endothelial cells than is currently available from the gross morphology. It is also noted in Blackshear et al. (1982) that the shear stress required to denude the endothelium once it has blistered is one to two orders of magnitude less than for an intact endothelium.

In Figure 11 we have plotted the subendothelial pressure distribution at z=1 for various wall thicknesses. To provide for a common standard of comparison, we have chosen a fixed intercellular cleft geometry for all curves, $\ell/w = 30$ and $2\varepsilon_{min} = 29.6\text{Å}$. These curves exhibit two important properties. First, the subendothelial pressure at the channel exit $x/\ell < 1.2\text{x}10^{-3}$ is nearly uniform and scales non-linearly with wall thickness, as already observed. For vessels 20 μm and under most of the pressure drop occurs across the endothelium and the fraction that does occur in the media is due primarily to the spreading of the exit jets. Second, the decay of the endothelial pressure under the cell occurs on a length scale which is much larger than the channel exit dimensions and for the larger vessels is only a small fraction of the peak pressure at the channel exit. Vessels whose media is 200 μm or thicker have a relatively uniform subendothelial pressure which varies by less than ten percent from its maximum to minimum value, whereas thin walled vessels have a larger subendothelial pressure variation governed by the jet interaction.

therefore might be used to provide an estimate of the back-pressure that can be built up in subendothelial blisters. To obtain a realistic estimate of this pressure one would need to know more about the geometry of the intercellular cleft between blistered endothelial cells than is currently available from the gross morphology. It is also noted in Blackshear et al. (1982) that the shear stress required to denude the endothelium once it has blistered is one to two orders of magnitude less than for an intact endothelium.

In figure 11 we have plotted the subendothelial pressure distribution at z=1 for various wall thicknesses. To provide for a common standard of comparison, we have chosen a fixed intercellular cleft geometry for all curves, $\ell/w = 30$ and $\varepsilon_{min} = 29.6\mathring{A}$. These curves exhibit two important properties. First the subendothelial pressure at the channel exit $x/\xi < 1.2\ 10^{-3}$ is nearly uniform and scales non-linearly with wall thickness, as already observed. For vessels 20 μm and under most of the pressure drop occurs across the endothelium and the fraction that does occur in the media is due primarily to the spreading of the exit jets, rather than their interaction, and thus is nearly constant for L < 20 μm. Second, the decay of the endothelial pressure under the cell occurs on a length scale which is much larger than the channel exit dimensions and for the larger vessels is only a small fraction of the peak pressure at the channel exit. Vessels whose media is 200 μm or thicker have a relatively uniform subendothelial pressure which varies by less than ten percent from its maximum to minimum value, whereas thin walled vessels have a larger subendothelial pressure variation governed by the jet interaction.

Figure 12 compares the average subendothelial pressure at the channel exit for three representative wall thicknesses as a function of intercellular cleft geometry. ℓ/w is held fixed at $\ell/w = 20$ but the minimum constriction of the junctional complex is varied. A thickwalled vessel is much more sensitive to its junction geometry since its resistance will be largely controlled by its media for $\epsilon_{min} > 20\mathring{A}$. The results for large vessels $L > 200$ μm have to be interpreted qualitatively because of the presence of vasa vasorum whose effect is not considered in the present model.

A final consideration which has not been considered in the present model is the possible existence of an extracellular matrix in the intercellular cleft. If such a matrix is diffuse, the present model does not need to be modified. This would be the case if the normal spacing of the cleft $200\mathring{A}$ is determined by macromolecular bridging as in red cell rouleaux. If the intercellular matrix is dense then a different type of model is necessary. The intercellular channels themselves would then be governed by porous matrix theory. This possibility has been studied by Currie and Michel (1980). The latter model has been confined to the endothelium and does not treat the coupled interaction with the underlying tissue.

4. REFERENCES

Baldwin, A., (1983), Columbia University Medical Center, personal communication.

Blackshear, P.L., Jr., Blackshear, G.L., Newell, M.K., Emerson, D.F., Kayser, S.J. Gross Endothelial Layer Blistering and Vascular Injury. Proceedings 6th International Symposium on Atherosclerosis, Berlin, Germany, June 13-17, 1982.

Curry, F.E. and Michel, C.C. (1980), Microv. Res. 20, 96.

Flory, L. and Sheppard, B.L., (1970). Proc. Roy. Sci., London, Series B 174: 435.

Fry, D.L., 1976 Circ. Res. 24, 363-67.

Harrison, R.G. and Massaro, T.A. (1976). Atherosclerosis 24:363.

Huttner, I., Boutet, M. and Katchalsky, A. (1973). Lab. Invest. 28:672.

Karnovsky, M.J. (1965). J. Cell. Biol. 27, 49A.

Keller, H.K. and Stein, T.R. (1967). Mathematical Biosciences 1:421.

Kelman, R.B. (1965). Bull. Biophys. 27, 57.

Kenyon, D.E. (1979). Bull. Math. Biol. 41, 79.

Landis, E.M., and J.R. Pappenheimer. Exchange of substances through the capillary wall. Handbook of Physiology Circulation, edited by W.F. Hamilton, Washington, DC: Am. Physiol. Soc. 1963, Sect. 2, vol. 2, Chapter 29, p. 961-1034.

Simionescu, M. and Simionescu, N. (1977). J. Cell. Biol. 74, 98.

Simionescu, N., Simionescu, M. and Palade, G.E. (1975). J. Cell. Biol. 64:586.

4. REFERENCES (cont.)

Vargas, B.C., Vargas, F.F., Pribyl, J.G. and Blackshear, P.L., (1978). Am. J. Physiol. 236: H53-H60.

Vargas, F.F. and Johnson, J.A. (1964). J. Gen. Physiol. 47:667.

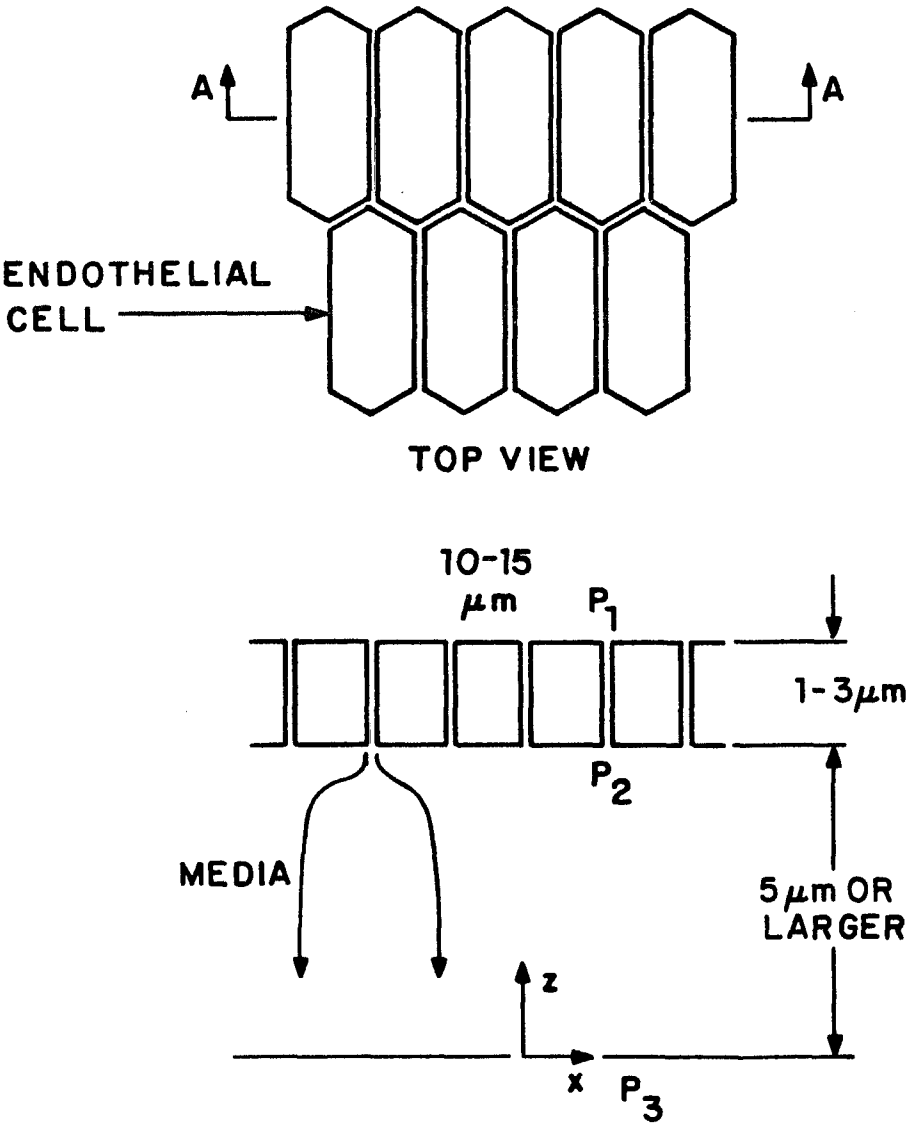

Figure 1. Schematic diagram for mathematical model for water filtration across arterial endothelium and media.

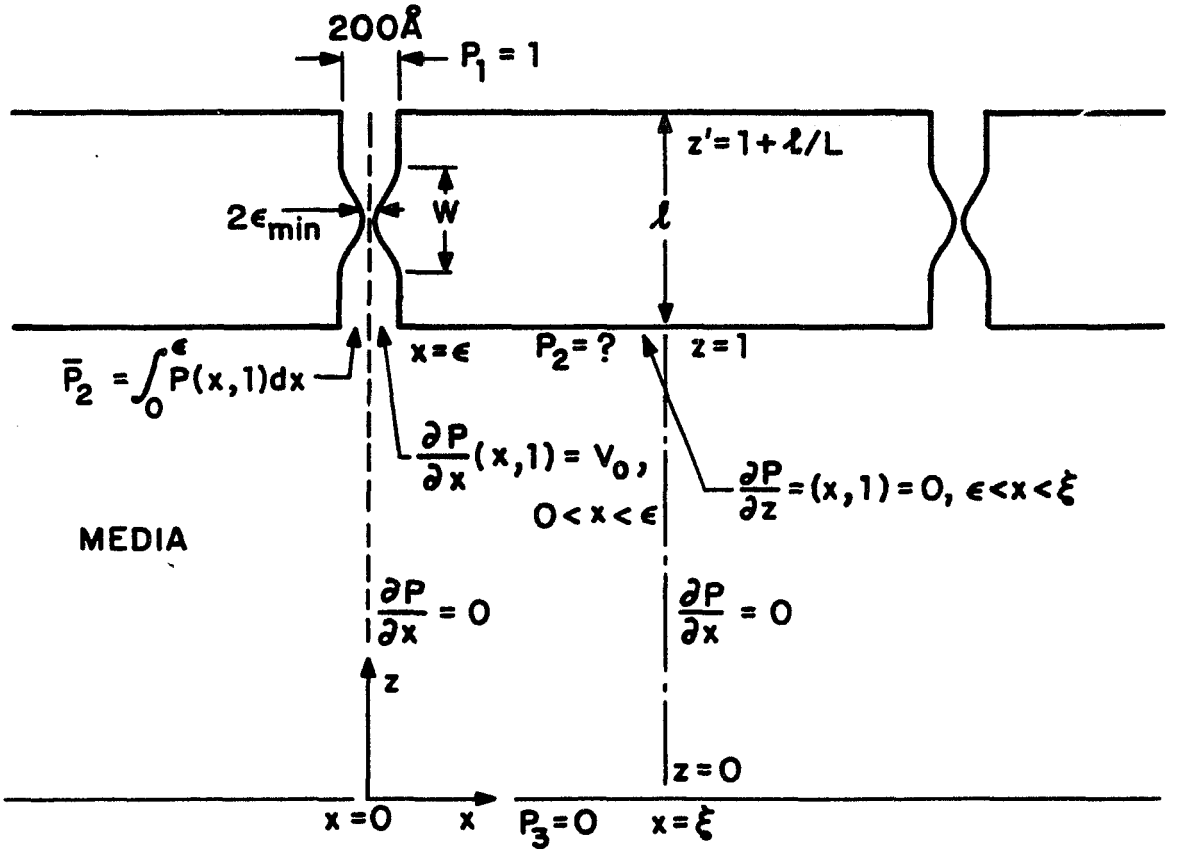

Figure 2. Schematic diagram of a unit cell in two-dimensional periodic arrangement; boundary conditions of the model are shown.

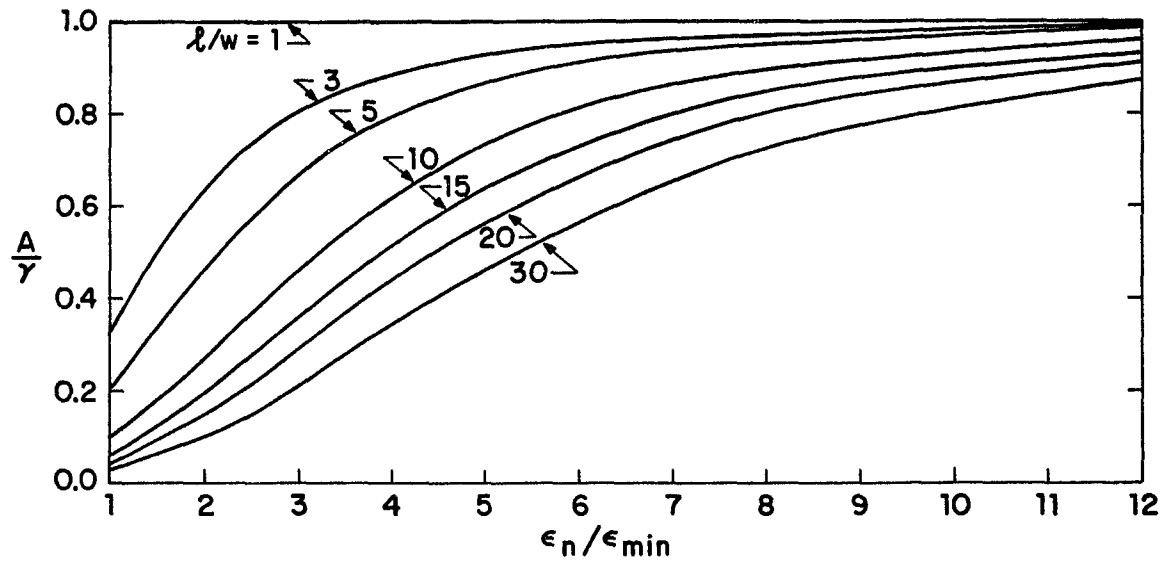

Figure 3. Resistance of tight junction region (w=1000Å) compared to total junctional resistance (ℓ = 0.3 to 3 μm) as a function of junctional width compared to tight junction width.

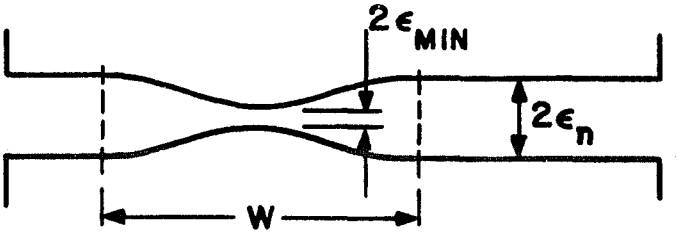

JUNCTION MODEL

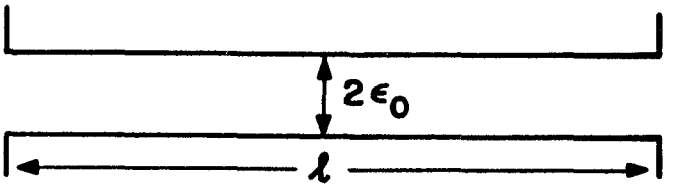

PARALLEL PLANE MODEL

Figure 4. Schematic diagram of endothelial junction with variable junctional geometry or with equivalent parallel plane channel of the same length and the same hydraulic resistance.

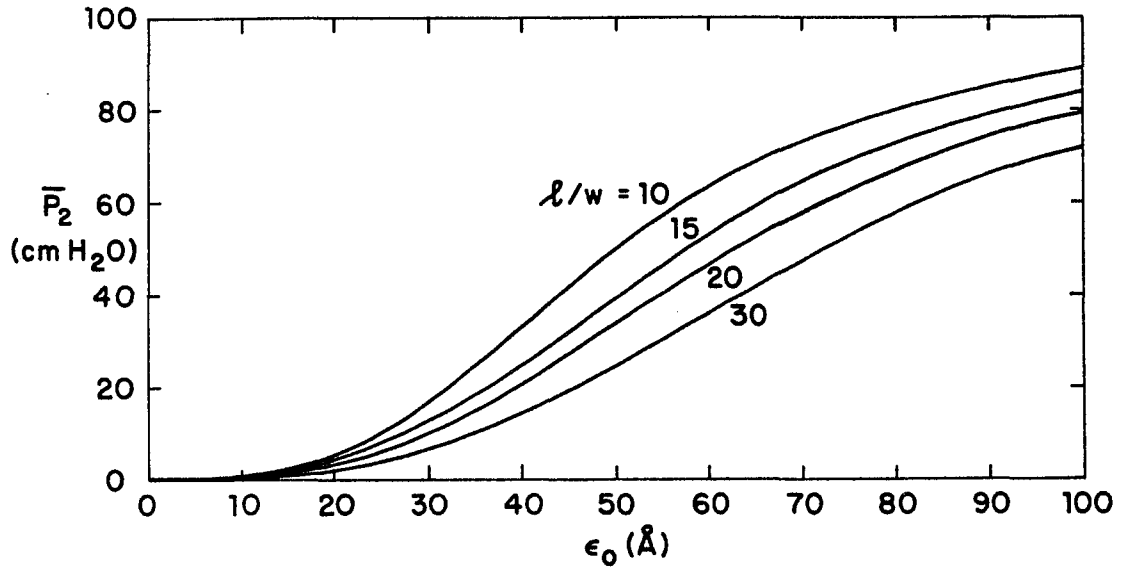

Figure 5. Average subendothelial pressure at the junction exit as a function of effective intercellular cleft (half) width; w = 1000Å, ℓ = 1 to 3 μm and L = 200 μm.

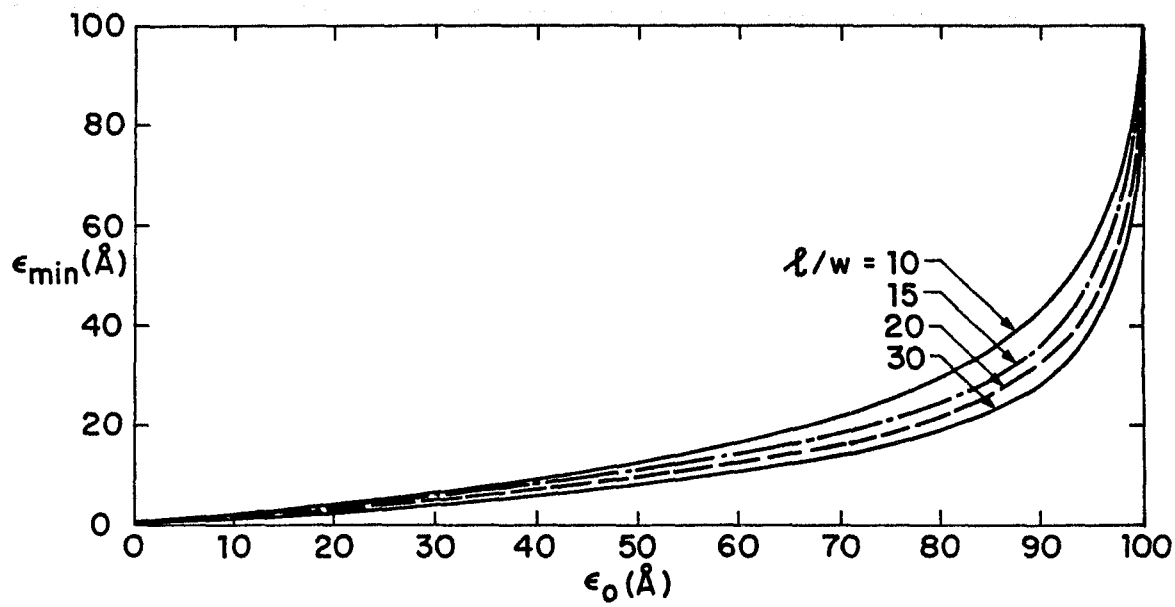

Figure 6. Minimum width of junctional complex ($2\epsilon_{min}$) as a function of equivalent width of parallel walled channel ($2\epsilon_o$); w = 1000Å, ℓ = 1 to 3 μm and L = 200 μm.

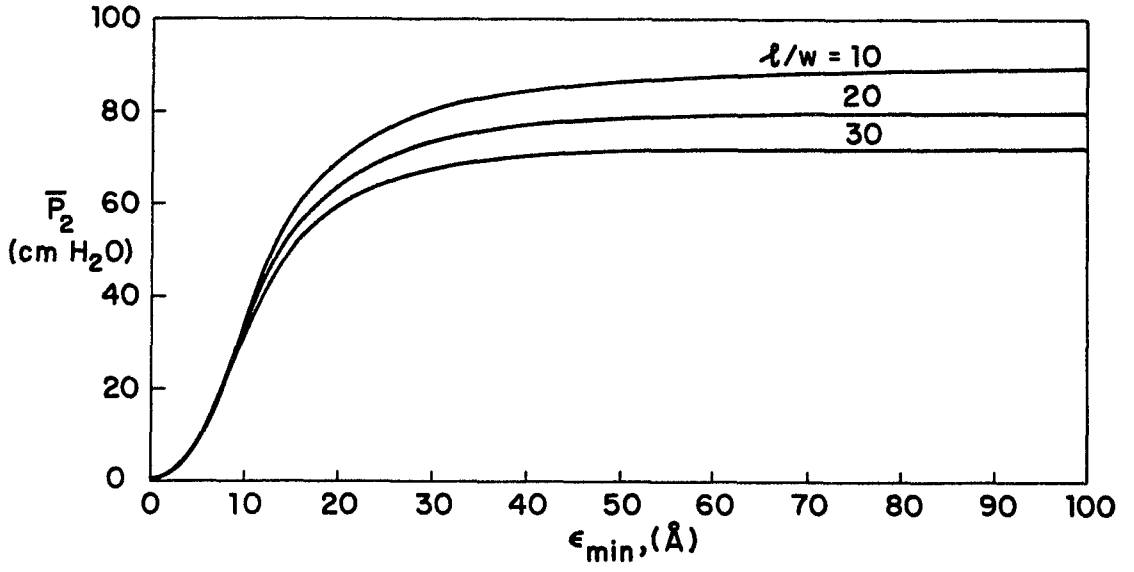

Figure 7. Average subendothelial pressure at the junction exit as a function of minimum (half) width of junctional complex, w = 1000Å, ℓ = 1 to 3 and L = 200 μm.

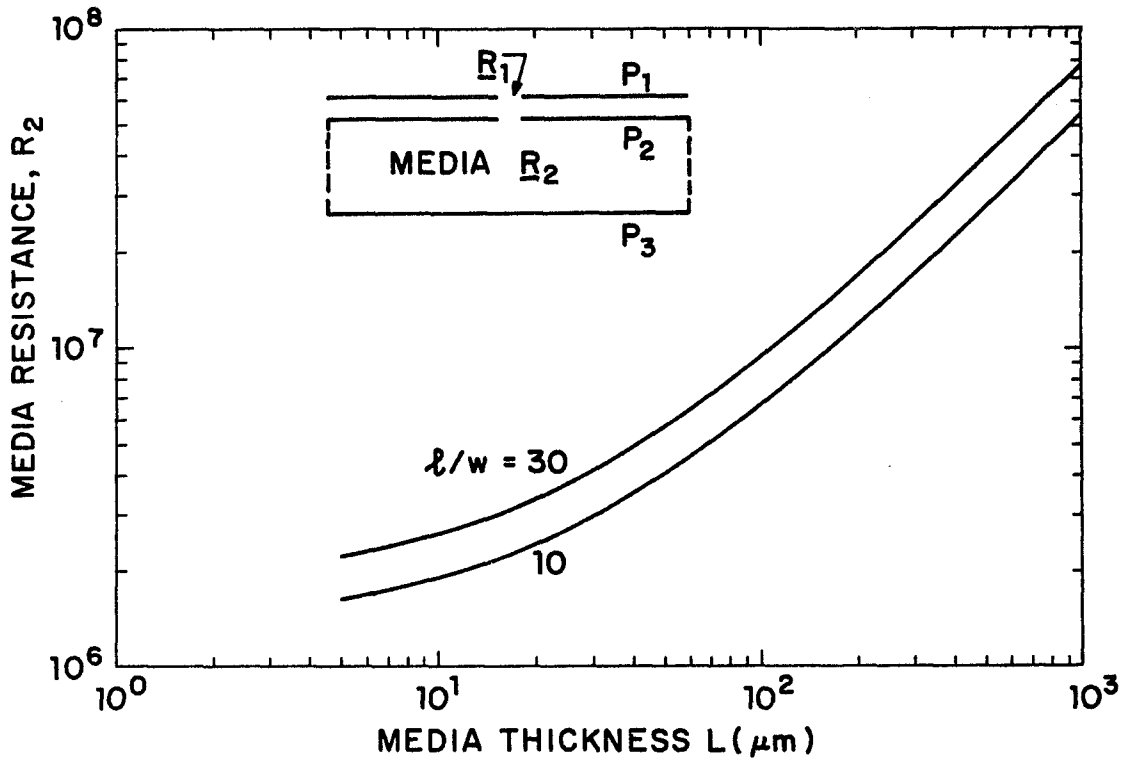

Figure 8. Hydraulic resistance of media as a function of media thickness; $2\epsilon_{min} = 26\text{Å}$ with $\ell/w = 10$, and $2\epsilon_{min} = 29.6$ with $\ell/w = 30$.

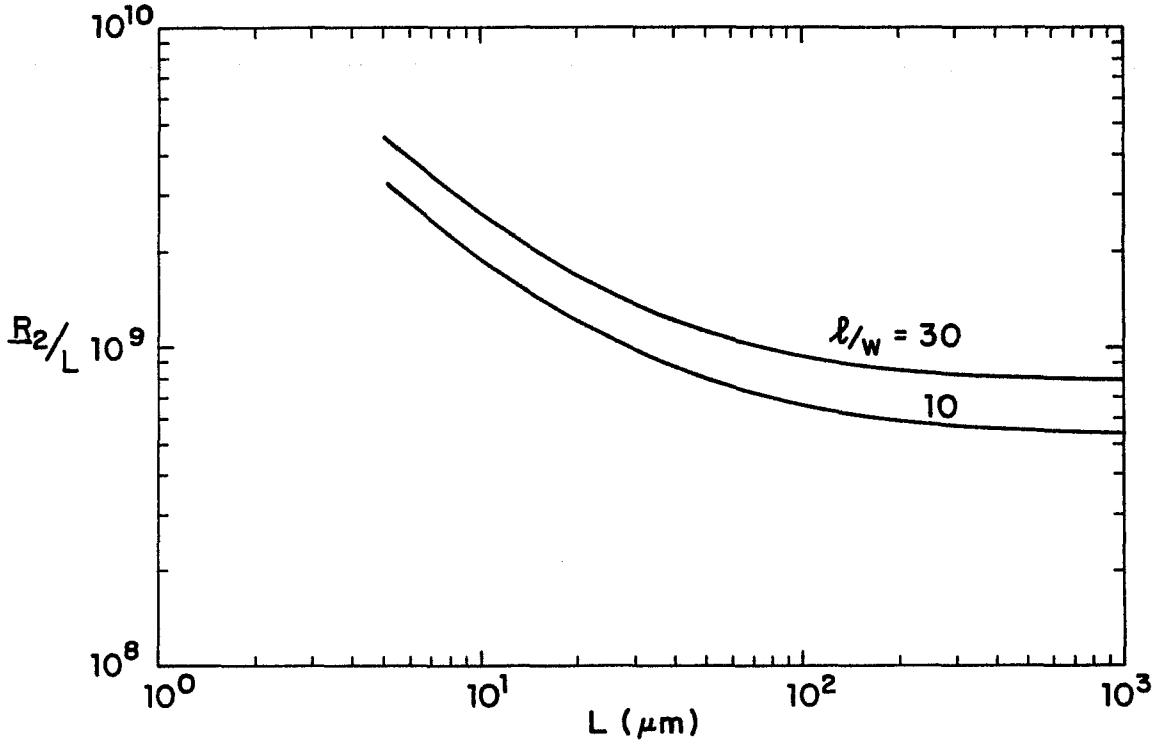

Figure 9. Media resistance per unit length as a function of media thickness.

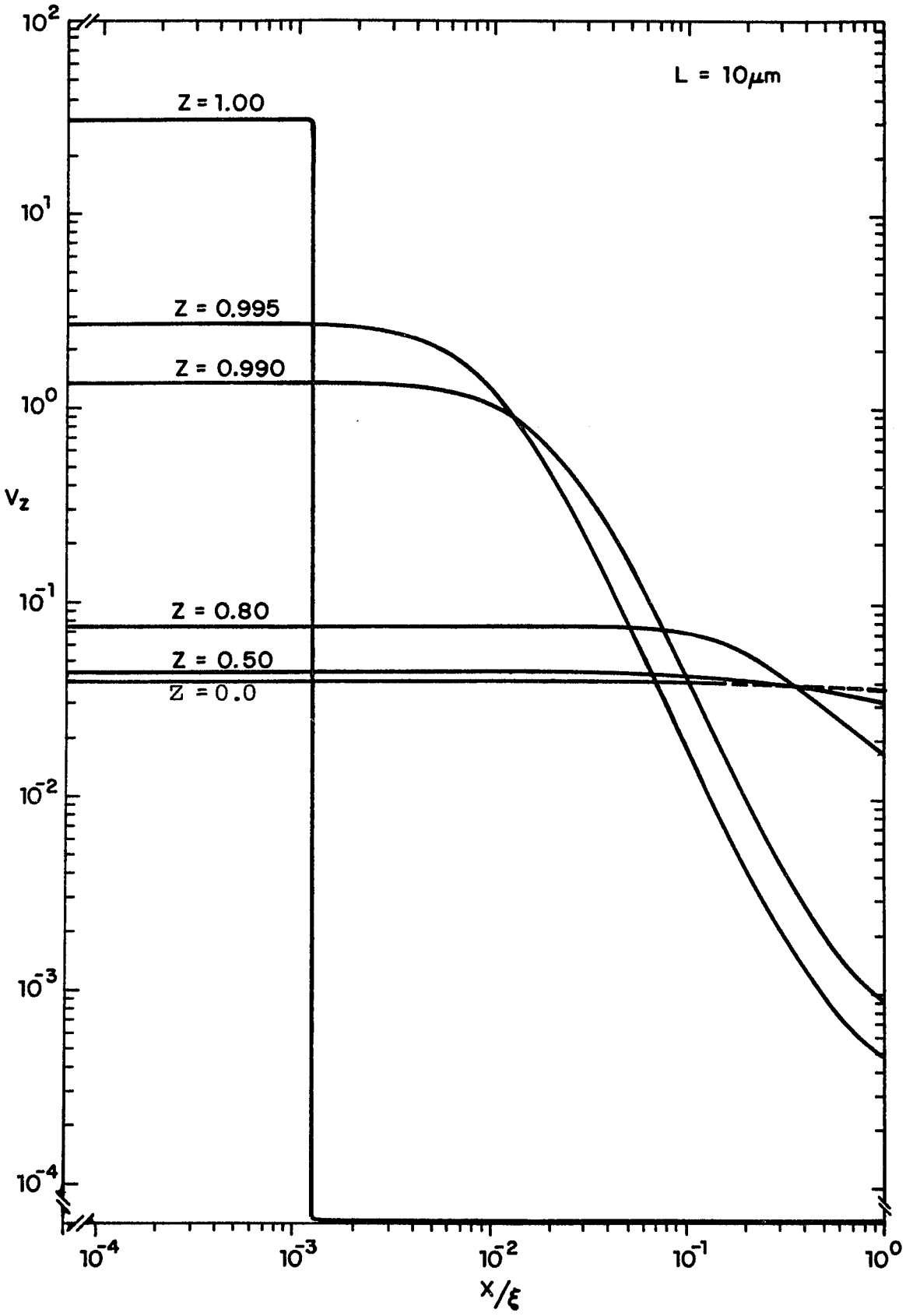

Figure 10a. Axial velocity profile at increasing depth below endothelial surface; $2\varepsilon_{min} = 29.6$Å, $\ell/w = 30$, and L = 10 μm.

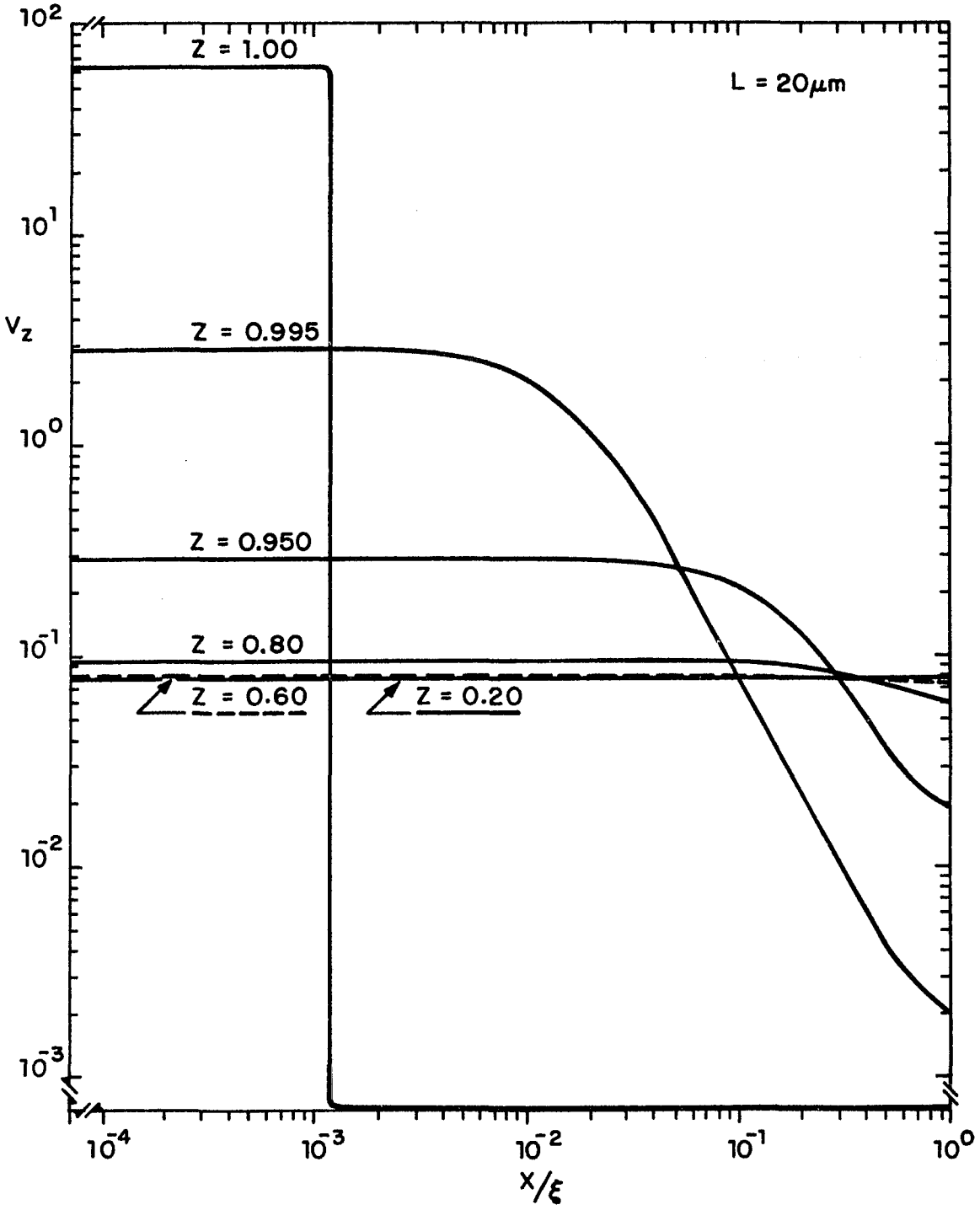

Figure 10b. Axial velocity profile at increasing depth below endothelial surface; $2\epsilon_{min}$ = 29.6Å, ℓ/w = 30 and L = 20 μm.

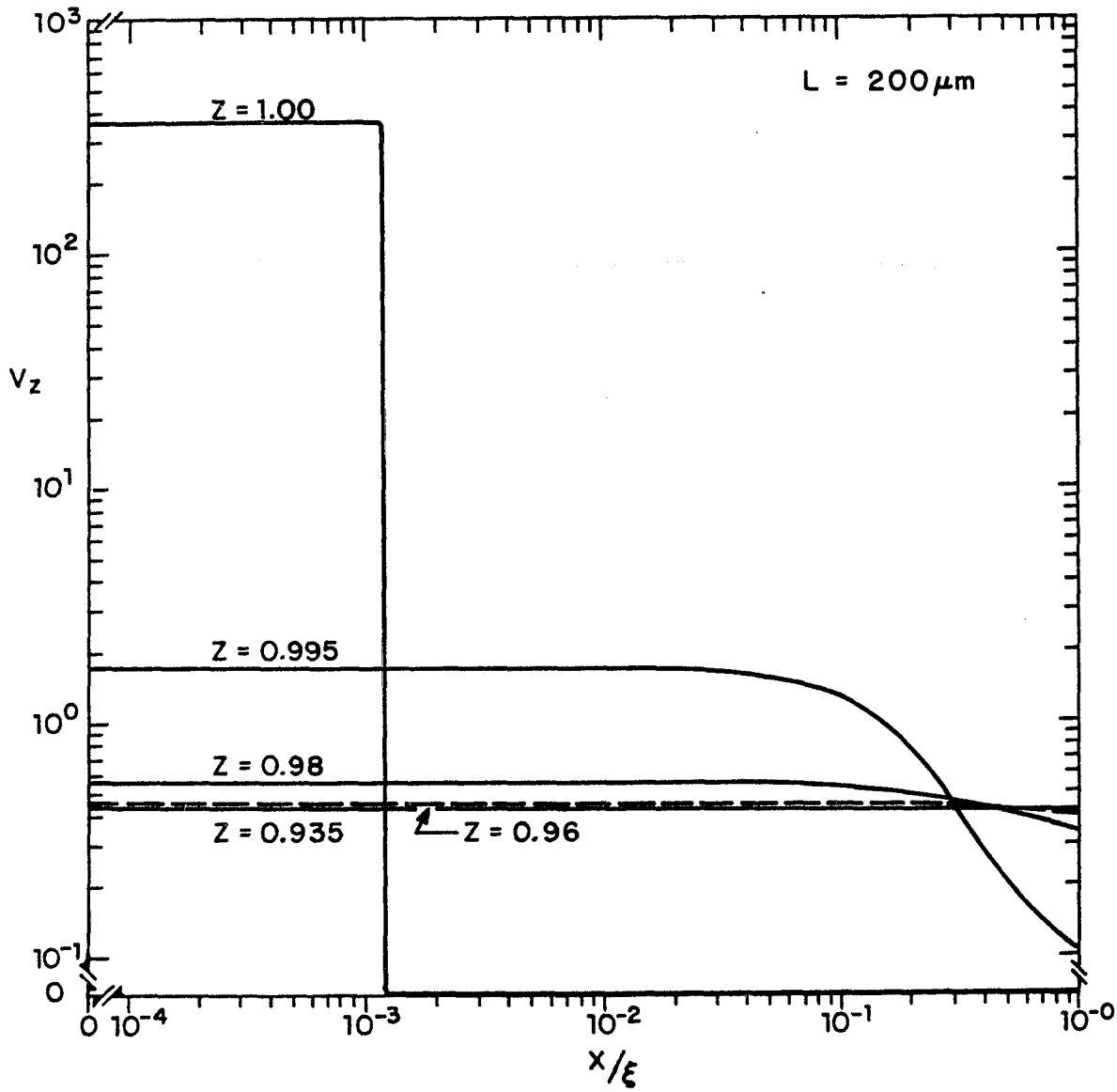

Figure 10c. Axial velocity profile at increasing depth below endothelial surface; $2\epsilon_{min}$ = 29.6Å, ℓ/w = 30 and L = 200 μm.

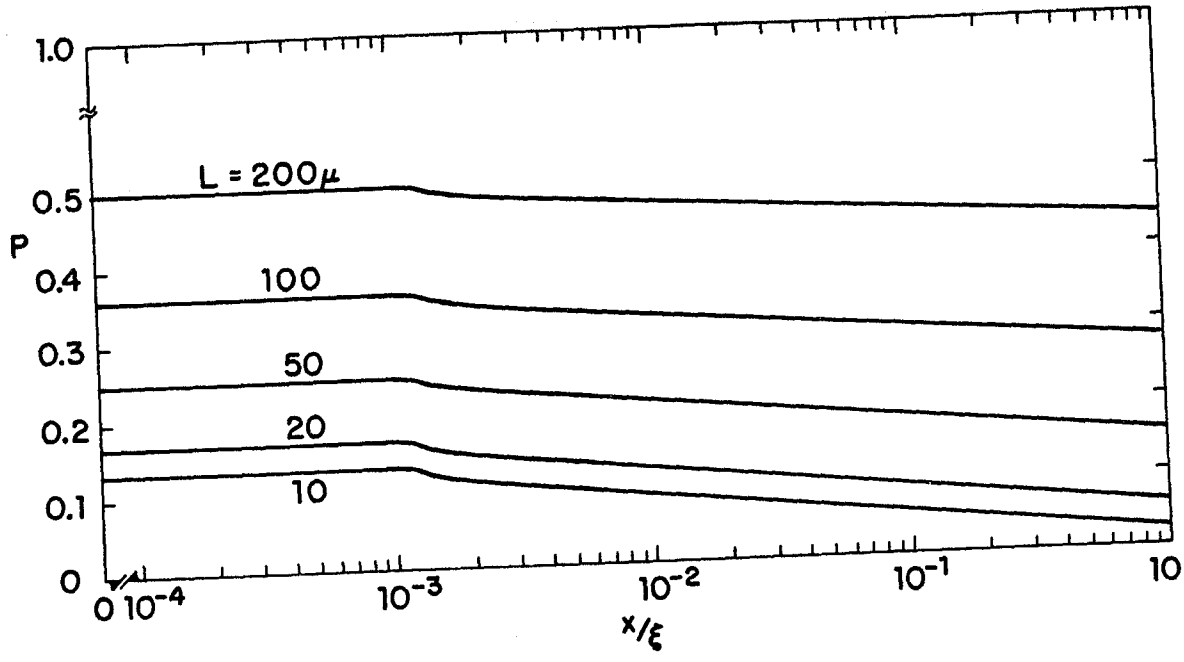

Figure 11. Subendothelial pressure distributiom at z = 1; $2\epsilon_{min}$ = 29.6 and ℓ/w = 30.

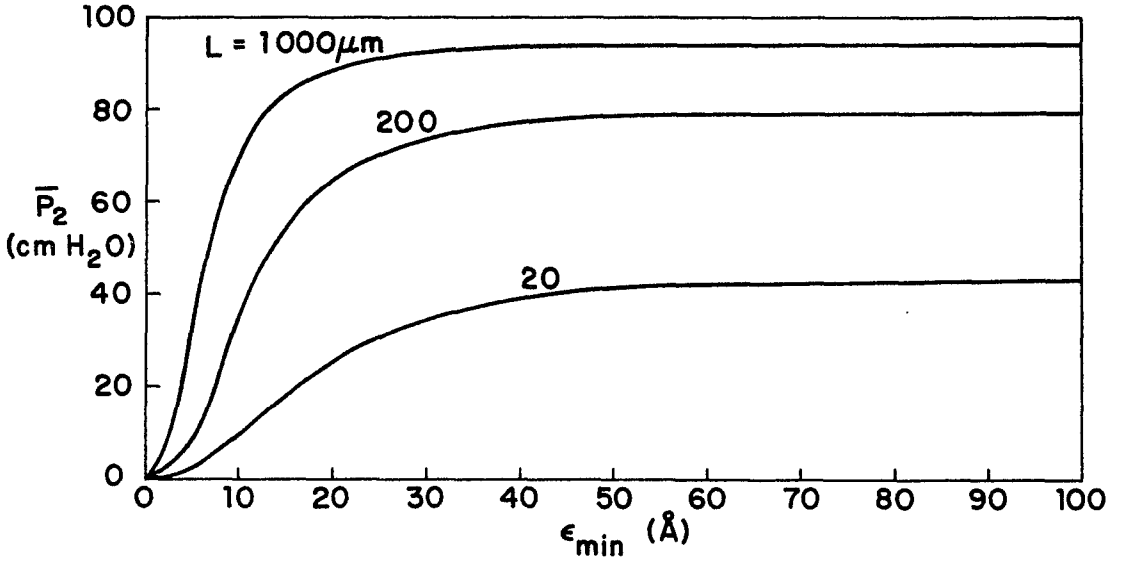

Figure 12. Average subendothelial pressure at channel exit as a function of intercellular cleft geometry; $\ell/w = 20$.

CHAPTER IV

CONVECTIVE AND DIFFUSIVE TRANSPORT OF MACROMOLECULES ACROSS ARTERIAL WALL IN THE PRESENCE OF MULTIPLE INTERACTING ENDOTHELIAL INJURIES OR LEAKY JUNCTIONS

SUMMARY

The theoretical study on the effect of cell turnover and leaky junctions on the transport of macromolecules across the arterial wall presented in Chapter II has been extended by incorporating into it, 1) a finite junctional transport resistance so that the concentration of macromolecules throughout the junction is not necessarily the same as that in the lumen, which was the case in the previous model, and 2) the effect of the lumen-adventitia pressure difference, which is of the order of 100mm Hg, so as to produce a more general theory enabling one to examine the effect of convection on the transport rate of macromolecules. In the leaky junction model (Chapter III), it was clearly shown that a small cell turnover rate could cause large changes in the equilibrium balance of the cholesterol carrying macromolecules in the arterial wall, and that the leaky junction hypothesis is a feasible mechanism of transport in the event of an endothelial injury. In addition to this, the present model shows that, 1) for small turnover rate (ϕ < 1%), the convective contribution to the flux or uptake of macromolecules by the arterial media is of some importance, but for ϕ > 1%, its effect is dramatically large, 2) convection tends to lower the macromolecule concentration in the media, owing to the increased transport of macromolecules from the media to the adventitia where they are removed by the lymphatic circulation system, and 3) the resistance of the leaky junction to the transport of macromolecules is not always negligible. The predictions of the model are in favorable agreement with the experimental work of Bell et al. (1974a) and with the in vivo experimental findings of Bondjers et al. (1973) and Colton et al. (1980).

1. INTRODUCTION

In the earlier related theoretical work, Nir and Pfeffer (1979) and Pfeffer et al. (1981) quantitatively examined the experimentally observed twofold increase in uptake of macromolecules in some focal regions of the mammalian arterial tree, where, cell turnover rate is higher than in other regions of the tree. Their hypothesis was that damaged or dying endothelial cells become permeable over their entire surface and thus offer no resistance to transendothelial diffusion of the cholesterol carrying and related macromolecules larger than 40Å which would normally cross the endothelial cell layer only via vesicular transport (a transport process that can not however explain the twofold increase in uptake, Chien and Weinbaum, 1981). Their findings clearly show that, 1) the endothelium is the controlling resistance to transarterial movement of macromolecules (> 40Å) that can not enter the arterial media through normal junctions between neighboring endothelial cells, and 2) if a small fraction (<3%) of the endothelial surface is damaged, it can cause a large increase ($\approx$ 2 fold) in the uptake of macromolecules. An important modification of the mechanism of the transendothelial diffusion during cell turnover was made by using a new model (see Chapter III) that is based on recent experimental evidence, Schwartz (1980), which suggests that the endothelial monolayer in vivo does not suffer denudation, but the junctions between dying or damaged cells and normal healthy cells may become wider allowing macromolecules larger than 40Å to enter the arterial wall. The findings of this model, i.e., the leaky junction model (Chapter II) are quantitatively in favorable agreement with experimental uptake studies. The findings also show that the rate of transport of molecules into the wall during cell turnover is controlled by the perimeter of the damaged or dying cell rather than its area, clearly

showing that the leaky junction hypothesis is a possible mechanism for the transendothelial transport when the integrity of the endothelium is not maintained.

However, in all of the above studies, the effect of convection on the flux, on the uptake and on the arterial wall concentration profiles of the macromolecules was ignored. However, the in vivo experiments of Björkerud (1969) and Bondjers et al.(1973), show that for a large endothelial injury, the uptake of cholesterol carrying macromolecules from the blood (lumen) by the arterial wall was 15 times greater in the region with the defective endothelium than in the other region where the integrity of the endothelium is not disturbed. Such an uptake difference, is much larger than what was experimentally observed by Bell et al.(1974a), which was a difference of only twofold, for a relatively smaller cell damage size and cannot be explained by the predictions of the theoretical models in which convection was neglected. A simplified arterial macromolecule transport model developed by Bratzler et al.(1977), together with their experimental work clearly indicates that both diffusion and convection play a significant role in the transport of macromolecules through the arterial media. Also, the in vivo experimental studies of Colton et al.(1980) although not at steady state show that the uptake with the endothelium removed was an order of magnitude greater than with the endothelium intact. Furthermore, the in situ experiments with elevated pressure and mechanical oscillation, and the supporting vesicle transport theory reported in Chien and Weinbaum (1981) strongly suggest that vecicular transport is not significantly affected by mechanical disturbances and thus the observed regional differences in uptake are difficult to explain on the basis of vesicular transport. This behavior suggests that the intercellular clefts between adjoining endothelial cells may become leaky at elevated pressure.

Thus, a better understanding of the actual (in vivo) transport of macromolecules across arterial wall in the presence of endothelial injuries or leaky junctions could be gained by also considering the effect of convection due to the pressure difference between the lumen and the adventitia which is about 100mm Hg. The plan here is to extend the leaky junction model (Chapter II) by incorporating into it, 1) the pressure effects and 2) a finite transport resistance in the junctions, so as to produce a more general theory enabling one to examine the effects of both convection and diffusion on the steady state flux, uptake and concentration distribution of macromolecules in the arterial wall, in the presence of multiple interacting endothelial injuries.

2. MODEL FOR CONVECTIVE AND DIFFUSIVE TRANSPORT

The accumulation of the cholesterol carrying low density lipoproteins (LDL) and related macromolecules in the arterial wall is governed by both the rate of uptake at the lumen-endothelium interface and by the rate of mass transport in the underlying wall tissue. In the mathematical model describing the steady state transport of macromolecules across arterial wall, and in particular through leaky junctions (Chapter II), the endothelial cell layer was treated as having zero thickness and the concentration of macromolecules throughout the leaky junction was assumed to be the same as in the lumen. In the present model, the endothelium is treated as having a finite thickness of length ℓ, with a non-zero junctional resistance. That is, the concentration of macromolecules throughout the junction need not be the same as that in the lumen. As in the model of Pfeffer et al. (1981), the endothelial cells which are in the process of turnover are assumed to be arranged in a periodic array. A unit cell of the array is shown in Figure 1. The endothelium is at $z = 1$, and the media-adventitia interface is at $z = 0$. R_1 is the radius of dying cell, R_2-R_1, is the width of the leaky junction, 2ξ is the distance between two neighboring damages and ξ is the radius of a unit cell of the array. All lengths have been non-dimensionalized by the thickness of the arterial media, L, except for the dimension of the junction which has been non-dimensionalized with respect to the junctional length, ℓ. The arterial media is represented by a dispersed cellular phase and interstitial fluid phase as in Weinbaum and Caro (1976), and the media is described by an effective diffusion coefficient, D_m. The dimensionless concentration is defined as $c = (C-C_A)/C_L-C_A)$, in which C_A is the macromolecule concentration at the media-adventitia interface ($z = 0$), and C_L is the concentration in the lumen.

For convenience, the formulation of the present mathematical problem has been divided into three sections: A) Leaky junctions, where the governing equation for the enhanced transport of macromolecules due to both convection and diffusion is integrated along the channel length to yield an expression for the flux through the junction in terms of an unknown interfacial concentration C_i (at $z = 1$, $R_1<r<R_2$). B) Media, in which the formulation for the concentration distribution of macromolecules follows along the same line as described in the leaky junction model (Chapter II) for the zero-thickness endothelial cell layer, except that the concentration just below the leaky junction is taken to be C_i instead of unity. C) Matching the media and junction fluxes results in a second equation for the flux through the channel as a function of the unknown concentration C_i. These equations are then solved simultaneously to yield the unknown interfacial concentration C_i, as well as the junctional flux, the media concentration distribution and the flux across the artery wall.

A. Transport Through Leaky Junctions

Here, it has been assumed that macromolecules >40Å enter the media via vesicular transport and through leaky junctions only. But the fluid velocity in the normal junctions is assumed to be the same as in the leaky junctions because of the fact that in the region of constriction a tight junction covers a very small distance when compared to the length of a junction (10^{-3} to 1, Baldwin, 1983) and thus its effect on the average junctional velocity is negligible. Assuming a parallel wall shape for the junctional complex adjacent to the injured endothelial cell, the one-dimensional diffusive and convective flux of macromolecules along the intercellular cleft is given by

$$D_j \frac{dC}{dX} + V_j C = \text{constant} = \tilde{J}_j \qquad (1)$$

where D_j is the effective junctional diffusion coefficient, V_j is the fluid velocity in the junction and $\mathfrak{J}_j$ is the flux through the junction, Equation (1) in dimensionless form is

$$\frac{dc}{dx} + P_j(c + \frac{\gamma}{1-\gamma}) = \mathfrak{J}\ell/D_j(C_L-C_A) = J_j \qquad (2)$$

in which J_j is the dimensionless flux through the junction, P_j is the Peclet number in the junction and γ is C_A/C_L.

Integrating (2) and using the condition that $c = 1$ at the lumenal end of the leaky junction ($x = 1$) and rearranging gives

$$c = (1 - (J_j-P_s)/P_j)\,\ell^{P_j(1-x)} + (J_j-P_s)/P_j \qquad (3)$$

where $P_s = P_j\gamma/(1-\gamma)$. At $x = 0$, that is at the media endothelium interface, Equation (3) gives an expression for the flux through the junction in terms of unknown interfacial concentration, C_i.

B. Convection and Diffusion in the Media

The equation which describes the steady-state concentration distribution of macromolecules in the media, in the presence of both convection and diffusion, in dimensionless form is

$$\frac{\partial^2 c}{\partial z^2} + \frac{1}{r}\frac{\partial c}{\partial r} + \frac{\partial^2 c}{\partial z^2} + Pe\,\frac{\partial c}{\partial z} = 0 \qquad (4)$$

in which Pe is the Peclet number in the media.

In Equation (1), the convective term in the r-direction has been dropped based on the steady-state water movement and pressure distribution studies (Chapter III), which show that for a vessel whose thickness L>150μm, the velocity field in the media can be accurately descriped as a plug flow. Figure 2 is a representative of the findings, in

which L = 1000μm and the leaky junction width (R_2-R_1) is 200Å. The fluid jets entering the arterial media through the junctions spread laterally very quickly and a uniform flow is established in the media after a penetration of only a few percent ($\simeq$1%) of its thickness.

In the present model, the boundary conditions to be satisfied by the concentration are

$$c(r,0) = 0 \qquad 0<r<\xi \tag{5}$$

$$\frac{\partial c}{dr}(0,z) = \frac{\partial c}{\partial r}(\xi,z) = 0 \qquad 0<z<1 \tag{6),(7}$$

$$c(r,1) = C_i \qquad R_1<r<R_2 \tag{8}$$

$$\frac{\partial c}{\partial z}(r,1) + Pe(c(r,1)) + \frac{\gamma}{1-\gamma}) = \sigma(1-c(r,1)) \qquad 0<r<R_1,\ R_2<r<\xi \tag{9}$$

Boundary condition (5) is at the media-adventitia interface where it is assumed that macromolecules are effectively removed by the lymphatic system. The symmetry conditon of the unit cell is given by Equation (6). At the edge of the unit cell, r = ξ, Equation (7) states that there be no net mass transfer, which is a required condition by the periodicity of the model. Boundary condition (8) requires that the concentration at the leaky junction exit and media interface be the unknown concentration C_i instead of one, which was the case in the leaky junction model (Chapter II). Condition (9) applies in the region where the endothelium is intact; where the net flux of molecules across the endothelium by vesicular transport is balanced by the net flux by molecular diffusion and convection directly beneath the endothelium. Here, σ is the Biot number, and physically represents the ratio of resistance to macromolecule transport of the arterial media to that of

the intact endothelium, Weinbaum and Caro (1976). As indicated above, condition (9) is also satisfied in the region $0<r<R_1$. Since the vesicular contribution of the dying cell is negligible, boundary condition (9) or a zero flux boundary condition would lead essentially to the same result.

The mathematical solution of the boundary value problem just outlined is not straightforward because of the complexity of the mixed boundary conditions at the endothelial surface, and the large difference in the required scale representation between R_1-R_2, i.e., leaky junction width, and the unit cell radius ξ. Therefore, the solution techniques presented in Chapter 2 are employed here as well to determine the fine structure of the concentration field underneath the endothelium and in particular at the leaky junction sites.

The solution for the steady-state concentration distribution is obtained using a superposition of two contributions

$$c = C_1 + C_2 \tag{10}$$

where C_1 is the contribution from the undamaged endothelium, in which, C_1 is required to satisfy condition (9) everywhere

$$\frac{\partial C_1}{\partial z}(r,1) + (Pe+\sigma)C_1(r,1) = \sigma - Pe\left(\frac{\gamma}{1-\gamma}\right) \qquad 0<r<\xi \tag{11}$$

and the C_2 accounts for the presence of the leaky junctions. From (8,9,10 and 11) the boundary conditions for C_2 at $z = 1$ are

$$C_2(r,1) = C_i - C_1 \qquad R_1<r<R_2 \tag{12}$$

and

$$\frac{\partial C_2}{\partial z}(r,1) + (Pe+\sigma)C_2(r,1) = 0 \qquad 0<r<R_1,\ R_2<r<\xi \tag{13}$$

For the case where the endothelium is intact, the concentration equation, that is, Equation (4) becomes

$$\frac{d^2C_1}{dz^2} + Pe\,\frac{dC_1}{dz} = 0 \qquad (14)$$

and the solution to C_1 is obtained by integrating (14) and applying the conditions (5) and (11)

$$C_1 = \left(\frac{\sigma - P_N}{H_0}\right)(1-e^{-Pez}) \qquad (15)$$

where $H_0 = Pe + \sigma(1-e^{-Pe})$ and $P_N = Pe(\gamma/(1-\gamma))$. Substituting (15) in (12) gives

$$C_2 = C_i - H_1(1-e^{-Pe}) \qquad R_1<r<R_2 \qquad (16)$$

where $H_1 = (\sigma - P_N)/H_0$.

The general solution for C_2 which satisfies boundary conditions (5,6 and 7), is of the form

$$C_2 = a_0(1-e^{-Pez}) + e^{-Pez/2}\sum_{j=1}^{\infty} a_j \sinh(\lambda_j' z) J_0(\lambda_j r) \qquad (17)$$

in which J_0 is the Bessel function of the first kind of order zero, $\lambda_j' = \sqrt{Pe^2/4 + \lambda_j^2}$, where λ_j are determined from the roots of the eigenfunction $J_1(\lambda_j \xi) = 0$, $j = 1,2,3...$, and the coefficients $a_j = 0,1,2....$, are unknown constants. In (17) when the Pe is zero, a_0 goes to infinity. To avoid this numerical difficulty, it is convenient to redefine the a_0 by another constant A_0 as $A_0 = a_o(1-e^{-Pe})$. The crucial mathematical problem is to determine these unknown coefficients by satisfying the mixed boundary conditions (12,13) at z = 1. Due to the small width of the leaky junctional complex compared to both the cell dimensions and the spacing between neighboring damaged cells 50,000 to 400,000 of the a_j coefficients are required

to adequately represent the solution $C_2(r,z)$, depending on the cell turnover rate. To determine the a_j coefficients it would be necessary to invert huge (j by j) matrices which require long computation times and a very large computer space (at least 10^9) easily exceeding our computer capacity. Thus, we use the special solution technique (Chapter II) and at z = 1 we require that

$$\frac{\partial C_2}{\partial z}(r,1) + (Pe+\sigma)C_2(r,1) = T(r), \quad R_1<r<R_2 \tag{18}$$

Using (10) and (15) in (18) it can easily be shown that

$$T(r) = \frac{\partial c}{\partial z}(r,1) + Pec(r,1) + P_N - \sigma(1-c(r,1))$$

Thus, T(r) physically represents the additional flux through the leaky junction above the value which would be obtained if the endothelium was intact and one side maintained at c = 1 and the other at $c = C_i$.

To determine the a_j coefficients in terms of T(r), we first evaluate (13) using (17) and then apply (18) to obtain

$$\frac{\partial C_2}{\partial z}(r,1) + (Pe+\sigma)C_2(r,1) = A_0H_3$$

$$+ e^{-Pe/2} \sum_{j=1}^{\infty} a_j[\lambda_j' \cosh\lambda_j' + H_2\sinh\lambda_j' \,]J_o(\lambda_j r)$$

$$= \begin{cases} 0 & 0<r<R_1, \quad R_2<r<\xi \\ T(r) & R_1<r<R_2 \end{cases} \tag{19}$$

in which $H_2 = \sigma + Pe/2$, $H_3 = \sigma + Pe + Pe\, e^{-Pe}/(1-e^{-Pe})$. Then, using the orthogonality of $J_0(\lambda_j r)$ in the region $0<r<\xi$ and using (19), the following expressions are obtained for the a_j coefficients in terms of the unknown function T(r),

$$A_0 = \frac{2}{H_3 \xi^2} \int_{R_1}^{R_2} r' \, T(r') dr' \tag{20}$$

and

$$a_j = \frac{2}{\xi^2} e^{Pe/2} \frac{1}{[\lambda_j \cosh \lambda_j + H_2 \sinh \lambda_j]}$$

$$\cdot \frac{1}{J_o^2(\lambda_j \xi)} \int_{R_1}^{R_2} r' T(r') J_o(\lambda_j r) dr' \tag{21}$$

$$j = 1,1,2,\ldots$$

where r' is a dummy variable in $R_1 < r < R_2$.

Substituting Equations (20) and (21) in (17) yields

$$C_2(r,z+ = \frac{2}{\xi^2} \frac{1-e^{Pez}}{H_3(1-e^{-Pe})} \int_{R_1}^{R_2} r' T(r') dr'$$

$$+ \frac{2}{\xi^2} \frac{e^{-Pez/2}}{e^{-Pe/2}} \sum_{j=1}^{\infty} \frac{\sinh(\lambda_j z)}{(\lambda_j \cosh \lambda_j + H_2 \sinh \lambda_j)}$$

$$\cdot \frac{J_0(\lambda_j r)}{J_0^2(\lambda_j \xi)} \int_{R_1}^{R_2} r' T(r') J_0(\lambda_j r) dr' \tag{22}$$

In order for this series representation (22) to also satisfy boundary condition (16), we multiply through by a Kernel solution function Kn(r), which is general enough to represent any solution function in the region R_1 to R_2, and can also be integrated when multiplied by the J_0 eigenfunction. Integrating this result from R_1 to R_2 and rearranging, one obtains

$$\{C_i - H_1(1-e^{-Pe}) - \frac{2}{H_3\xi^2}\int_{R_1}^{R_2} r'T(r')dr'\}\int_{R_1}^{R_2} Kn(r')dr'$$

$$= \frac{2}{\xi^2}\sum_{j=1}^{\infty} \frac{1}{(\lambda_j/\tanh\lambda_j)+H_2} \frac{1}{J_0^2(\lambda_j\xi)}\int_{R_1}^{R_2} r'T(r')J_0(\lambda_i r)dr'$$

$$\cdot \int_{R_1}^{R_2} Kn(r')\, J_0(\lambda_j r)dr' \qquad (23)$$

Now, we seek a function representation for T(r) and Kn(r) that satisfies an appropriate Sturm-Liouville problem at the end points R_1 and R_2. Thus, we choose (as in Chapter 2) a general series representation for T(r) of the form

$$T(r) = E_0 + \sum_{j=1}^{\infty}[E_m J_0(\alpha_m r) + F_m Y_0(\alpha_m r)] \qquad (24)$$

where Y_0 is Bessel function of the second kind of order zero. The appropriate Sturm-Liouville problem for T(r) which is orthogonal on the interval $R_1<r<R_2$, requires that T(r) and dT/dr vanish at R_1 and R_2. However, this may not be true in the present model. Thus, to ensure that T(r) is general enough, the series representation is made orthogonal in a slightly larger integration interval $R_1-\Delta r$ and $R_2+\Delta r$, satisfying the following artificial conditions

$$\text{at } r = R^- = R_1 - \Delta r, \quad \frac{dT(r)}{dr} = 0 \qquad (25)$$

$$\text{and at } r = R^+ = R_2 + \Delta r, \quad \frac{dT(r)}{dr} = 0 \qquad (26)$$

where $\Delta r << (R_2-R_1)$.

Using (25) in (24) gives

$$T(r) = E_0 + \sum_{m=1}^{\infty} E_m[J_0(\alpha_m r) - T_m Y_0(\alpha_m r)] \qquad (27)$$

and (26) in (24) gives

$$-J_1(\alpha_m R^+) + T_m Y_3(\alpha_m R^+) = 0 \qquad (28)$$

in which $T_m = J_1(\alpha_m R^-)/Y_1(\alpha_m R^-)$, the E_m are unknown constants still to be determined, and the α_m are eigenvalues obtained from the roots of the eigenfunction (28).

Having derived a suitable representation for T(r), Equations (27) and (28), we next choose a Kernel function Kn(r) with the following properties: (1) it is general enough to represent any function in the interval $R<r<R_2$, (2) it is integrable when multiplied by the J_0 function, and (3) it enables the generation of n linearly independent equations to determine the unknown E_m, $m = 0,1,2,\ldots$, coefficients in (24). A suitable form of the Kernel solution function with the above properties is

$$Kn(r) = \begin{cases} r & n = 0 \qquad (29a) \\ r[J_0(\alpha_n r) - T_n Y_0(\alpha_n r) & \qquad (29b) \end{cases}$$

where $\alpha_n = \alpha_m$ and $T_n = T_m$, in which m is replaced by n.

Substituting (27) and (29) in (23), performing the necessary integration and rearranging gives

$$C_i(-\bar{R}\frac{\xi^2}{2}) + E_0(\frac{\bar{R}^2}{H_3} + \sum_{j=1}^{\infty} f_3(j) f_4^2(j)) + \sum_{m=1}^{\infty} E_m \{\frac{f_1(m)\bar{R}}{H_3} + \sum_{j=1}^{\infty} f_3(j) f_2(m) f_4(j)\} = -H_1(1-e^{-Pe})\bar{R}\frac{\xi}{2}, \text{ for } n = 0 \qquad (30a)$$

and

$$C_i(-f_1(m)\ \frac{\xi^2}{2}) + E_0[\frac{f_1(m)\bar{R}}{H_3} + \sum_{j=1}^{\infty} f_3(j)f_2(n)f_4(j)]$$

$$+ \sum_{m=1}^{\infty} E_m[f_1(m)f_2(n) + \sum_{j=1}^{\infty} f_3(j)f_2(m)f_2(n)] \qquad (30b)$$

$$= H_1(1-e^{-Pe})\ \frac{\xi^2}{2}\ f_1(n),\ \text{for } n>0$$

where, $\bar{R} = (R_2^2-R_1^2)/2$

$$f_1(m) = \int_{R_1}^{R_2}[J_0(\alpha_m r') - T_m Y_0(\alpha_m r')]r'dr'$$

$$= \left\{r'\ \frac{J_1(\alpha_m r')}{\alpha_m} - T_m Y'\ \frac{Y_m(\alpha_m Y')}{\alpha_m}\right\}\Bigg|_{R_1}^{R_2}$$

$$f_2(m) = \int_{R_1}^{R_2}(J_0(\alpha_m r') - T_m Y_0(\alpha_m r'))r'J_0(\lambda_j r)dr'$$

$$= \left\{\frac{r'}{\alpha_m^2-\lambda_j^2}\ [-\lambda_j J_0(\alpha_m r')J_1(\lambda_j r') + \alpha_m J_1(\alpha_m r')J_0(\lambda_j r')\right.$$

$$\left.-(-\lambda_j Y_0(\alpha_m r')J_1(\lambda_j r') + \alpha_m Y_1(\alpha_m r')J_0(\lambda_j r'))]\right\}\Bigg|_{R_1}^{R_2}$$

$$f_3(j) = \frac{1}{(\lambda_j/\tanh\lambda_j)+H_2}\cdot\frac{1}{J_0^2(\lambda_j\xi)}$$

and

$$f_4(j) = \int_{R_1}^{R_2} r'J_0(\lambda_j r)dr' = r'\ \frac{J_1(\lambda_j r')}{\lambda_j}\Bigg|_{R_1}^{R_2}$$

From Equation (30), for every value of n, a linearly independent equation is obtained. Applying (27) in (20)

and (21) and integrating gives

$$A_0 = \frac{2}{\xi^2}\left(\frac{\bar{R}}{H_3}\right)E_0 + \frac{1}{H_3}\frac{2}{\xi^2}\sum_{m=1}^{\infty} E_m f_1(m) \tag{31}$$

and

$$\begin{aligned} A_j &= a_j \sinh\lambda'_j \\ &= \frac{2}{\xi^2} e^{Pe/2}\{f_3(j)(f_4(j)E_0 + \sum_{m=1}^{\infty} E_m f_2(m))\} \end{aligned} \tag{32}$$

in which the A_j has been introduced so as to avoid overflow problems in the computer from the hyperbolic functions when the index j is large. From (15,17,31 and 32) the concentration in terms of the unknown constants is

$$\begin{aligned} c(r,z) = {} & H_1(1-e^{Pez}) + \frac{2}{\xi^2}\left\{\frac{\bar{R}}{H_3} + \sum_{m=1}^{\infty}\frac{E_m f_1(m)}{H_3}\right\}\cdot\left(\frac{1-e^{-Pez}}{1-e^{-Pe}}\right) \\ & + \frac{2}{\xi^2}\frac{e^{-Pez/2}}{e^{-Pe/2}}\sum_{j=1}^{\infty} f_3(j)\{E_0 f_4(j) \\ & + \sum_{m=1}^{\infty} E_m f_2(m)\}\frac{\sinh(\lambda'_j z)}{\sinh\lambda'_j} J_0(\lambda_j r) \end{aligned} \tag{33}$$

C. Matching the Junction Flux to the Media Flux at $z = 1$ in $R_1<r<R_2$

The area averaged media flux in $R_1<r<R_2$, in dimensionless form is

$$J_m = \frac{\tilde{J}_m L}{D_m(C_L-C_A)} = \frac{2\pi}{\pi(R_2^2-R_1^2)}\int_{R_1}^{R_2}\left(\frac{\partial c}{\partial z} + Pe\left(c + \frac{\gamma}{1-\gamma}\right)\right)r'dr' \tag{34}$$

in which $\tilde{J}_m$ is the dimensional media flux and D_m is the effective diffusion coefficient of the media. However, $\tilde{J}_j = \tilde{J}_m$. Thus from (2) and (34)

$$J_j = J_m\left(\frac{\ell}{L}\right)\left(\frac{D_m}{D_j}\right) = J_m\left(\frac{P_j}{Pe}\right)\cdot\left(\frac{A_j}{A_m}\right) \tag{35}$$

where A_j/A_m is the area ratio of the leaky junction to that of an endothelial cell or the area of media covered by a single endothelial cell.

If, we let $(\ell/L)(D_m/D_j) = S_r$, then from (35)

$$P_j = PeS_r\, A_m/A_j \tag{36}$$

Applying (35) and (34) in (33), integrating and rearranging gives

$$J_j\left(\frac{-\bar{R}\xi^2}{2S_r}\right) + E_0\left(\bar{R}^2H_4 + \sum_{j=1}^{\infty} f_3'(j)f_4{}^2(j)\right) + \sum_{m=1}^{\infty} E_m\{f_1(m)H_4\bar{R}$$

$$+ \sum_{j=1}^{\infty} f_3'(j)f_2(m)f_4(j)\} = -\left(H_1Pe\,\frac{\xi^2}{2}\,\bar{R} + P_N\,\frac{\xi^2}{2}\,\bar{R}\right) \tag{37}$$

where

$$H_4 = \frac{Pe}{H_3(1-e^{Pe})}$$

and

$$f_3'(j) = \left[\frac{\lambda_j' + Pe/2(\tanh\lambda_j')}{\lambda_j' + \tanh\lambda_j'}\right]\cdot\frac{1}{J_0{}^2(\lambda_j\xi)}$$

Equation (37) gives a second condition for the flux through the channel as a function of the unknown E_m coefficients which are in turn dependent in C_i.

Thus far, we have developed the expressions for: (1) the junctional flux as a function of C_i, (2) the A_j coefficients as a function of the E_m coefficients, (3) the E_m constants in turn as a function of C_i. Thus, using (3) and (37), one can eliminate the C_i from (30). For such a case, if the infinite series indexed by j (in Equation (30)) is truncated at some large number j, and the m series is

truncated at some number m = n, a system of (n+1) linear algebraic equations are obtained for the unknown coefficients E_m, m = 0,1,2,...,m. The coefficient matrix of the system of equations may be solved for the E_m coefficients via standard matrix reduction techniques. Then J_j and C_i may be determined from (37) and (3) respectively, or simply, (3), (30) and (37) may be solved simultaneously (n+3 equations) to yield the values for C_i, J_j and the E_m coefficients. Having determined these values, this completes the solution of the concentration distribution.

The average axial flux across any plane in the arterial media is defined by

$$\psi = \frac{2\pi}{\pi\xi^2} \int_0^{\xi} \frac{\partial c}{\partial z} \, r dr \tag{38}$$

For the case where the endothelium is intact

$$\psi_i = P_N + \frac{Pe\sigma}{H_0} \tag{39a}$$

whereas for the case where the endothelium has damage(s) or leaky junctions

$$\psi = P_N + H_1 Pe + \frac{A_0 Pe}{1-e^{-Pe}} \tag{39b}$$

Furthermore, the total uptake of macromolecules per unit volume is

$$u = \frac{2\pi}{\pi\xi^2} \int_0^1 \int_0^{\xi} c r dr dz \tag{40}$$

and with intact endothelium

$$u_i = H_1 (Pe + e^{-Pe} - 1)/Pe \tag{41a}$$

However, with endothelial damage(s) or leaky junctions

$$u = (H_1 + \frac{A_0}{1-e^{-Pe}})(Pe + e^{-Pe} - 1)/Pe \qquad (41b)$$

Here also, as was shown for a single localized damage (Nir and Pfeffer, 1979), the periodic model (Pfeffer et al, 1981), and for the leaky junction model (Chapter 2), the flux and the uptake depend only on the leading coefficient A_0.

3. NUMERICAL RESULTS AND DISCUSSIONS

In obtaining numerical results for the flux, uptake and concentration distribution from the present model, in the m series, only 20 terms were found to be sufficient for accurate convergence of the solution series for all turnover rates (ϕ) of interest. However, the j series required more than 50,000 terms depending on ϕ; in particular, for $\phi < 1\%$, more than 120,000 terms were needed. In the solution techniques presented herein, the j terms enter the solution in the form of a summation, and thus present no difficulty.

The main results of this study are presented in Figure 3. The steady-state flux ratio ψ/ψ_i and uptake ratio u/u_i, that is for damaged to an intact endothelial cell layer, are given as a function of cell turnover rate, ϕ. Since the diffusion coefficient in the junction, D_j, is not known, the diffusion coefficient of albumin in free solution, i.e., 7.1×10^{-7} cm^2/sec (Keller et al., 1971) has been used as the upper limit. Using a diffusion coefficient for albumin in the media, $D_m = 5.05 \times 10^{-9}$ cm/sec (Thurn, 1982) gives $D_j/D_m = 140$. However, the medium of transport in the junction is not strictly free solution. Thus, we assume a D_j that is an order of magnitude smaller so that $D_j/D_m = 14$ is taken as the lower limit. Furthermore, we assume a leaky junction (R_2-R_1) of 200Å (Thurn, 1982), a junctional length of 2μm (Baldwin, 1983), an endothelial cell length ($2R_1$) of 30μm (Caplan and Schwartz, 1973), a media thickness (L) of 1mm, a C_A/C_L of zero, and a Biot number (σ) of 0.2. Experimental estimates of cell turnover rate vary depending on the experimental techniques and animals used. Gerrity et al. (1979) observed morphologic alterations of endothelial cells as well as cell death in the pig aortic arch, an area which stains readily by Evans blue dye. However, they rarely observed such conditions in areas of the arterial tree that did not stain (white areas) with Evans blue dye. Using

silver-nitrate staining, the above authors have reported cell turnover rate of 2.91% in the blue areas compared with only 0.71% in the white areas. However, DeBruijn et al. (1974) and Schwartz et al. (1981) have reported that the silver stain itself is noxious and can produce changes in the endothelium, complicating the determination of the cell turnover rate. In general, the cell turnover rate predicted by silver staining is five to tenfold greater than that reported using thymidine labeling. Thus, turnover rates of 1% or less are more likely to be physiologically correct.

From Figure 3, the important observation is that, for the physiologically relevant turnover rates ($\phi \lesssim 1\%$), the convective contribution to the flux and uptake is only 15 to 22% and less. This explains the apparent favorable agreement between the theoretical studies reported earlier (Pfeffer et al., 1981, and those in Chapter II) and the physiological experimental results of Bell et al. (1974a). However, as the cell turnover rate increases ($\phi > 1\%$), the effect of convection on flux and uptake can be dramatic, as is evident when observing the deviation of the Pe = 4 curves from the Pe = 0 curves. The use of a media Pe of approximately four is based on the physiological data of Vargas et al. (1978). From Figure 3 one observes that as the cell turnover rate or number of leaky junctions increase from 1/1000 to 5/1000, the flux or uptake ratio increases 20 to 50% for Pe = 0, and 29 to 67% for Pe = 4, clearly showing the transport rate controlling effect of the endothelial cell monolayer. Thus, significant changes in the equilibrium balance of the cholesterol carrying LDL molecules in the arterial wall can occur due to a very small fraction of leaky junctions.

Bell et al. (1974a) reported 66% increase in albumin influx in the blue stained areas of the pig aortic arch as compared to the unstained or white areas. This may be

denoted by $(\psi/\psi_i)_{\phi blue}/(\psi/\psi_i)_{\phi white}$ as in the previous models. Taking ϕ = 2.9% in the blue and 0.7% in the white areas, from Figure 3 (referring to results for the D_j/D_m of 140 as the upper limit and the results for the D_j/D_m of 14 as the lower limit), the equivalent ratios or increases in uptake are 55-74% for Pe = 0 and 93% to 134% for Pe = 4. In the in vivo experiments of Bondjers et al. (1973), although the exact sizes of the endothelial damages were not measured, they have reported that the damages were large and periodic, for the uptake difference of 15 times between the damaged and intact endothelial regions of the arterial tree. This large uptake difference can be explained only when taking into account the effect of convection. Such an increase is observed, for example in the Pe = 4 curve when ϕ increases from 0.1% to 50% when D_j/D_m is 14 and when ϕ increases from 0.1% to 20% when D_j/D_m is 140. Similarly, the large uptake difference reported by Colton et al. (1980) can only be explained by these curves.

The fraction of the total macromolecule flux that enters the arterial wall through the leaky junctions (or damages) is presented in Figures 4a and 4b. The results for Pe = 0 and Pe = 4 are nearly the same indicating that convection sharply increases the flux through the junction but has very little effect on the vesicular transport. The importance of the leaky junction or the leaky junction hypothesis is evident here again when one notices that when $\phi > 2\%$ and D_j/D_m = 14 or when $\phi > 0.7\%$ and D_j/D_m = 140, more than half of the total flux enters the arterial wall through the leaky junctions.

Another prediction of the present model that is of interest is the leaky junction-media interface concentration C_i, as a function of ϕ, presented in Figures 5a and 5b for D_j/D_m = 14 and D_j/D_m = 140, respectively. In these figures, and especially in 5a, it is clear that 1) the junctional resistance is important and that the concentration

throughout the junction is not the same as in the lumen and 2) a higher hydraulic flux tends to depress tissue concentration. A deeper insight into the mechanism on how a small turnover rate can effectively destroy the diffusional resistance of the endothelium can be obtained by examining the radial concentration profiles in Figure 6 for ϕ = 1% and D_j/D_m = 140. Due to the small dimensions of the leaky junctions, steep concentration gradients are found only in the vicinity of the leaky junctions; however, the radial spread of macromolecules is very significant and is nearly independent of r away from the damage site. Here also it is evident that hydraulic flux lowers the tissue concentration, by increasing the flow of macromolecules away from the media and into the adventitia where they are removed by the lymphatics. A similar observation about the effect of hydraulic flow on the concentration of macromolecules in the arterial media was also made by Bratzler et al. (1977).

Figure 7 shows the flux and uptake curves, and these are plotted for the same conditions as in Figure 3 except that σ has been changed to 0.086, which is the Biot number for rabbit estimated from the experimental work of Caro et al. (1980) for a media thickness of 0.2mm. Based on the definition of σ, as σ decreases or as the wall thickness decreases, the importance of the endothelium as a rate controlling resistance increases. It is clear that the convective contribution is dramatic for $\phi > 1\%$, as is evident in Figures 3 and 7. However, the slightly higher sensitivity to cell turnover by arteries with thinner walls can be noticed when one compares Figures 3 and 7.

The theoretical model presented herein has been evaluated using the adventitia-lumen concentration ratio (C_A/C_L) of zero; i.e., it was assumed that when molecules cross the media, they are totally removed by the lymphatic system at the adventitia. This assumption makes the flux and uptake ratios to be equal. However, the mathematical formulation

of the model is exact and is valid for any C_A/C_L ($0<C_A/C_L<1$) ratio and cell turnover rate or number of leaky junctions. The results from the present model show that the effect of pressure on transarterial transport is important especially for cell turnover rates greater than 1%, and that the leaky junction hypothesis is feasible. However, the apparent favorable agreement between the model and experimental data should be viewed with caution because of the simplified treatment of the complicated wall structure and because of the fact that the wall kinetics has been neglected which can be added easily as an extension to the present model.

4. REFERENCES

Baldwin, A. (1983), Columbia University Medical Center, personal communication.

Bell, F.P., Adamson, I.L. and Schwartz, C.J. (1974a). Exp. Mol. Path. 20, 57.

Björkerud, S. (1969). J. Ather. Res. 9, 209

Bondjers, G. and Björkerud, S. (1973). Atheroclerosis 17, 85.

Bratzler, G.L., Colton, C.K. and Smith, K.A. (1977). In G.W. Manning and M.D. Haust (Eds.), Atherosclerosis: Metabolic, Morphologic and Clinical Aspects, Plenum Press, New York, p. 943.

Caplan, B.A. and Schwartz, C.J. (1973). Atherosclerosis 17, 401.

Chien, S. and Weinbaum, S. (1981). ASME Biomech. Eng. 103, 176.

Colton, C.K. Schneiderman, G., Ramirez, C.A., Smith, K.A., Lee, R.S. and Stemerman, M.B. (1980). Proc. NSF Specialists Meeting, Hydrodynamics and the Artery Wall, eds. R.M. Nerem and J.R. Guyton, University of Houston, Houston, Texas, Nov. 5-7.

Gerrity, R.G., Richardson, M., Somer, J.B., Bell, F.P. and Schwartz, C.J. (1977). Am. J. Pathol. 89, 313.

Lezczynski, D.E. and Kummenow, F.A. (1981), J. Biomech. 14, 307.

Nir, A. and Pfeffer, R. (1979). J. Theor. Biol. 81, 685.

Pfeffer, R., Ganatos, P., Nir, A. and Weinbaum, S. (1981). ASME J. Biomech. Eng. 103, 197.

Schwartz, S.M., Gajdusek, C.M. and Seldon, S.C., III (1981). Atherosclerosis 1, No. 1.

Thurn, A.L. (1982). Doctoral Thesis, Columbia University.

4. REFERENCES (cont.)

Vargas, C.B., Vargas, F.F., Pribyl, J.G. and Blackshear, P.L., (1978). Am. J. Physiol. 236:H53-H60.

Weinbaum, S. and Caro, C.G. (1976). J. Fluid Mech. 74, 611.

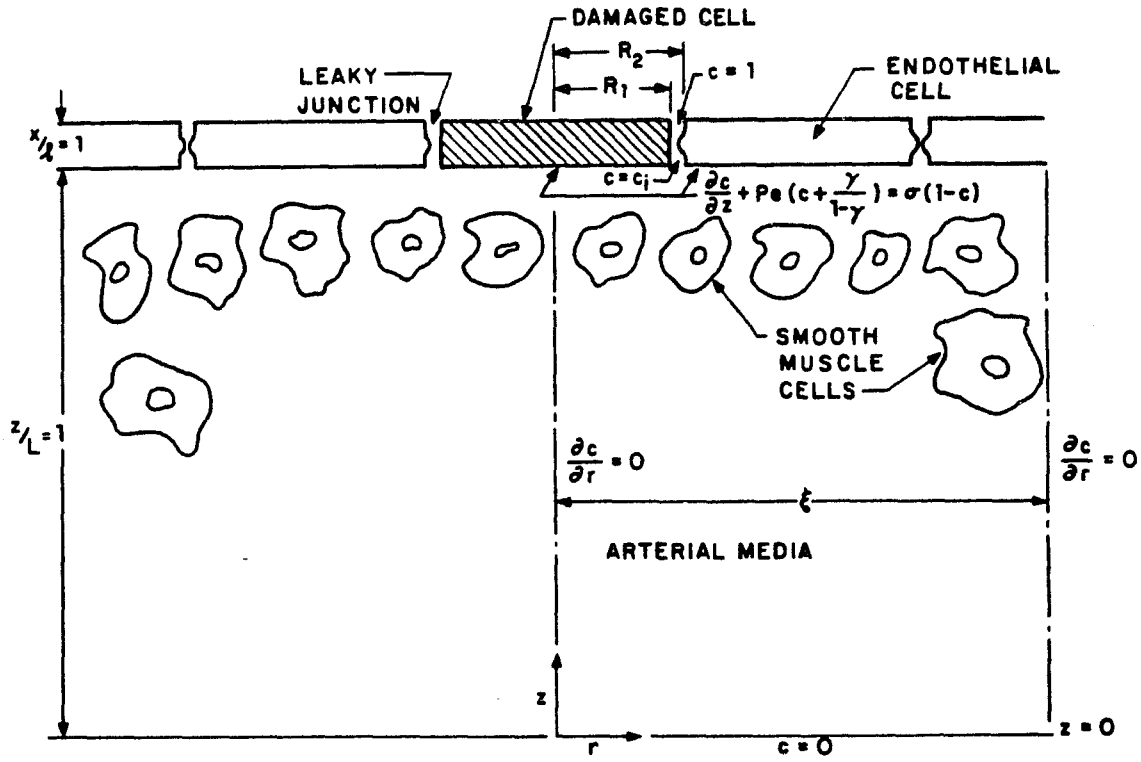

Figure 1. Schematic diagram of the mathematical model describing convective and diffusive transport of macromolecules across an artery wall having endothelial cell layer of finite thickness and leaky junctions.

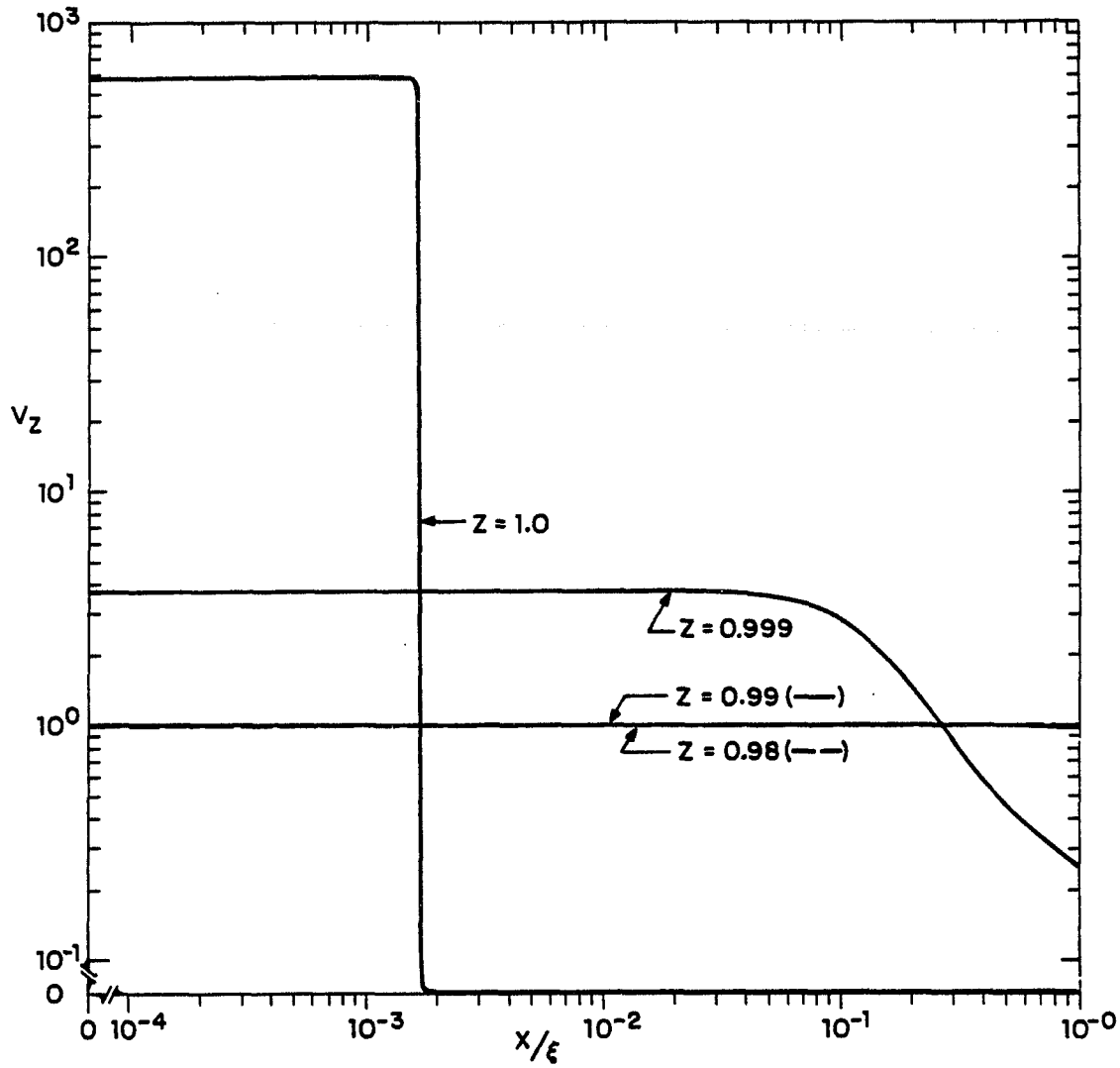

Figure 2. Axial velocity profile at increasing depth below endothelial surface; junctional width of 200Å and wall thickness of 1mm.

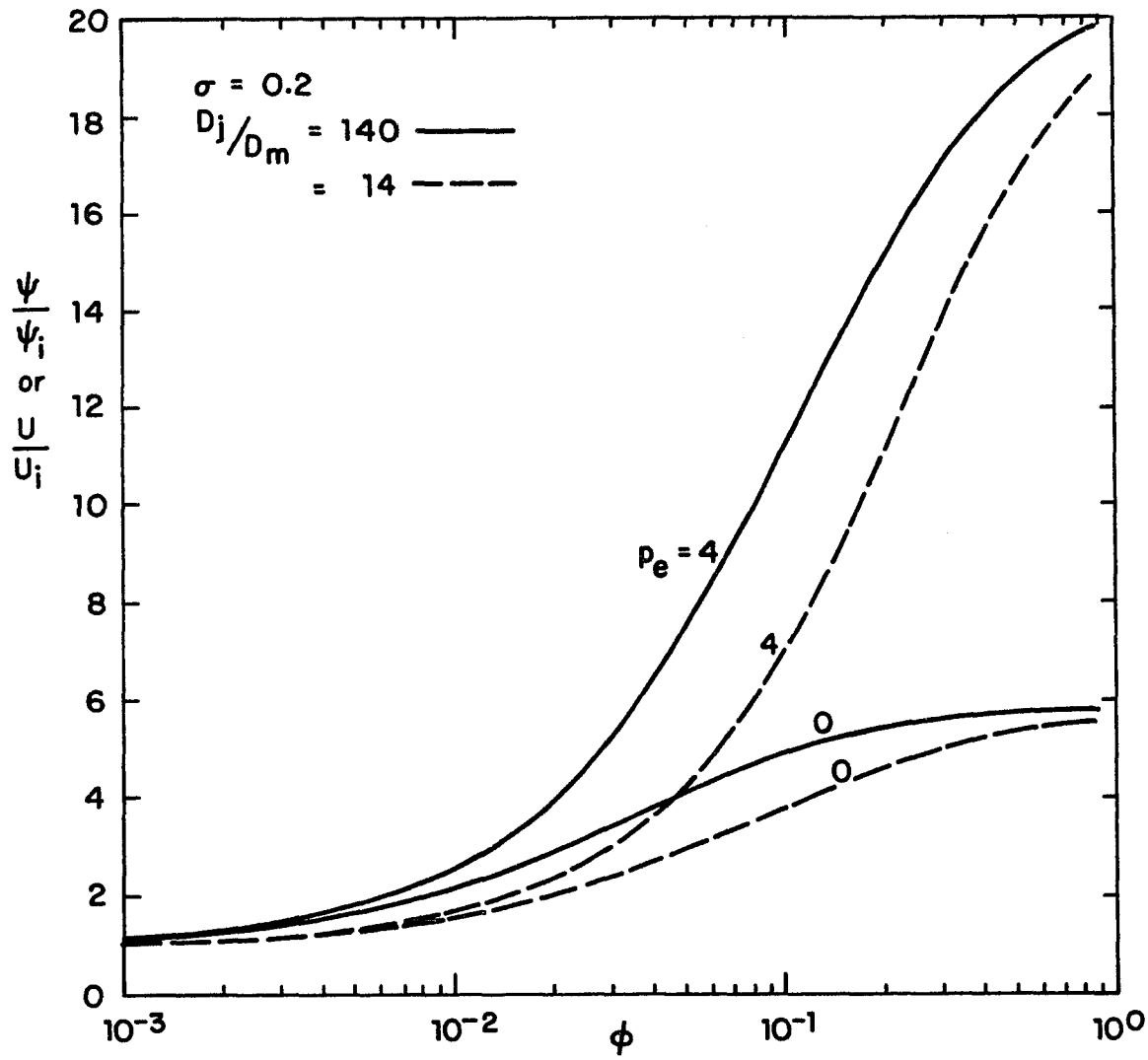

Figure 3. Relative enhancement of flux or uptake as a function of cell turnover rate for Pe = 0 and for Pe = 4; σ = 0.2, ℓ = 2μm and L = 1mm (D_j/D_m = 14-dashed curves and D_j/D_m = 140-solid curves).

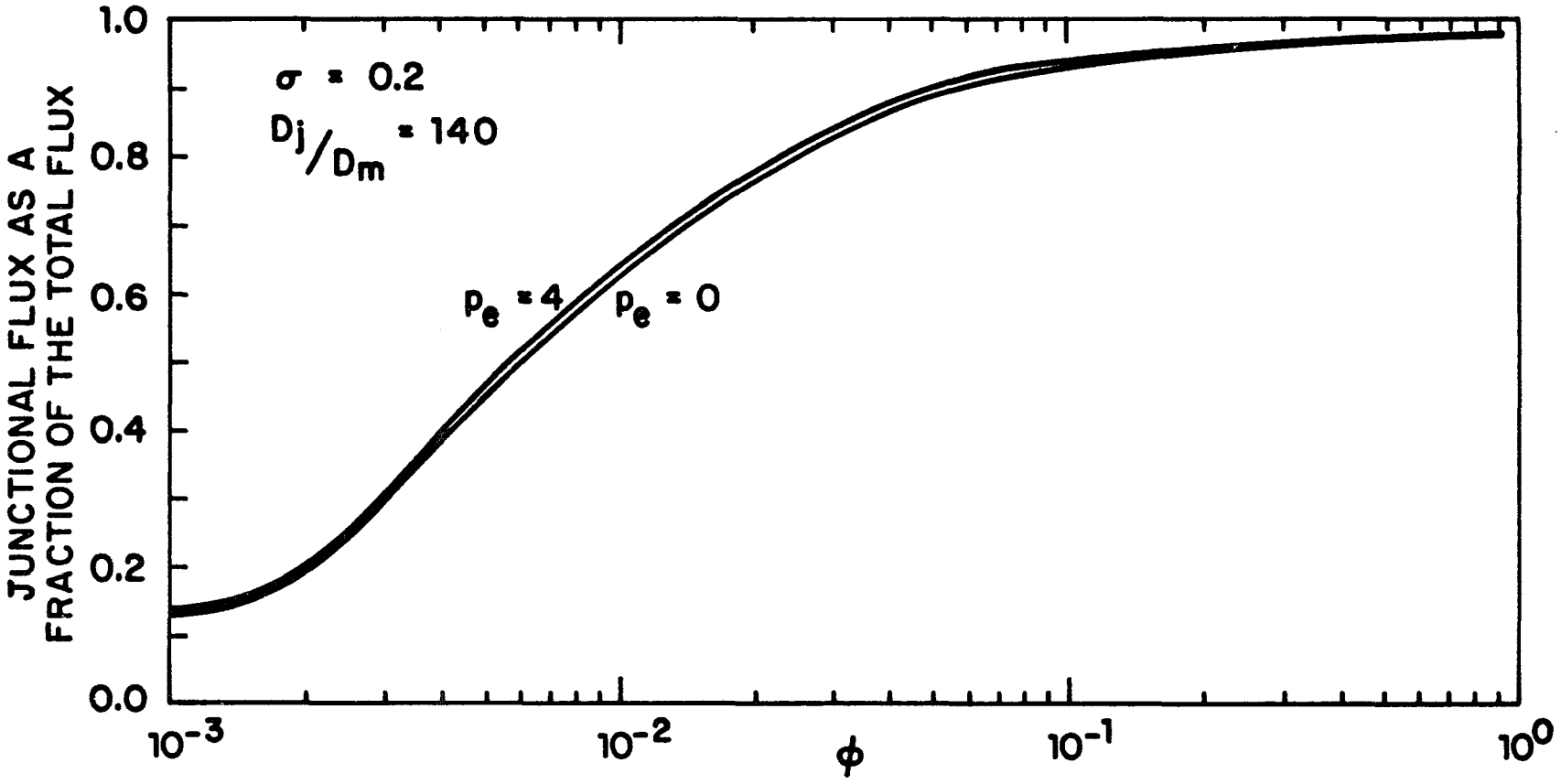

Figure 4b. Junctional flux as a fraction of the total flux as a function of cell turnover rate for Pe = 0 and Pe = 4; σ = 0.02, ℓ = 2μm, L = 1mm and D_j/D_m = 140.

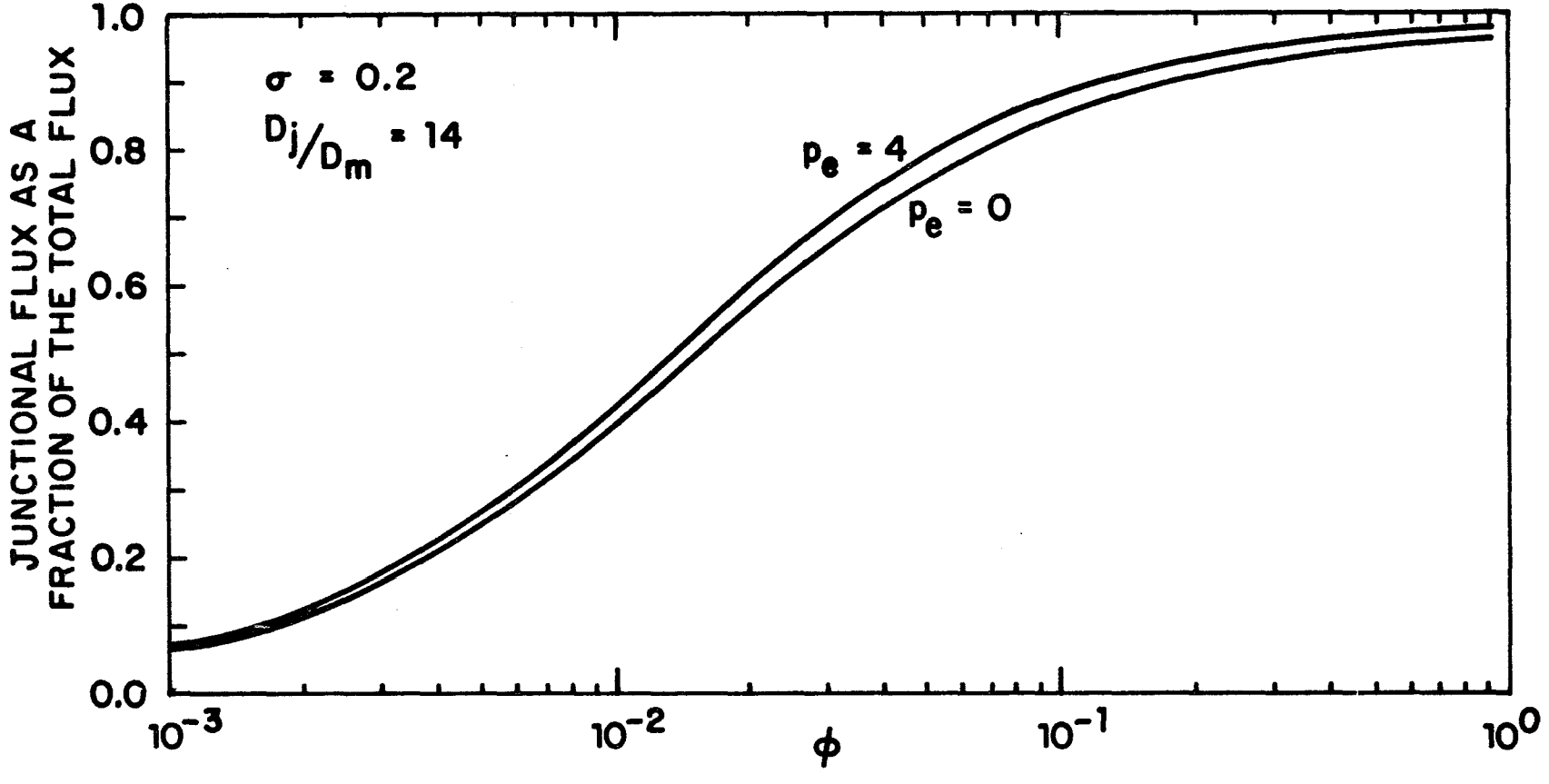

Figure 4a. Junctional flux as a fraction of the total flux as a function of cell turnover rate for Pe = 0 and for Pe = 4; $\sigma = 0.2$, $\ell = 2\mu m$, L = 1mm and $D_j/D_m = 14$.

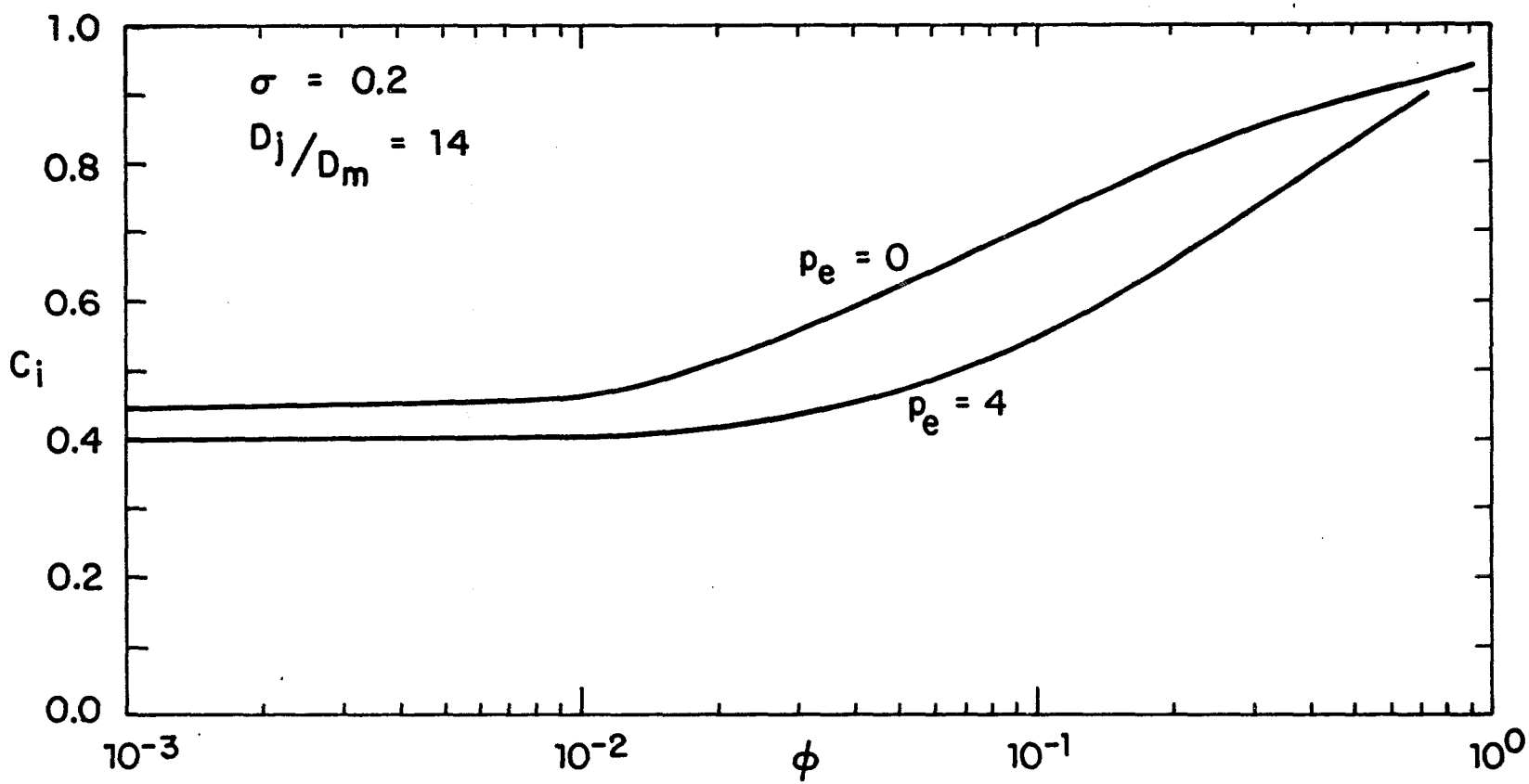

Figure 5a. Leaky junction and media interface concentration as a function of cell turnover rate for Pe = 0 and Pe = 4; σ = 0.2, ℓ = 2μm, L = 1mm and D_j/D_m = 14.

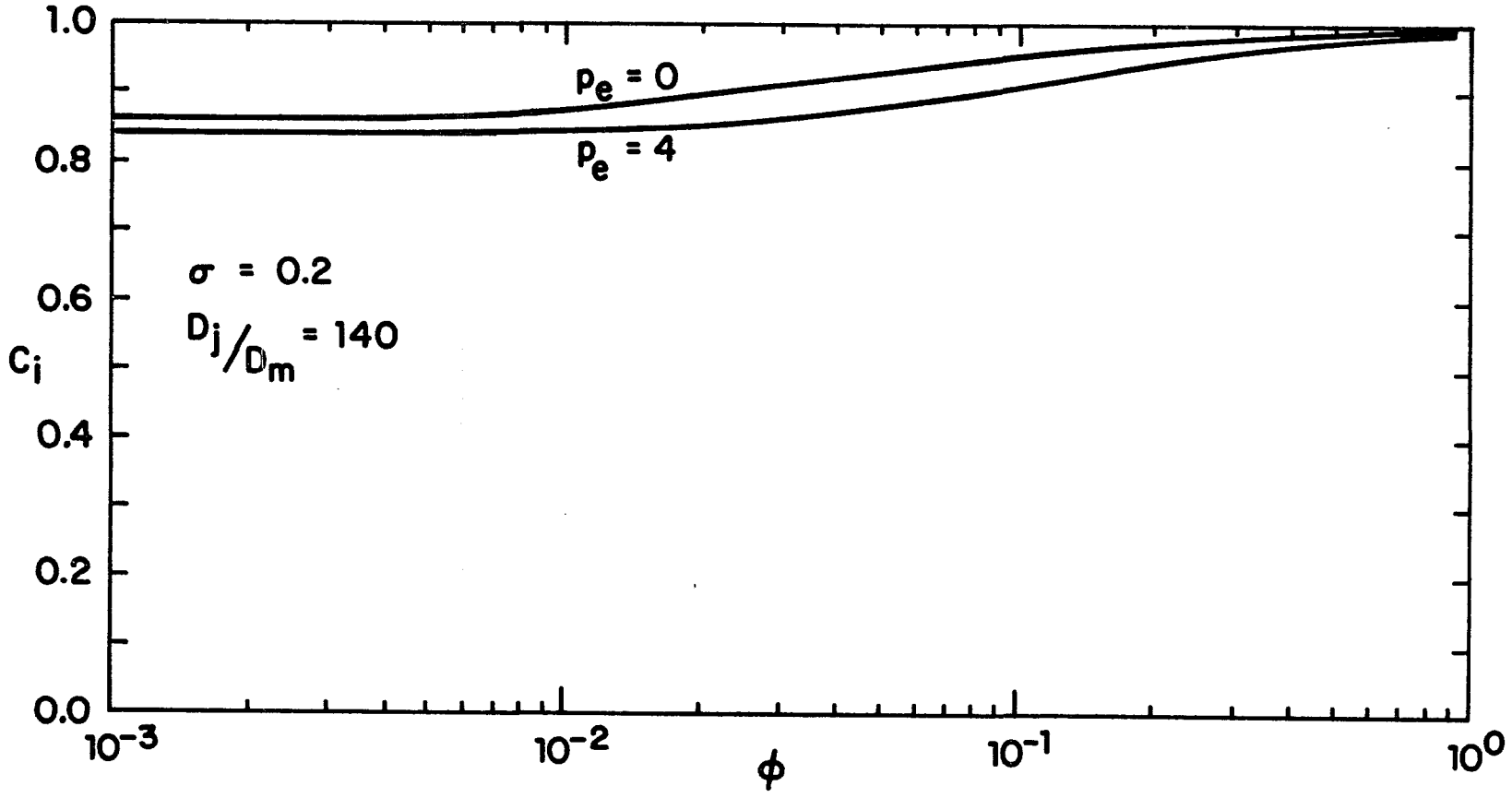

Figure 5b. Leaky junction and media interface concentration as a function of cell turnover rate for Pe = 0 and Pe = 4; σ = 0.2, ℓ = 2μm L = 1mm and D_j/D_m = 140.

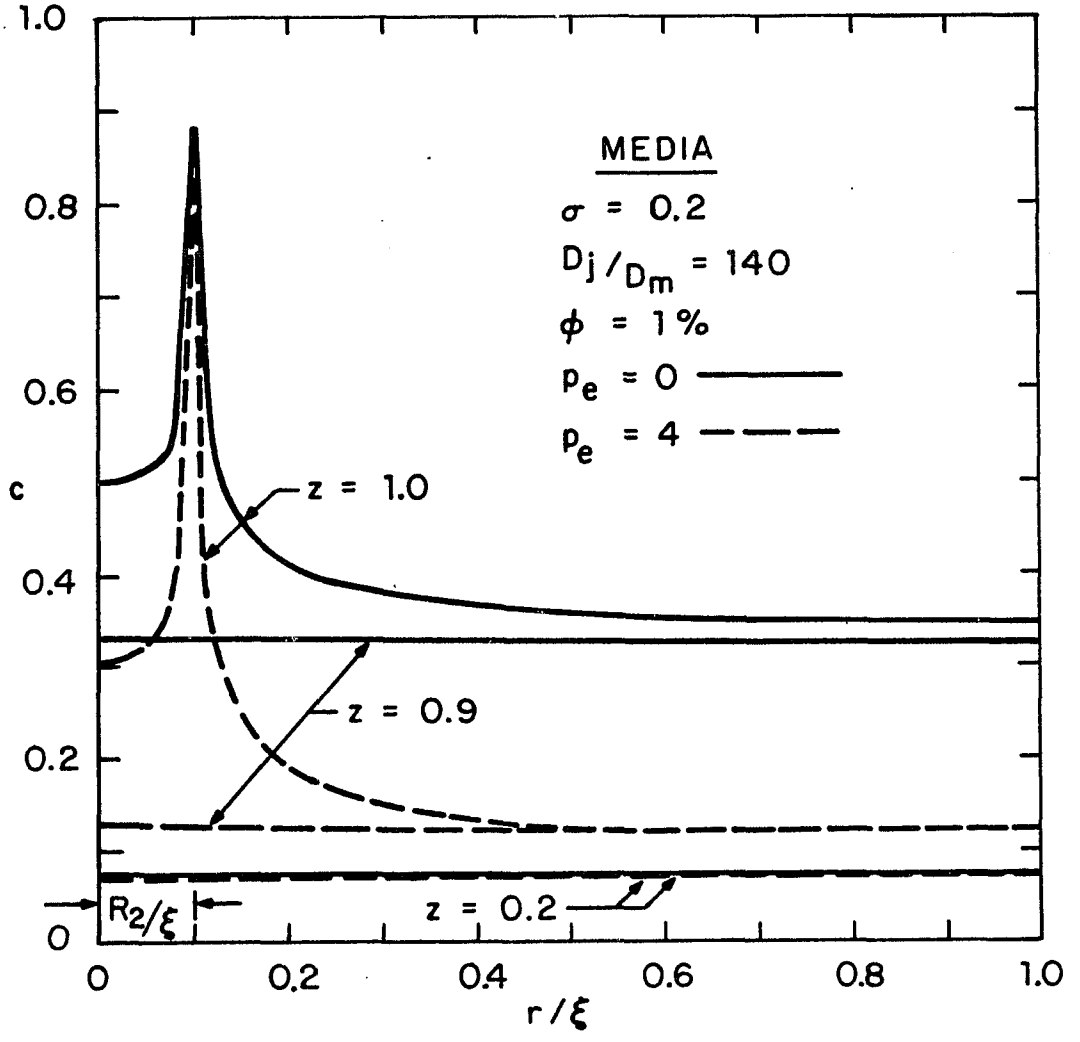

Figure 6. Radial concentration profiles for Pe = 0 (solid curves) and Pe = 4 (dashed curves); $\sigma = 0.2$, $\ell = 2\mu m$, L = 1mm, $\phi = 0.01$ and $D_j/D_m = 140$.

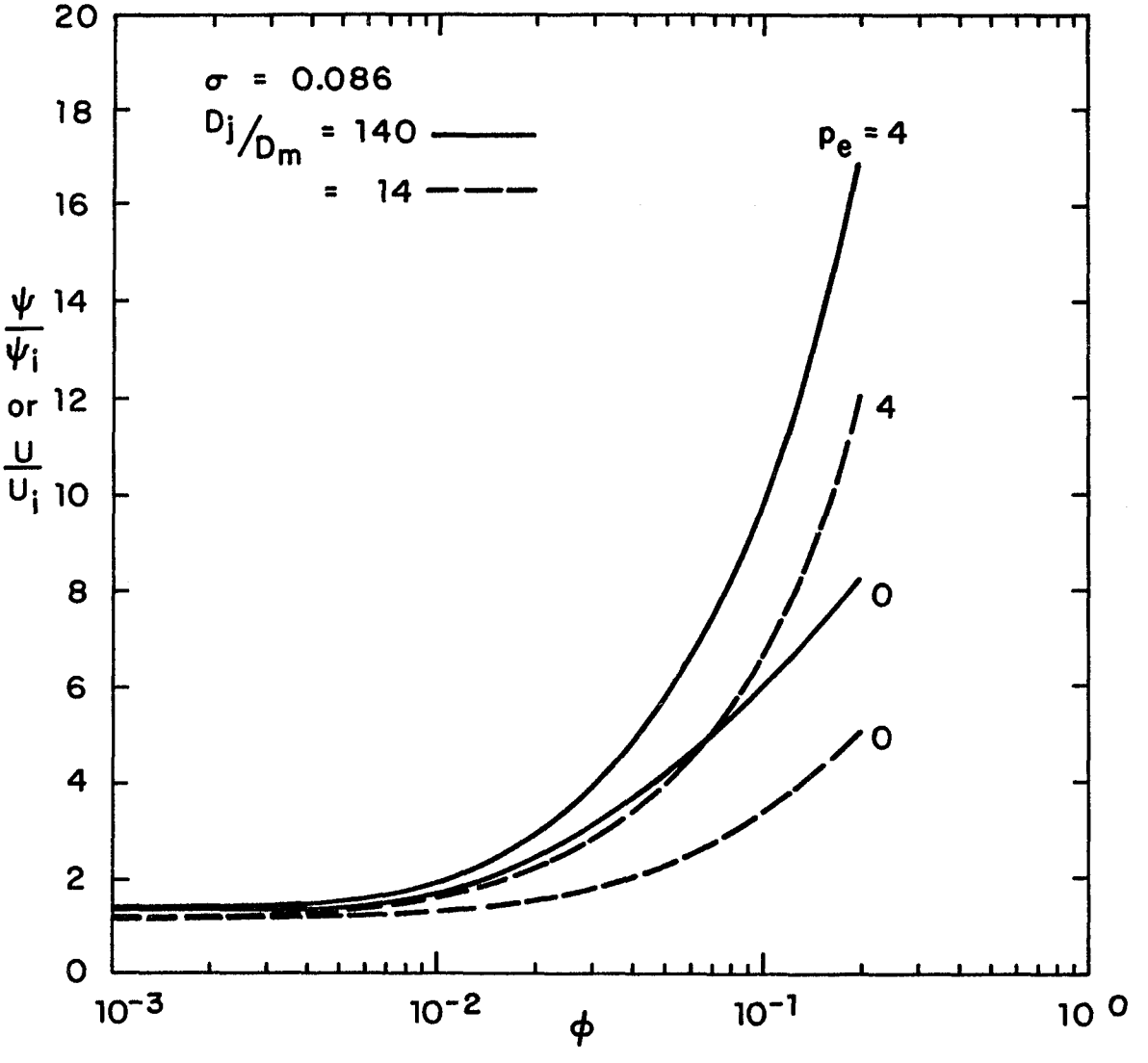

Figure 7. Relative enhancement of flux or uptake as a function of cell turnover rate for Pe = 0 and Pe = 4; σ = 0.086, ℓ = 2μm and L = 200μm (D_j/D_m = 14-dashed curves and D_j/D_m = 140-solid curves).

CHAPTER V

A SIMPLE THEORETICAL MODEL FOR ESTIMATING THE INTERSTITIAL CONCENTRATION AND DISTRIBUTION VOLUME IN THE ARTERIAL WALL USING TISSUE ACTIVITY MEASUREMENTS

SUMMARY

A theoretical model has been developed herein for estimating the interstitial concentration and distribution volume in the arterial wall. The validity of the model is illustrated here using experimental data from tissue activity measurements.

Key words: Atheroclerosis, Distribution volume, Diffusion coefficient

INTRODUCTION

Atherosclerosis is a multifactor disease; however, its ultimate manifestation is the build up of plaque in the arterial wall. In order to gain a better understanding of atherosclerosis and its prevention, it is necessary to seriously consider a model which; 1) could explain the resistance to the transport of macromolecules such as the cholesterol-carrying low density lipoproteins (LDL) by the different layers in the wall and 2) could predict the distribution volume in the different layers, thus allowing the computation of the actual concentration of macromolecules across the arterial wall.

The various experimental procedures presently used to determine the extracellular fluid volume (distribution volume) in the arterial wall usually result in either an overestimation of the volume if an electrolyte is used as the tracer substance, or an underestimation of the volume if a non-electrolyte tracer is used (1). However, a reasonable estimate can be obtained by very carefully selecting the tracer molecule size and the experimental technique. From such studies (1,2,3,4) the fact that the distribution volume is much greater in the adventitia than in the media is now clear and well-documented. It has also been observed that regions of the wall with lower distribution volume show a higher resistance to the transport of macromolecules, indicating the presence of a variable diffusion coefficient across the arterial wall. However, the tracer studies do not provide an estimate of either the change in the local resistance of the local distribution volume which are both necessary in order to scale the observed concentration distribution of macromolecules to obtain the true concentration profile and concentration gradient across the wall.

It is in the intima, the region between the media and the endothelium, that atheromatous lesions develop. Thus the

media provides a barrier or resistance to the influx or efflux of LDL molecules and in order for a steady-state flux to exist from the lumen to the adventitia the interstitial concentration must drop monotonically from the endothelium to the outer portion of the artery. This property of the media is not apparent when inspecting the available experimental data, e.g., (1,4) in which the uptake of macromolecules is reported as the ratio of tissue concentration to plasma concentration (C_T/C_P) as a function of distance (Z) across the wall from the lumen or from the adventitia. In fact, these data show that the concentration ratio C_T/C_P appears to be lower in the media than in the adventitia. However, when these data are presented taking into account both the variable distribution volume and diffusion coefficient across the wall as predicted by the proposed model, it is seen that the opposite is true, which is the expected result.

THEORETICAL MODEL

A relatively simple model is developed herein which relates the concentration, distribution volume and diffusion coefficient in the arterial wall. The experimental data of Caro et al. (4) are used to illustrate the validity of the model. Figure 1 is a plot of the steady-state concentration distribution ratio C_T/C_P (counts per minute gm^{-1} of wet tissue/counts per minute gm^{-1} plasma) of radioactively labeled albumin in rabbit carotid artery, as measured in situ by Caro et al. as a function of Z, the dimensionless distance across the arterial wall measured inward towards the lumen which is at Z=1. At first glance it seems puzzling that the measured radioactivity per gram of tissue is greater at the adventitial than at the luminal side of the wall. However, this does not necessarily indicate a net flux of labeled albumin out of the wall and into the lumen since the flux is based on the actual concentration in the available

interstitial space. Thus, it is necessary to estimate the distribution volume as a function of Z.

The model developed herein assumes: 1) a steady-state distribution of macromolecules in the wall, 2) the effects of hydrodynamic stress on the distribution volume are negligible, and 3) the distribution volume is known at both, a) the innermost part of the wall, or lumen, Z=1, and b) at the outermost part of the wall, Z=0. As stated above, experimental results have shown that the arterial wall is inhomogeneous indicating the presence of a variable diffusion coefficient in the artery wall due to the non-uniform distribution of smooth muscle cells in the various laminae. If we consider the smooth muscle cells in the arterial wall to be impermeable to the label and let each cell and its surrounding matrix of collogen fibers and other impermeable material be arbitrarily represented by a cube of length L, and the effective void distance between neighboring cubes is ℓ, where $\ell = \ell(Z)$, then the void or available volume associated with every cube of smooth muscle cell is $(L+\ell)^3-L^3$. Assuming $L>>\ell$, the void volume fraction, ε, is approximately given by

$$\varepsilon = \frac{3L^2\ell}{L^3} = \frac{3\ell}{L} \tag{1}$$

Similarly, the available surface area for diffusion in a cross-sectional plane surrounding each cell is its perimeter times one half its effective void distance

$$A = \frac{2L\ell}{L^2} = \frac{2\varepsilon}{3} \tag{2}$$

Now, denoting the experimentally measured data, C_T/C_P as $\bar{C}$, the apparent diffusion coefficient as $\bar{D}$, the true concentration as C and the true diffusion coefficient as D where both C and D are functions of Z, it is clear that:

$$C = \bar{C}/\varepsilon \tag{3}$$

and

$$D = \bar{D}A = \frac{\bar{D}2\varepsilon}{3} \tag{4}$$

In order to determine $\varepsilon(Z)$ we write down the one-dimensional steady-state conservation of mass equation in the arterial wall in the absence of convection

$$\frac{d}{dZ}\left(D\,\frac{dC}{dZ}\right) = 0, \tag{5}$$

and substitute equations (3) and (4) in (5). This substitution gives:

$$\frac{d}{dZ}\left(\varepsilon d\,\frac{(\bar{C}/\varepsilon)}{dZ}\right) = 0 \tag{6}$$

Integrating equation (6) once yields:

$$\frac{d\bar{C}}{dZ} - \frac{\bar{C}}{\varepsilon}\,\frac{d\varepsilon}{dZ} = \underline{C}_1, \tag{7}$$

where $\underline{C}_1$ is an integration constant. Rearranging equation (7) we obtain:

$$d\ \ell n\ \bar{C} - d\ \ell n\ \varepsilon = \underline{C}_1\,\frac{dZ}{\bar{C}} \tag{8}$$

From steady-state distribution studies in rabbit carotid arteries, Caro (5) found that the available volume ε is approximately 7% at Z=1 and 35% at Z=0. Since $\bar{C}$ was not measured at Z=1 and Z=0, the above information is arbitrarily used as boundary conditions at Z=0.95 and Z=0.05 respectively where $\bar{C}$ is known at both points (see Figure 1). Integration of equation (8) therefore yields:

$$\varepsilon(Z) = \varepsilon(0.05)\,\frac{\bar{C}(Z)}{\bar{C}(0.05)}\ e^{-\underline{C}_1\ B_1} \tag{9}$$

where

$$B_1 = \int_{0.05}^{Z} \frac{dZ}{\bar{C}}$$

$$C_1 = \ell n \frac{\bar{C}(0.95)}{\bar{C}(0.05)} \cdot \frac{\varepsilon(0.05)}{\varepsilon(0.95)} / B_2 \qquad (10)$$

$$B_2 = \int_{0.05}^{0.95} \frac{dZ}{\bar{C}}$$

The integral $\int_{0.05}^{Z} dZ/\bar{C}$ is determined after curve fitting the data in Figure 1, using a least square approximation by cubic splines with variable knots.

Equations (9) and (10) permit the evaluation of $\varepsilon(Z)$, which in turn permits the evaluation of C(Z) using Equation (3). A plot of C(Z) is shown in Figure 2. By extrapolating the curve in Figure 2 to Z=1 it is possible to obtain an estimate of the concentration C at Z=1, from which an independent estimate of the Biot number σ for rabbit carotid artery can be obtained. The Biot number is a very important parameter in determining the transport of macromolecules across the arterial wall. It represents the ratio of the resistance to the transport of macromolecules offered by the arterial media to the resistance of the intact endothelium. From Figure 2, C=0.16 at Z=1 and since Weinbaum and Caro (6) have shown that $dC/dZ = \sigma(1-C)$ across the intact endothelium, a value of $\sigma = 0.086$ is obtained.

DISCUSSION

The simple model presented above was applied to the steady-state distribution data in Figure 1. The data was replotted in Figure 2 taking into account the variable local distribution volume and diffusion coefficient. Figure 2 indicates that the artery wall consists essentially of two

distinct regions of relatively constant diffusion coefficient, the media and the adventitia, with an abrupt change in diffusion coefficient occurring at their interface. The concentration of albumin is highest at the lumen and decreases monotonically in both the media and the adventitia which is the expected result but is opposite to what is seen in Figure 1. Furthermore, the estimated value of 0.086 for the Biot number indicates that the resistance of the endothelial wall layer is more than 9 times greater than the resistance of the media and is clearly the controlling resistance to the passage of macromolecules in an intact rabbit carotid artery.

REFERENCES

1. Chien, S. and Gregersen, M.I., Determination of Body Fluid Volumes. In: W.L. Nastuk (Ed.), Physical Techniques in Biological Research, Academic Press, New York, 4, p. 1 (1962).
2. Torok, J., Nedergaard, C.A. and Bevan, J.A., Distribution of Inulin Space in the Rabbit Thomi Aorta, Experimentia (Basel), 27, 55 (1971).
3. Ghosh, S., Finkelstein, J.N., Moss, D.B. and Schweppe, J.S., Evaluation of Permeability Parameters of Arterial Wall for LDL and Other Proteins. In: C.E. Day (Ed.) Atherosclerosis Drug Discovery, Plenum Press, New York, p. 191 (1975).
4. Caro, C.G., Lever, M.T., Laver-Rudich, Z., Meyer, F., Livon, N., Ebel, W., Parker, K.H. and Winlove, C.P., New Albumin Transport Across the Wall of the Rabbit Common Carotid Artery Profused in Situ, Atherosclerosis 37, 497 (1980).
5. Caro, C.G. Personal Communication.
6. Weinbaum, S. and Caro, C.G., J. of Fluid Mechanics, 74, 611 (1976).

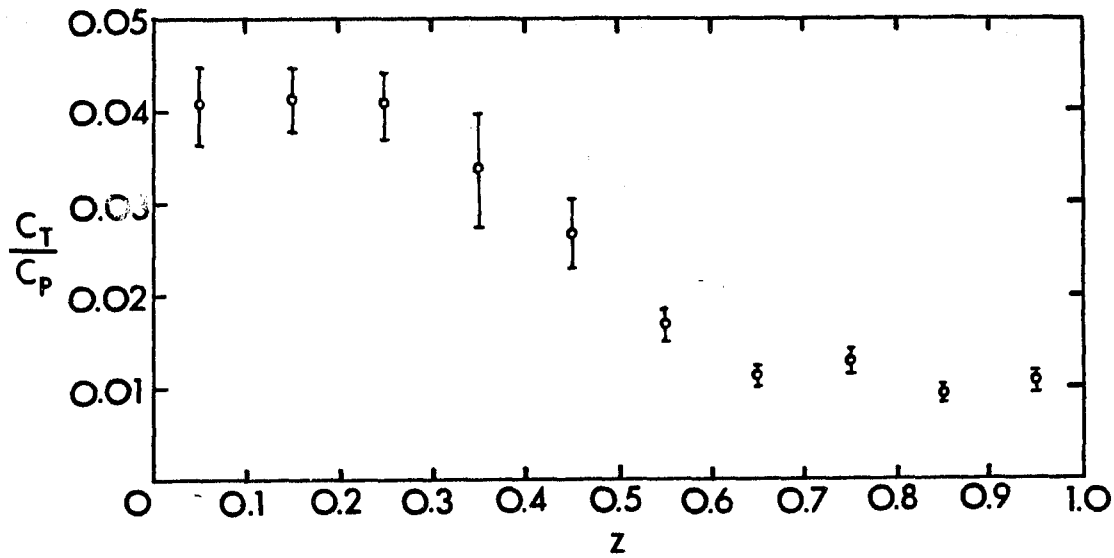

Figure 1. Caro (1980) experimental data for steady-state concentration ratio C_T/C_P (counts per minute gm^{-1} of wet tissue/counts per minute gm^{-1} plasma) of radioactively labeled albumin in rabbit carotid artery as a function of distance Z across the arterial wall; adventitia at Z = 0, lumen at Z = 1.

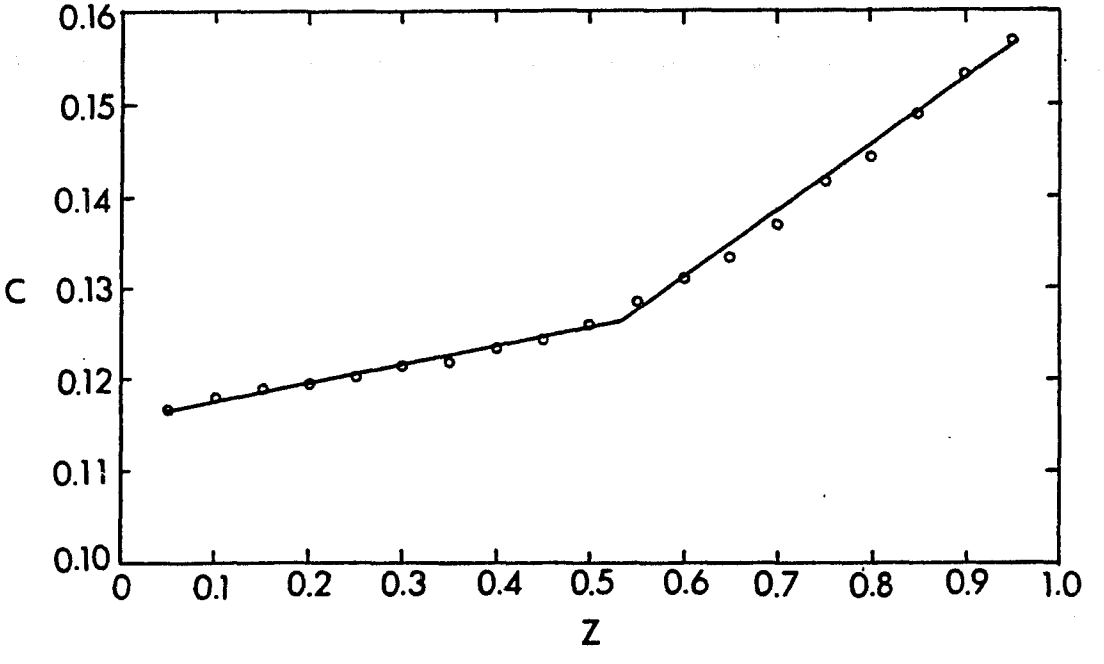

Figure 2. Data of Figure 1 replotted taking into account the available volume, diffusion and spatial dependence of the diffusion coefficient.

CHAPTER VI

CONCLUDING REMARKS

As stated earlier, atherosclerosis is a multi-factor disease and its ultimate manifestation is in the build up of plaque in the arterial wall. Therefore, the studies presented herein have concentrated on developing theoretical models which, together with the available physiological data, can lead to a better understanding of the transport mechanisms in the wall.

In the leaky junction model (Chapter II), based on recent experimental observation, it is assumed that when an endothelial cell is in the process of turnover, it becomes leaky only along its perimeter so as to allow the transport of macromolecules larger than 40Å. The results from this model clearly show that the leaky junction hypothesis is a feasible mechanism of transport into the arterial wall when the integrity of the endothelium is disturbed due to normal cell turnover. Extension of this model (Chapter IV) shows that the junctional resistance even in these leaky junctions can have significant effect on transendothelial transport. Furthermore, the model shows that the effect of convection on the uptake or flux of macromolecules into the wall is important, and the convective contribution to flux and uptake increases dramatically with an increase in endothelial damage size or with an increase in the number of leaky junctions.

Furthermore, the coupling of the endothelial junction resistance with the arterial media resistance (Chapter III) and the available distribution volume (Chapter V) have been quantified for the first time. In Chapter III, a theoretical model is developed which gives a detailed view of the fine structure of the water movement and pressure distribution in the arterial wall, and shows the quantitative relationship between the dimension of the intercellular cleft and the water movement and pressure distribution in the subendothelial space. Based on the results of this model, it can be shown that for a 0.2mm thick wall, more than half

of the total pressure drop will occur across the endothelium if the minimum width of the junction is less than 26Å. Using measured resistances for the wall and endothelium (see Chapter III), the theory provides a novel independent means of estimating the width of the junctional complexes from filtration data. Chapter V deals with an estimation of the distribution volume and interstitial concentration in the wall using tissue activity measurements. The results indicate that the artery wall consists essentially of two distinct regions, the media and the adventitia where the distribution volume is much larger in the latter and the diffusion coefficient changes abruptly at the interface between the two. However, it is also clear that both the media and the adventitia can be described by a relatively constant (although different) effective diffusion coefficient.

Results from all of the above models have shown a very favorable agreement with experimental data whenever a direct comparison was possible. However, because of the many simplifications which were applied when describing the complicated structure of the arterial wall, these theory and experiment comparisons should be viewed with caution. The methods of solutions presented here are also applicable to a variety of problems in different fields where similar mixed boundary conditions are applicable. For example, the solution procedure can be applied to the study of the transpiration of water vapor by plant leaves, where, the bulk of the diffusion occurs through the leaf pores but some may occur through the leaf surface. Another application is found in electrostatic potential theory, where, in order to determine the series resistance of a transister, the potential distribution must be found. Here, the voltage of current density may be specified on the emitter and collector plates while the remaining area adjacent to the emitter is

insulated, leading to a mixed boundary value problem similar to the ones which were solved herein.

Some important experimental and theoretical problems related to this research which still need to be addressed are, 1) to predict the time dependent accumulation of macromolecules in the arterial wall following an endothelial injury, 2) to clearly show by definitive experiments that the junctions of dying or newly formed endothelial cells are leaky to macromolecules while those of normal neighboring cells are not, 3) to determine the role of macromolecular charge in vesicle loading and transport through junctions, and 4) to produce a more general model based on the results in Chapters II to V, so as to present a unified theory which can describe the transport phenomenon in all vessel sizes. A variety of new experiments are now in progress at The Columbia University College of Physicians and Surgeons in close coordination with additional theoretical studies at The City University of New York in order to elucidate the above problems.

LIST OF SYMBOLS

a = a constant = $(\varepsilon_n+\varepsilon_{min})/2$, Å

A = area, cm^2

$a_j, j=0,1,2,\ldots,$ = constant coefficients

$A_j, j=1,2,3,\ldots,$ = $a_j \sinh(\lambda_j)$

b = a constant = $(\varepsilon_n-\varepsilon_{min})/2$, Å

B_1, B_2 = known integrals

c = concentration, dimensionless

C = concentration, g/cm^3

C_1 = concentration distribution in an arterial wall with intact endothelium

C_2 = contribution to the arterial wall concentration distribution due to leaky junctions

$\underline{C}_1$ = integration constants

D = diffusion coefficient, cm^2/sec

$D_m, m=0,1,1,\ldots,$ = constant coefficients

$E_m, m=0,1,2$ = constant coefficients

$f_i, i=1$ to 7 = known functions

$f_i(m), f_2(m)$ = known functions

$f_3(j), f_4(j)$ = known functions

$f_3^i(j)$ = known functions

$f(r)$ = local flux at $z=1$ in $R_1<r<R_2$

$F_m, m=1,2,3,\ldots,$ = integration constants

H_0 = a constant, $Pe+\sigma(1-e^{Pe})$

H_1 = a constant, $(\sigma-P_N)/H_0$

H_2 = a constant, $\sigma+Pe/2$

H_3 = a constant, $\sigma+Pe+e^{-Pe}/(1-e^{-Pe})$

J_0 = Bessel function of the first kind of order zero

J_1 = Bessel function of the first kind of order one

$\mathcal{J}$ = flux, $g/(cm^2-sec)$

J = dimensionless flux

LIST OF SYMBOLS (cont.)

k = hydraulic conductivity, cm/(sec cm-H_2O)

$Kn(r), n=0,1,2,\ldots,$ = Kernel solution functions

ℓ = intercellular channel, length, μm

$\ell(z)$ = void distance between two neighboring model cubes

L = arterial media thickness, μm or mm or cm

p = pressure, cm-H_2O

p_1 = lumen pressure, cm-H_2O

p_2 = subendothelial pressure

p_3 = media-adventitia in interface pressure, cm-H_2O

$\bar{p}_2$ = average subendothelial pressure, cm-H_2O

$P_1, P_2, P_3, \bar{P}_2$ = dimensionless pressures

Q = volumetric flow rate, cm^3/sec

r, r' = space variables

R_1 = radius of damaged endothelial cell

$\underline{R}_1$ = hydraulic resistance of an endothelial junction, $g/(cm^2\text{-sec})$

R_2 = R_1+leaky junction width

$\underline{R}_2$ = hydraulic resistance of an arterial media

$\bar{R}$ = $(R_2^2-R_1^2)/2$

R^+ = $R_2+\Delta r$

R^- = $R_1-\Delta r$

S_m, S_r = known constants

$T(r)$ = additional flux through a leaky junction at $z=l$ in $R_1<r<R_2$

u = uptake of macromolecules per unit volume, $(g/cm^3)cm^3$

V = fluid velocity, cm/sec

V_1 = fluid velocity in the intercellular channels, cm/sec

LIST OF SYMBOLS (cont.)

V_2 = fluid velocity in the media, cm/sec

w = length of a localized constriction in the channel, Å

x = space variable

Y_0 = Bessel function of the second kind of order zero

Y_1 = Bessel function of the second kind of order one

z, z', Z = space variables

∇ = differential operator

Greek Letters

α_n, α_m = eigenvalues

γ = C_A/C_L

γ_c = known constant

Δ = incremental or a difference quantity

ε = half width of an intercellular junction, Å

ε' = width of a leaky junction, Å

ε_{min} = half width of a tight junction, Å

ε_n = half width of junction at its wider region(s), Å

ε_0 = an equivalent junctional half width, Å

$\varepsilon(z)$ = fraction of void volume in an arterial media

$\lambda_j, \lambda'_j, \lambda_m$ = eigenvalues

μ = viscosity g/(cm-sec)

ξ = radius of a unit model cell

ϕ = fraction of junctions that are leaky (R_2^2/ξ^2) or the ratio of junction area to endothelial cell area (ε/ξ)

ψ = average axial flux in the media

ψ_i = average axial flux with intact endothelium

LIST OF SYMBOLS (cont.)

$\underline{\psi}$ = a known constant

Superscripts

* indicates dimensionless quantity

' indicates a modified definition of a quantity or variable

Subscripts

A, refers to the arterial adventitia

c, refers to the intercellular channel

i, refers to the endothelial junction-media interface

j, refers to the intercellular junction

L, refers to the arterial lumen

m, refers to the arterial media

P, refers to the arterial plasma

T, refers to the arterial tissue

Dimensionless Quantities

Pe = Peclet number in the media = $V_m L/D_m$

P_j = Peclet number in the junction = $V_j \ell/D_j$

$P_N = Pe\gamma/(1-\gamma)$

$P_s = P_j\gamma/(1-\gamma)$

σ = Biot number = $\theta I_v L/D_m$, in which, θ is the transendothelial vesicle number flux and I_v is the internal volume of the vesicles